Theoretical Studies on the Role of Silver Salt Additives in Palladium Catalysis: Insights on Heterobimetallic Cooperativity

by

Megha Anand

(Under the Direction of Prof. Henry F. Schaefer III)

Abstract

A wide variety of additives are frequently used in homogenous transition-metal catalyzed reactions, however, their role at the molecular level has not been well understood. An exhaustive mechanistic study has been done to find the plausible role of silver additives in seven different palladium catalyzed reactions by locating all conceivable transition states (both in the presence and the absence of additives) for the key steps of the reaction. The lower energy transition states display intermetallic Pd–Ag interaction with bridging ligands such as acetate, triflate, etc., bringing the two metals together. These results provide credence to existence of heterobimetallic (Pd–Ag) cooperativity in palladium catalyzed homogenous reactions with silver salts as additives.

Index words: C–H activation, Transition metal Catalysis, Palladium Acetate, Additives, Cooperativity, Reaction mechanisms, Transition states

Theoretical Studies on the Role of Silver Salt Additives in Palladium Catalysis: Insights on Heterobimetallic Cooperativity

by

Megha Anand

MS (Chemistry), Indian Institute of Technology Bombay, 2012

A Dissertation Submitted to the Graduate Faculty
of The University of Georgia in Partial Fulfillment
of the
Requirements for the Degree

Doctor of Philosophy

Athens, Georgia

2016

©2016

Megha Anand

All Rights Reserved

Theoretical Studies on the Role of Silver Salt Additives in Palladium Catalysis: Insights on Heterobimetallic Cooperativity

by

Megha Anand

Approved:

Major Professor:	Henry F. Schaefer III
Committee:	Shanta Dhar
	Eric Ferreira
	P. V. R. Schleyer

Electronic Version Approved:

Suzanne Barbour
Dean of the Graduate School
The University of Georgia
May 2016

Theoretical Studies on the Role of Silver Salt Additives in Palladium Catalysis: Insights on Heterobimetallic Cooperativity

Megha Anand

May 2, 2016

Acknowledgments

Firstly, I would like to express gratitude to my advisor Prof. Henry F. Schaefer III who has been very kind and supportive and gave me the freedom to work on research problems of my choice in collaboration with Prof. Paul Schleyer at the Center for Computational Quantum Chemistry (CCQC) and Prof. R. B. Sunoj from IIT Bombay.

I am also grateful to Prof. R. B. Sunoj who has been a longtime mentor and a friend since I was an undergraduate student at IIT Bombay. His encouragement and constant support during tough times in graduate school helped me to stay focused on my goals. I have immensely enjoyed working with him both as an undergraduate and graduate student.

I was fortunate to be able to work with the renowned Prof. Paul Schleyer, one of my committee members and his post-doctoral student Dr. Judy Wu. They greatly influenced my scientific outlook in the early days of my PhD and helped me to move closer towards my academic and personal development goals in the graduate school. I would also like to thank my other committee member Dr. Shanta Dhar who has been a great role model by encouraging me to further my career in science.

I would like to special mention my CCQC friend Andrew Launder who has been meticulous in proofing and commenting on my drafts and this thesis. Andrew and my office mate Xiao Wang are great friends always willing to help me at work and outside work. All of my CCQC friends have extended great support helping me to adjust with the American system.

I did not realize how fast the last four years in Athens passed and I became good friends with my colleagues, who will be missed.

Lastly, I would like to thank God to embrace me with wonderful family in India who has been there with me throughout this journey in life. Mom and Dad are the pillars of my strength. Even though they are miles apart I derive inspirations from their struggle in life and never give up when I come across difficult times in my personal and professional life. My siblings are my best friends and helped me through the stressful homesickness in the initial years in Athens. Thank you God for blessing me with great family and friends who make this life meaningful.

Table of Contents

1 Introduction **2**

1.1 Catalysis by Transition Metals 2

1.2 Computational Methodology 9

1.3 Density Functional Theory 10

1.4 Basis Sets 15

1.5 Condensed Phase Computations 19

1.6 Prospectus 21

2 Non-Innocent Additives in a Palladium(II)-Catalyzed C–H Bond Activation Reaction: Insights into Multi-Metallic Active Catalysts in an amination reaction **23**

2.1 Abstract 24

2.2 Introduction 25

2.3 Computational Details 27

2.4 Results and Discussion 30

3 Palladium–Silver Cooperativity in an Aryl Amination Reaction through C–H functionalization **35**

3.1 Abstract 36

3.2 Introduction 37

3.3 Computational Methods 39
3.4 Results and Discussion 40
3.5 C–H Activation 42
3.6 N–O Activation 48
3.7 Conversion from Intermediate **6** → **7** → **8** 52
3.8 Reductive Elimination 53
3.9 Conversion of Intermediate **9** → **10** 57
3.10 Comparison of Gibbs Free Energy Profiles with and without the Participation of Additives 60
3.11 Conclusions 61

4 New Insights on C–H Activation and Reductive Elimination in a dual C–H activation reaction **63**
4.1 Abstract 64
4.2 Introduction 65
4.3 Computational Methods 66
4.4 Results and Discussion 69
4.5 Conclusions 82

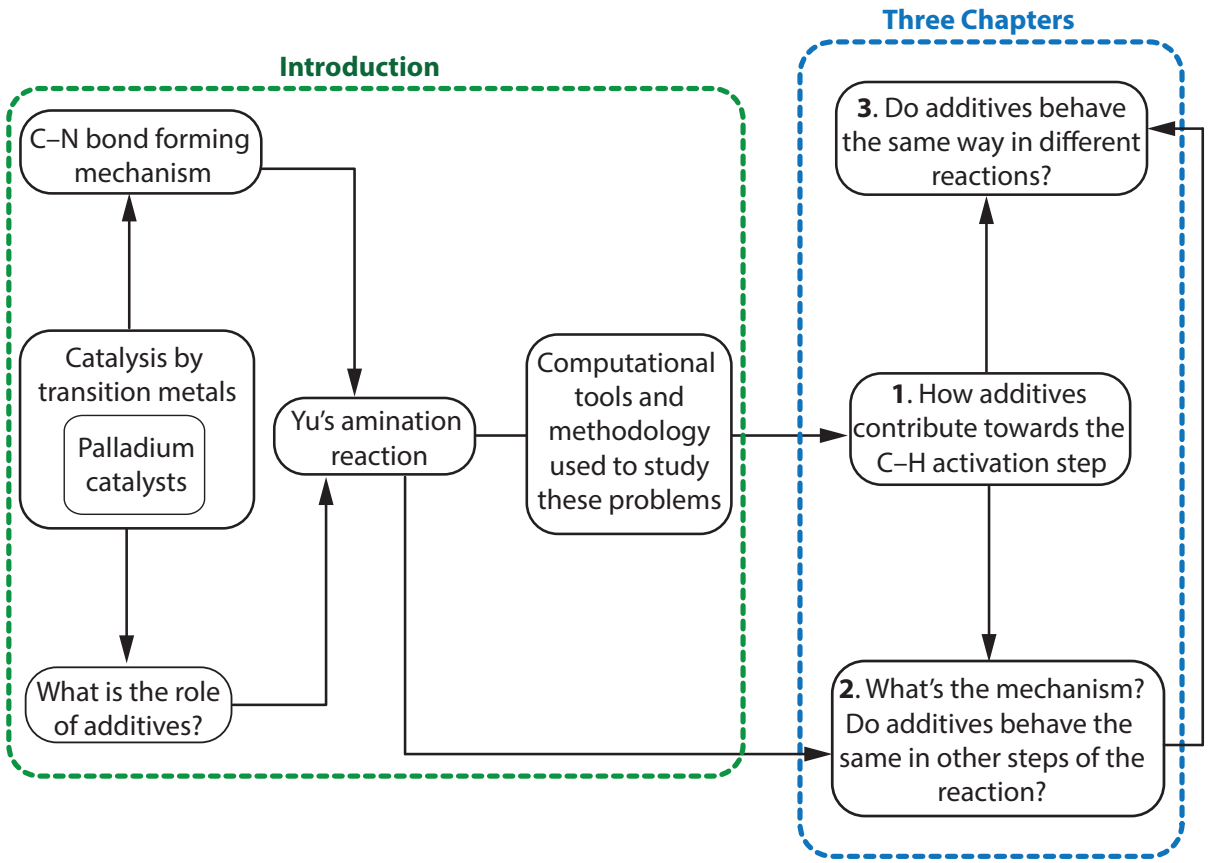
5 Conclusions **83**

Appendices **85**

A For Chapter 2 **86**

B For Chapter 3 **93**

C For Chapter 4 **103**
C.1 Atoms In Molecules (AIM) Analysis 103



Scheme 1: Outline of introduction and three chapter in the thesis.

Chapter 1

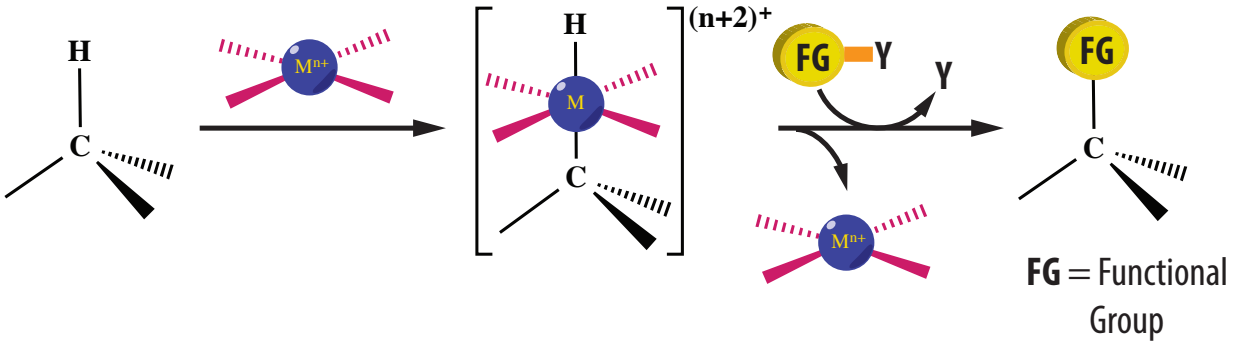
Introduction

1.1 Catalysis by Transition Metals

Transition metal (TM) catalysts have revolutionized the way C–C and C–heteroatom bonds are constructed in the synthesis of complex compounds. The advancement in the area of TM catalysis is evident from the large number of research articles and reviews published in the chemical literature.[1–6] The earliest indication of TM complexes as potential catalysts came in late sixties[7] and it intrigued chemists to explore further in this area.[8–10] Once considered intractable, the use of Pd, Rh, Co, Ni, Pt, etc., complexes has now become a standard protocol for target synthesis in medicine, electronics, and materials science, surpassing the traditional methods (like Grignard reagents) for making C–C and C–X (X = heteroatom) bonds.[11]

TM complexes under appropriate reaction conditions can activate an otherwise inert C–H bond (BDE = 80–110 kcal mol^{-1}), which is eventually functionalized (see Scheme 1.1) to obtain the desired product. Metals initially develop a weak interaction with the C–H bond, often termed the *agostic* interaction, and then get inserted between the C–H bond as shown in Scheme 1.1. This step is called the oxidative insertion step, as it results in the increment

of the oxidation state and the coordination number of the metal by two. The carbon–metal bond is far more reactive than the initial C–H bond. Thus, it is easily functionalized by the species available in the vicinity of the complex. In most TM–catalyzed reactions, the reductive elimination is another key step wherein the coupling of two ligands on the metal releases an organic product and the catalyst is regenerated in its original state to resume the next catalytic cycle.



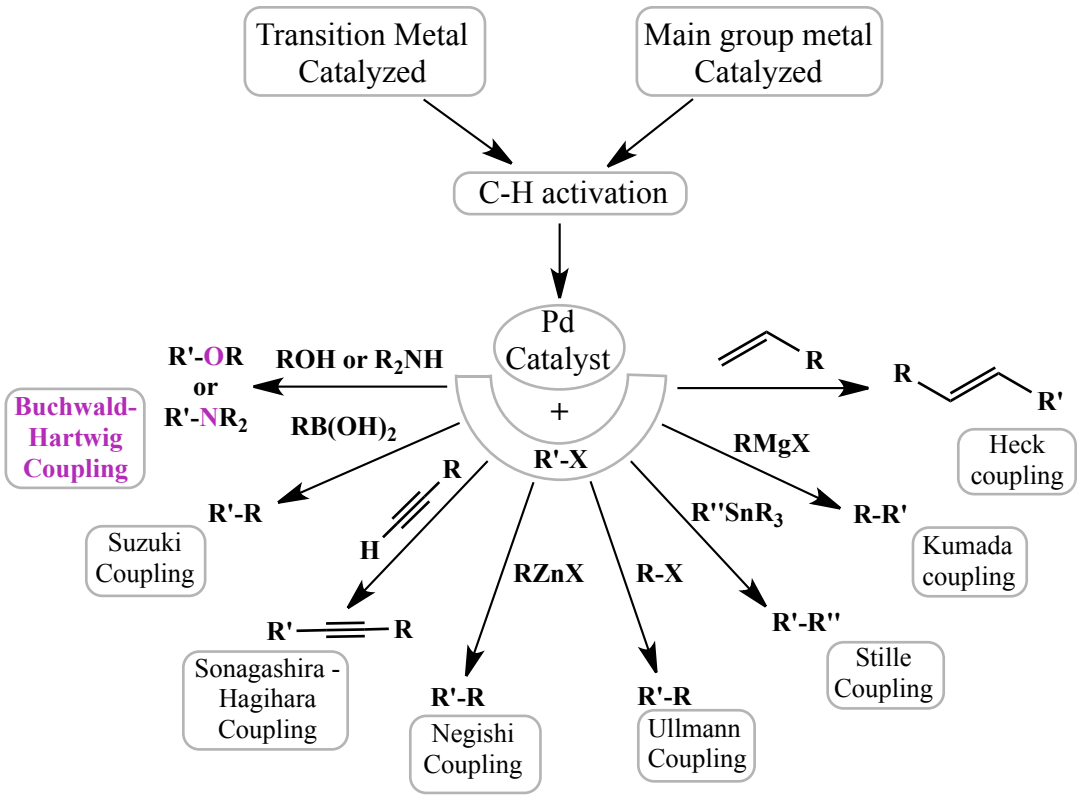
Scheme 1.1: Simple cartoon demonstrating the activation of an inert C–H bond in an alkane by a transition metal catalyst followed by the substitution of a functional group.

However, given the large number of equivalent C–H bonds in alkanes, selective C–H functionalization is a major challenge in these processes.[12] Most often, alkenes or alkyl halides ($R_3C{-}X$ where X is a halogen) are used as starting materials. The heteroatom (or the double bond) coordinates to the TM, directing it to activate the specific C–H bonds in its proximity. This idea of *directed C–H functionalization* is well-studied with a myriad of directing groups in the functionalization of arenes. More details on this topic will be discussed in the next chapter.

Development in the area of homogenous TM catalysis has made it possible to convert long-chain hydrocarbons, major byproducts from the petroleum industry, to useful compounds. Chemists are now able to install functional groups at positions in a molecule that were generally regarded as tedious before. Complex drug molecules have been synthesized in much

fewer steps, as opposed to conventional multistep syntheses. Despite these notable advances, there are still associated challenges that have engaged scientists worldwide in this field. The need for high catalyst loading, harsh reaction conditions, lower substrate scope, lower yields, and, most importantly, the use of external ligands are a few outstanding examples in TM catalysis. Some of these limitations can be improved through better understanding of the factors controlling the elementary steps in these catalytic reactions, and thus the detailed reaction mechanism. This is the main focus of the upcoming chapters and we disclose our interesting findings in palladium catalyzed reaction mechanisms.

1.1.1 Catalysis by Palladium



Scheme 1.2: Various palladium catalyzed cross-coupling reactions in industries and research laboratories.

Among the wide array of 3d, 4d, and 5d transition metal catalysts developed to date,[6,8] palladium catalysis is the most variant and has been studied extensively both experimentally and computationally.[13–20] Palladium complexes like $Pd(OAc)_2$, $Pd(PPh_3)_4$, and $PdBr_2$ are some of the popular catalyst precursors.[21,22] These precursors supersede other TM catalysts due to their ease of handling and compatibility with a broad range of substrates. In fact, the 2010 Nobel Prize in chemistry was awarded to Heck, Negishi, and Suzuki for their pioneering contribution to the area of palladium catalyzed cross-coupling reactions.

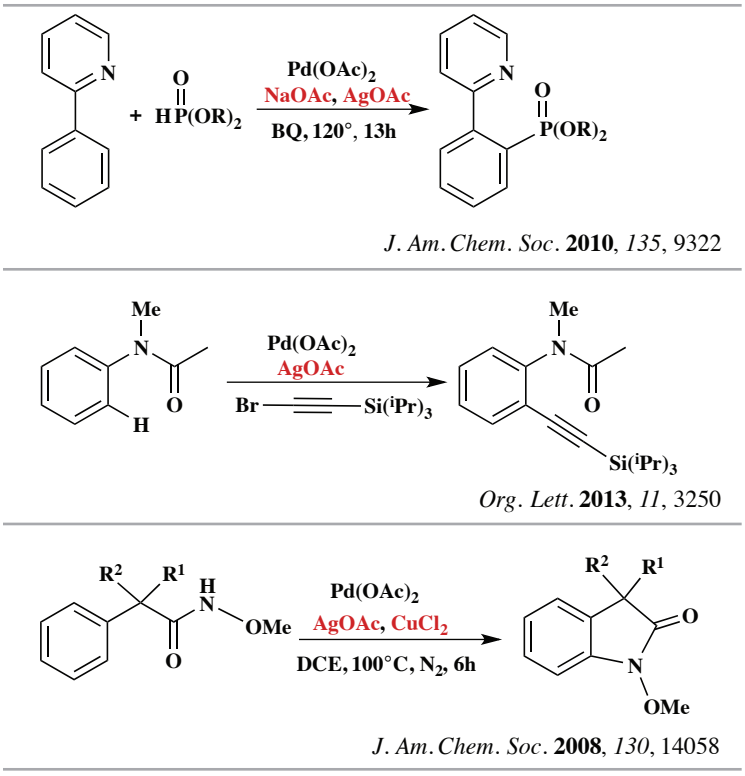
Scheme 1.2 lists some of the named cross-coupling reactions that constitute important sections of the industrial processes involving C–H activation by palladium catalysts. While most of the available cross-coupling reactions are good for the construction of C–C bonds, as shown in Scheme 1.2, the Buchwald-Hartwig coupling offers a way to make C–heteroatom bonds.[23–25] This insinuates that C–X (X = O, N, P, etc.) bonds are probably harder to synthesize as compared to the various C–C bonds. The ligands enabling TM catalyzed amination reactions have been developed recently in the last ten years. Consequently, there has been fewer mechanistic studies and we became interested in exploring the mechanism of the palladium catalyzed C–X bond-formation reaction.

1.1.2 Additives in Catalysis

Although rapid progress in TM catalyzed C–H activation reactions has enabled access to complex synthetic targets,[26–31] the reaction conditions appear to become increasingly more complex as noted from Scheme 1.3.[32–34] An analysis of the current practices in homogenous TM catalysis reveals the use of an increasing number of additives besides the main catalyst, in an effort to improve the yield and selectivity in such reactions.[35–38] Though a myriad of different additives, ranging from simple acids or bases to complex salts, are used in homogeneous transition-metal (TM) catalysis,[39–42] the molecular origin of their role has not been

adequately understood. It poses a few fundamental questions concerning TM catalysis such as:

1. How do additives influence the energetics and the yield of the reaction?
2. Are additives explicitly involved in the pertinent intermediates and transition states of the reaction?
3. How is the additive for a particular reaction decided?
4. Will the reaction happen without it? If not, why?
5. Can we design catalytic reactions where fewer additional reagents are required?



Scheme 1.3: A few examples on the use of additives in palladium catalysis.

It is anticipated that molecular insights on elementary steps in such catalytic reactions with additives will offer ways to overcome the current limitations and designing more efficient catalysts.

1.1.3 Transition metal catalyzed amination reactions

Nitrogen-containing compounds are ubiquitous in medicines, dyes, synthetic products and materials science(Figure 3.1).[43–52] The prevalence of nitrogen-containing compounds in diverse fields underscores the importance of C–N bond-forming reactions such as the Buchwald-Hartwig coupling, which involves coupling between aryl halides and amines in the presence of phosphine ligands using palladium(II) catalysts.[23–25] The initial step is the C–H bond functionalization, followed by C–N bond formation between the two reacting substrates. Buchwald-Hartwig amination (BHA) has facilitated synthesis of many pharamaceutically relevant compounds containing arylamines achieved earlier using multistep syntheses. It is a common synthetic protocol for making heterocycles containing C–N, C–O, and C–S bonds in both academic and industrial settings.

Yu's amination reaction

Along similar lines as the BHA, Yu *et. al.* recently reported a direct *ortho*-amination of *N*-Arylbenzamide using a variety of alkylamines, like morpholine and piperidine.[53] The substrate has an interesting auxiliary group (p-$C_6F_4CF_3$), which is expected to make it more acidic.[14] It is one of the few examples of TM catalyzed intermolecular C–H amination reaction using alkylamines in literature. Yu's synthetic strategy is appealing, as there are no external ligands involved (unlike in BHA). However, the mechanism of the reaction is expected to be complex due to the presence additives - cesium flouride and silver acetate, besides the primary catalyst palladium acetate. More discussion on this reaction will be presented in the introduction of the next two chapters.

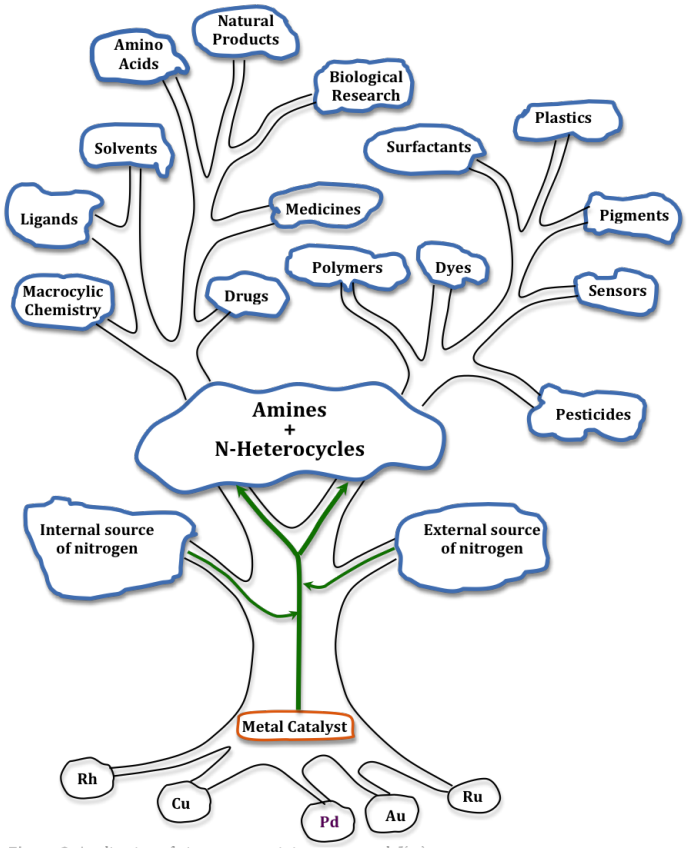
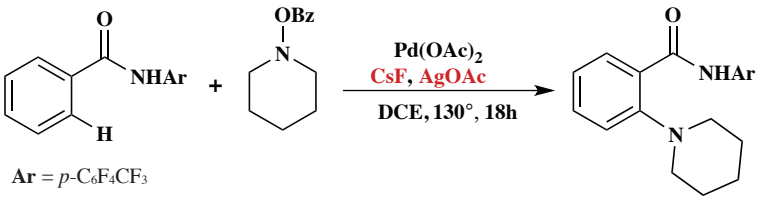


Figure 1.1: Application of nitrogen containing compounds.



Scheme 1.4: Palladium acetate catalyzed *ortho*-Amination of *N*-arylbenzamide.[53]

We became interested in Yu's reaction primarily because of two reasons. First, we have a long-standing interest towards understanding the mechanisms of TM-catalyzed carbon–heteroatom bond formation reactions.[54–57] Though there are a few experimental reports on the mechanism of C–N bond formation reactions,[25,58–61] transition-state models, as well as the energetics of such reactions, are seldom reported.[62] Secondly, the reaction employs two additives in the presence of which the yield is improved. Yu's reaction in Scheme 1.4 gives an opportunity to study palladium acetate catalyzed C–N bond-forming reaction mechanisms with the main focus on the role of additives. The mechanism of Yu's reaction would step up our understanding of the role of silver acetate, cesium flouride, and similar additives in other reactions at the molecular level. We have used computational tools to locate pertinent intermediates and transition states for this reaction. The underlying concepts and theories for the same are discussed in the next section.

1.2 Computational Methodology

Computational studies have enabled chemists to gain specific insights on chemical reactions that are otherwise difficult to obtain using only experiments.[63] Theory could help identify transient intermediates, as well as the transition states for the reactions involving several reagents. These reactive species are quite elusive and hard to trace using standard experimental techniques. Theory complements the experiments and thus, provide better picture of the TM–catalyzed reaction mechanisms.

Homogenous catalytic reaction mechanisms has been widely studied using computational techniques. Of the vast and wide array of theories developed so far, Density Functional Theory (DFT) is the foremost choice for studying large systems of the order of 10–1000 (or more) atoms. Moreover, the advent of fast supercomputers has made it even easier for studying such huge systems with a reasonable computational cost. Walter Kohn shared the

Nobel Prize with John Pople in 1998 for his pioneering work towards the development of DFT. Before we move on to the description of DFT, it is worthwhile to mention the most fundamental equation in quantum mechanics, the Schrödinger equation,

$$\hat{H}|\Psi\rangle = E|\Psi\rangle \tag{1.1}$$

where $\hat{H}$ is the time-independent Hamiltonian operator that operates on a wavefunction Ψ to give the energy E of the system.[a] A wavefunction is a mathematical construct that contains all knowable information about the system. Operators are used to derive values of physical observables from the wavefunction. For example, $\hat{H}$ is an energy operator and its expectation value over entire space gives the corresponding energy of the system,

$$E = \frac{\langle\Psi|\hat{H}|\Psi\rangle}{\langle\Psi|\Psi\rangle} \tag{1.2}$$

$$= \frac{\int \Psi^* \hat{H} \Psi d\tau}{\int \Psi^* \Psi} \tag{1.3}$$

where the integration is done over the whole space. For the reaction of our interest, we compute the energies of intermediates and the transition states to adequately map the potential energy surface. In this way, a plausible mechanism of the reaction can be proposed.

1.3 Density Functional Theory

The theoretical foundation of DFT is based on two theorems proposed by Hohenberg and Kohn.[64] The first theorem called the *existence theorem* (see Figure 1.2) states that there is one-to-one mapping between the total electron density $\rho(r)$ and the nuclear potential

[a] $|a\rangle$ is another way of representing state vector a while $\langle a|$ represents the complex conjugate a^* of vector a. This is called the bra-ket notation proposed by Dirac.

(ν_{ext}) of the system.[b] This implies that all the ground-state properties of a system can be determined exactly if its total electron density is known. Therefore, $\rho(r)$ is the fundamental variable in DFT, which depends on only three coordinates i.e., $[r(x, y, z)]$. The energy is thus a functional[c] $E[\rho(r)]$ of $\rho(r)$. This is different from the wavefunction-based methods where energy is a functional of $3N$ variables comprising of the (x, y, z) coordinates of the N particles in the system. The second theorem called uniqueness theorem states that $E[\rho(r)]$

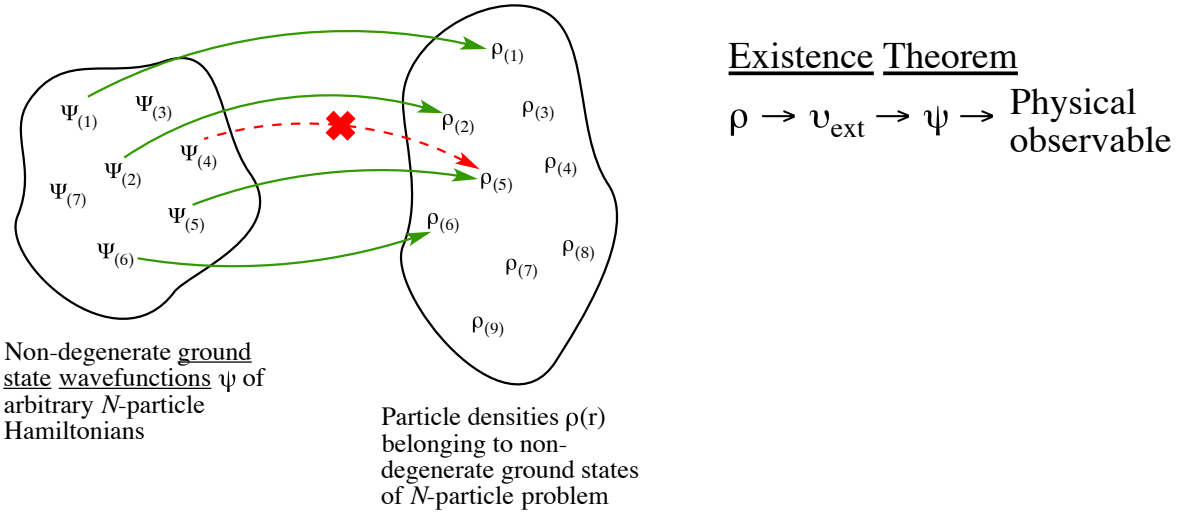


Figure 1.2: Diagrammatic illustration of the existence theorem proposed by Hohenberg and Kohn. Once the electron density $\rho(r)$ is known, we get the nuclear potential by the virtue of the existence theorem. From the nuclear potential ν_{ext}, the wavefunction is derived, from which the energy can be computed.

is a minimum if and only if the $\rho(r)$ is the true ground-state density. This is in line with the wave mechanical variational principle where one starts with a trial density and minimizes it variationally to reach the ground state energy. The trial electron density $\tilde{\rho}$ must satisfy the criteria: $\tilde{\rho} > 0$ and integration of electron density over all space should result in the total number of electrons, i.e., $\int_0^\infty \tilde{\rho} d^3r = N$. Thus, the Hohenberg-Kohn procedure is a

[b] ν_{ext} refers to the charges and the positions of the nuclei.

[c] Functionals is a rule that transforms a function into a number. For e.g., let $f(x) = x^2$. Then a functional may be $F[f(x)]$ defined as $F[f(x)] = \int_a^b x^2 dx$ which will give a numerical value.

constrained minimization of the energy, $\delta\{E[\rho] - \mu(\int_0^\infty \rho d^3r - N)\} = 0$, where μ is the Lagrange multiplier.

Though the existence theorem ensures a connection between the density and the wave-function, it does not offer a way of computing the ground-state density of a system in practice. Kohn and Sham, a year later devised a method to calculate the ground-state energy of the system that retained the structure of the initial formulation of DFT.[65–67] This is often referred to as Kohn-Sham (KS) DFT.

In KS-DFT, the real system of electron density ρ_r is replaced by a fictitious system of non-interacting electrons of the same electron density ($\rho_0 = \rho_r$). Because of the existence theorem, both the real and the fictitious system would correspond to the same Ψ. The total electronic energy is given as follows,

$$E[\rho_0] = T_{\mathrm{ni}}[\rho_0] + V_{\mathrm{ne}}[\rho_0] + V_{\mathrm{ee}}[\rho_0] + E_{\mathrm{XC}}[\rho_0] \tag{1.4}$$

where T_{ni} is the kinetic energy of non-interacting electrons, V_{ne} is the nucleus-electron interaction energy, V_{ee} is the electron-electron repulsion energy and E_{XC} is the exchange-correlation energy of the system. The E_{XC} term also includes other correction terms such as the classical self-interaction energy, the kinetic energy difference between the real and the fictitious system (ΔT) depending upon the type of the functional used for the computation. Finding the mathematical form of E_{XC} is the biggest challenge and an active area of research in the

development of DFT functionals. The first three terms in 1.4 are given by expressions:

$$T_{\mathrm{ni}}[\rho_0] = \sum_{i}^{n} \langle \Psi_i | -\frac{1}{2}\nabla^2 | \Psi_i \rangle, \quad i \text{ runs over all the electrons in the system.} \tag{1.5}$$

$$\begin{aligned} V_{\mathrm{ne}}[\rho_0] &= \int_{\nu} \rho_0(r) v_{\mathrm{ext}} dr \\ &= -\sum_{\text{nuclei A}} Z_A \int_{\nu} \frac{\rho_0(r_1)}{R_{1A}} dr_{1A} \quad (\nu \text{ is the integration over entire space.}) \end{aligned} \tag{1.6}$$

$$V_{\mathrm{ee}}[\rho_0] = \frac{1}{2} \int_{\nu_1} \int_{\nu_2} \frac{\rho_0(r_1)\rho_0(r_2)}{r_{12}} dr_1 dr_2 \tag{1.7}$$

While the V_{ne} and V_{ee} terms are functionals of ρ, the kinetic energy term T_{ni} depends on Ψ (equation 1.5). Therefore, it is not straightforward to obtain the kinetic energy portion of the energy. In KS-DFT, since the electrons are non-interacting, Ψ_i can be written as a single Slater determinant of occupied spin molecular orbitals.[68] For example, the Ψ_i a four electron non-interacting system is a single Slater determinant like shown below.

$$\Psi_i = \frac{1}{\sqrt{4!}} \begin{vmatrix} \Psi_1^{\mathrm{KS}}(1)\alpha(1) & \Psi_1^{\mathrm{KS}}(1)\beta(1) & \Psi_2^{\mathrm{KS}}(1)\alpha(1) & \Psi_2^{\mathrm{KS}}(1)\beta(1) \\ \Psi_1^{\mathrm{KS}}(2)\alpha(2) & \Psi_1^{\mathrm{KS}}(2)\beta(2) & \Psi_2^{\mathrm{KS}}(2)\alpha(2) & \Psi_2^{\mathrm{KS}}(2)\beta(2) \\ \Psi_1^{\mathrm{KS}}(3)\alpha(3) & \Psi_1^{\mathrm{KS}}(3)\beta(3) & \Psi_2^{\mathrm{KS}}(3)\alpha(3) & \Psi_2^{\mathrm{KS}}(3)\beta(3) \\ \Psi_1^{\mathrm{KS}}(4)\alpha(4) & \Psi_1^{\mathrm{KS}}(4)\beta(4) & \Psi_2^{\mathrm{KS}}(4)\alpha(4) & \Psi_2^{\mathrm{KS}}(4)\beta(4) \end{vmatrix} \tag{1.8}$$

where Ψ_x^{KS} is the Kohn-Sham spatial orbital of the reference system. The kinetic energy can thus be calculated as the expectation value of the kinetic energy operator over these Kohn-Sham orbitals.

The last and the most important term is the $E_{\mathrm{XC}}[\rho_0]$, whose exact functional form is not known. Therefore, even though the KS energy equation is exact, it is solved approximately because we do not know the functional form of E_{XC}. The functional dependence of E_{XC} on

the electron density is expressed as,

$$E_{\mathrm{XC}}[\rho(r)] = \int \rho(r)\varepsilon_{\mathrm{XC}}[\rho(r)]dr \tag{1.9}$$

where $\varepsilon_{\mathrm{XC}}$ is treated as sum of exchange and correlation contributions. Therefore,

$$E_{\mathrm{XC}} = E_{\mathrm{X}} + E_{\mathrm{C}}$$

The E_X and E_C refers to the exchange and correlation functionals respectively. The correlation energy is often much smaller than the exchange energy and thus more research has been done to find formulations for the E_{X} part. Different strategies have been employed to approximate E_{X} and E_{C} energies that can be easily computed. In this current investigation, we have used the B3LYP and M06 functionals to obtain the geometric and energetic data for the reaction studied.

B3LYP (Becke 3-parameter Lee-Yang-Parr) is one of the most popular DFT functionals among quantum chemists and gives remarkable performance over a wide range of systems for various chemical properties of systems. The formulation of the B3LYP functional was first suggested by Becke in 1993,[69]

$$E_{\mathrm{XC}}^{\mathrm{B3LYP}} = a_0 E_{\mathrm{X}}^{\mathrm{HF}} + (1-a_0)E_{\mathrm{X}}^{\mathrm{S}} + a_{\mathrm{X}}E_{\mathrm{X}}^{\mathrm{B88}} + (1-a_C)E_{\mathrm{C}}^{\mathrm{VWN}} + a_C E_{\mathrm{C}}^{\mathrm{LYP}} \tag{1.10}$$

where $E_{\mathrm{X}}^{\mathrm{A}}$ and $E_{\mathrm{C}}^{\mathrm{B}}$ are exchange and correlation energies of functional A and B. The coefficients a_0, a_{X}, and a_{C} have values 0.2, 0.72 and 0.81. Thus, the B3LYP functional combines portions of Becke (B88) exchange,[70] Lee-Yang-Parr (LYP) correlation[71] GGA functionals,[d] Slater (S) exchange,[72] Vosko-Wilk-Nusair (VWN) correlation[73] LDA functionals,[e] and the

[d] *Generalized Gradient Approximation* (GGA) functionals depend both on the density ρ and gradient of density at a given point. Therefore, $E_{XC}^{GGA} \approx \int \rho(\mathrm{r})\epsilon_{XC}(\rho, \nabla\rho)d\mathrm{r}$, where $\rho(\mathrm{r})$ refers to the electron density.

[e] *Local density approximation* (LDA) functionals are designed with the assumption that the exchange-correlation energy density at every position in space for the molecule is the same as it would be for the uniform electron gas as found at that position. The VWN functionals are LDA correlation functionals. Most GGA functionals are constructed by adding a gradient correction term to the LDA functionals.

HF exchange integral with 3 parameters a_0, a_X and a_C determined by fitting G1 set of experimental data.

The M06 hybrid functional belongs to the M06 suite of functionals (M06-L, M06-2X, M06-HF) developed by Truhlar's group.[74] It contains 27% of HF exchange and provides significant improvement over the various other DFT functionals. It has been constructed by fitting parameters from a large set of chemically important species and thus are particularly well-suited for studying kinetics and non-covalent interactions of main-group and organometallic systems.[75]

1.4 Basis Sets

The term *basis set* refers to the set of (non-orthogonal) mathematical functions used to create molecular orbitals (MOs). The obvious choice for MOs would be atomic orbitals (AOs) that are linearly combined to build MOs. The AOs thus form the 'minimal basis set' for molecular systems since there is only one basis function for each core or valence orbital of the atom. The AOs are often represented using Slater-type functions (or Slater-type Orbitals, STOs) that have mathematical forms similar to that of the orbitals of the hydrogen atom. These STOs comprise of a radial part and an angular part, as shown below,

$$\Phi_{STO}(r) : N r^L e^{-\zeta r}\, Y_{lm}(\theta, \phi) \tag{1.11}$$

where N is the normalization constant, L depends on the total angular momentum of the orbitals (e.g., $L = 0$, 1, 2, etc., for s, p, d-orbitals, etc. respectively), ζ is the orbital exponent (which depends on how tight or diffused the orbital is), and $Y_{lm}(\theta, \phi)$ are the spherical harmonics describing the angular part of the orbital. The STOs decay exponentially and vanish at large distances from the nucleus ($\Phi \to 0$ as $r \to \infty$). Even though they

provide the correct short- and long-range behavior of the orbitals, they lack radial nodes and hence cannot appropriately model orbitals like $2s$, $2p$ or $3s$ etc. It is also very tedious to compute electron repulsion integrals using Slater-type functions. In 1950, Boys suggested using Gaussian-type functions to mimic STOs. The product of two Gaussian functions is also a Gaussian function and therefore it is easier to compute electron repulsion integrals when GTOs are used.

$$\Phi_{GTO}(r) = N r^{L} e^{-\alpha r^2}\, Y_{lm}(\theta, \phi) \tag{1.12}$$

where N is the normalization constant, L depends on the total angular momentum of the orbitals, α is the orbital exponent and $Y_{lm}(\theta, \phi)$ are the usual spherical harmonics.

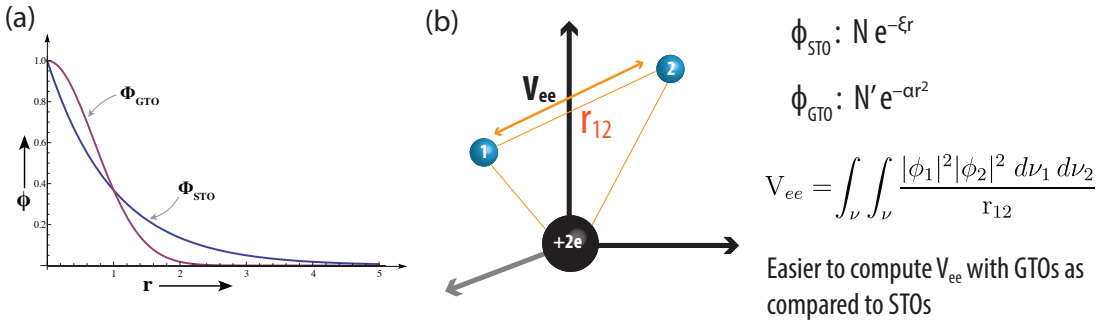


Figure 1.3: (a) Slater type orbitals (STOs) vs Gaussian type orbitals (GTOs) for a $1s$-orbital. (b) The electron-electron repulsion is obtained by evaluating the integral V_{ee} over the entire volume around electron 1 (ν_1) and 2 (ν_2).

Several primitive gaussians are combined to get basis functions closer to that of STOs. Such basis functions are called STO-nG, where n denotes the number of primitive gaussians in the basis set. For example, the STO-3G basis set for a hydrogen atom has the form as shown in Figure 1.4.

(a) $\Psi_{1s} = \underbrace{0.50907N_1e^{-0.1233r^2} + 0.47449N_2e^{-0.453757r^2} + 0.13424N_3e^{-2.01330r^2}}$

CGTO basis function made of three primitive Gaussians (single contraction)

(b) DZ quality basis set (Two contractions)

$$\Psi_{1s} = 145.88(0.6234\ N_1e^{-0.1233r^2} + 0.2379\ N_2e^{-0.453757r^2}) + 2.30(0.54394N_3e^{-2.01330r^2})$$

Figure 1.4: (a) STO-3G basis function for the $1s$ orbital of hydrogen atom, where three primitive gaussian functions are combined to give a single contracted GTO. (b) Double-zeta (DZ) basis set with two contractions for the $1s$ orbital of hydrogen atom.

All of the basis sets (STOs, GTOs, and CGTOs[f]) are minimal basis sets of single zeta quality[g] whose coefficients and exponents are fixed for all AOs in the atom. However, the valence orbitals in a molecule undergo noticeable changes as compared to the core orbitals during the course of a reaction. Therefore, split-valence basis sets are designed such that one basis function is used to model the core AOs while larger basis functions are used to represent valence AOs. These basis sets give more flexibility and provide better results compared to the SZ basis sets.

Basis sets are further improved by adding polarization and diffuse functions. Functions of higher angular momentum (L) are included for better description of the polarization of atomic orbitals in a molecule. Diffuse functions with smaller ζ values are essential for accurately describing anions, molecules with very electronegative atoms such as O or F, etc., where electrons are spatially more diffused and not tightly bound to the nucleus.

[f]CGTO stands for contracted Gaussian type orbital where several gaussian functions are linearly combined to form one basis function.

[g]Single zeta implies only one basis function for an atomic orbital. A double-zeta (DZ) basis set has two basis functions for every atomic orbital of the system. Likewise, TZ (triple-zeta), QZ (quadruple-zeta), etc., basis sets have been developed.

1.4.1 Pople Basis Sets

We have used split-valence basis sets (6-31+G**) belonging to the family of Pople-basis sets to model smaller atoms like H, C, N, O, F, S, and Cl in this work.[76,77] These were first developed by Nobel laureate John Pople and have been implemented in most electronic structure theory programs, including Gaussian.

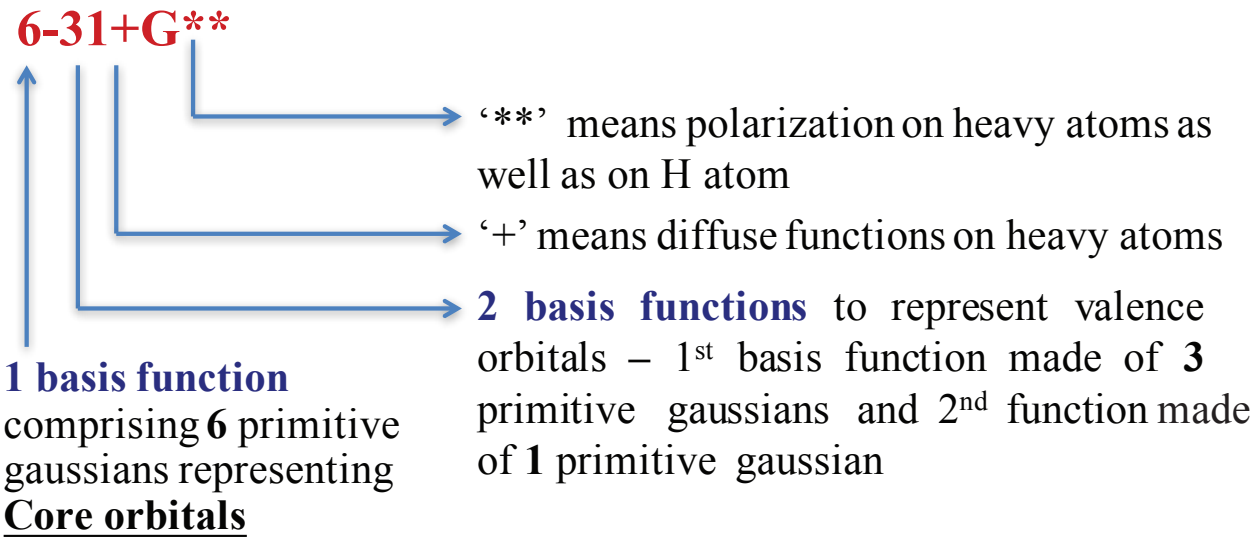


Figure 1.5: Description of the notation for the split-valence double zeta basis set, 6-31+G**.

1.4.2 Effective Core Potentials (ECPs)

The reactions in the present investigation involve palladium, silver, cesium, iodine, and bromine. Due to the large atomic number of these atoms, it becomes difficult to explicitly treat all the electrons of each atom. For example, Cs ($1s^2 2s^2 2p^6 3s^2 3p^6 3d^{10} 4s^2 4p^6 4d^{10} 5s^2 5p^6 6s^1$) has many core electrons which should be described properly to get energy but would require several basis functions. ECPs are thus developed where core electrons are modeled by a suitable potential function, and only the valence electrons are treated explicitly. The key

idea is to treat the core electrons as effective averaged potentials rather than actual particles. Thus, ECPs tremendously reduce the computational effort and may be constructed to give better results for relativistic effects which become prominent as we go down in periodic table. We have used the Los Alamos pseudopotential (LANL2DZ) basis set consisting of an effective core potential (ECP) for 28 core electrons and a double-ζ quality valence basis set for remaining valence electrons in the Pd, Ag, I, Cs, and Br atom.

1.5 Condensed Phase Computations

Most homogenous catalytic reactions are conducted in condensed phase. The charges on the solute interact with the solvent in a solution. As a result, the dipole moment of the solute changes depending on its polarizability and the strength of the reaction field induced by the solvent molecules during the solvation process. Thus, solvents can influence the overall outcome of the catalytic reaction. It is imperative to incorporate solvent effects in transition state modeling studies.[78] Many solvation models have been developed to reliably include a term accounting for solute-solvent interactions in the solute Hamiltonian.

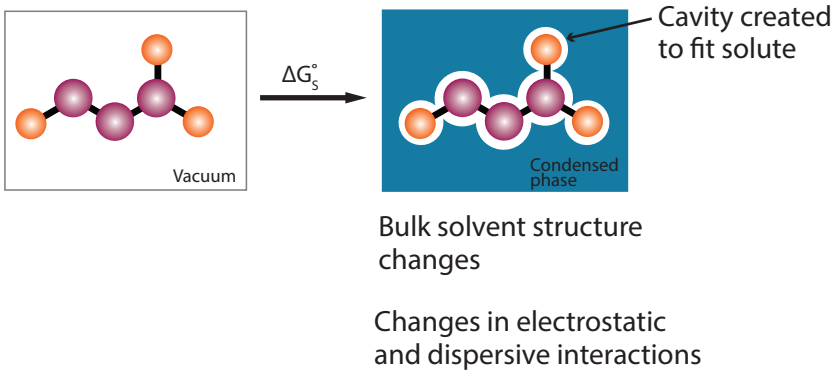


Figure 1.6: The free energy of transfer of solute from vacuum to condensed media is the free energy of solvation (ΔG_S°).

The fundamental quantity describing the interaction of the solute with the surrounding solvent is the free energy of solvation ($\Delta G_{\mathrm{S}}^{\circ}$). It is also referred to as the free energy of transfer since it is essentially the phenomenon of a molecule leaving the gas phase and entering a condensed phase.[79] The overall solvation process is accompanied by the creation of a cavity in the bulk solvent to accommodate the solute, along with changes in electrostatic and dispersive interactions. The protocol for defining a cavity to fit the solute inside the continuum is vital in the process of developing solvation models. Poorly shaped cavities fail to adequately include the solvent effects in the free energy of solvation.

We have used a polarized continuum solvation model[h] based on the *Poisson–Boltzmann equation* (vide infra), abbreviated as PCM for the majority of our computations in this mechanistic study.[80–100] Continuum solvation models treat solvent as continuous dielectric media.[101] Thus, the charges of the solvent are replaced by a continuous electric field that represents a statistical average over all solvent degrees of freedom at equilibrium. Some of the other underlying assumptions are:

1. The solvent is isotropic and at equilibrium at the given temperature, T.

2. Solute-solvent interactions are of electrostatic origin.

3. Single solute molecule is immersed in an infinite solvent reservoir.

The equations in the condensed-phase computations are solved in usual fashion as the Hartree-Fock equations, with an extra term for the solute polarization energy added.

$$\left\{\hat{H} + \hat{G}_{\mathrm{P}}\right\} \Psi = E\Psi \tag{1.13}$$

The Fock operator is modified accordingly,

$$\left\{F_i + G_{\mathrm{P}i}\right\} \psi = e_i \psi \tag{1.14}$$

[h]The PCM model is used for the amination work (chapter 2 and 3) and the Solvation model based on Density (SMD) by Truhlar and Cramer has been used for chemical systems in chapter 4. In the PCM computations, cavities have been defined by taking the union of spheres about the solute atoms.

where F_i is the usual gas-phase Fock operator for i^{th} MO and convergence is achieved when both the energy, as well as the polarization, of the solute becomes stationary with respect to the iterations in the coefficients of the molecular orbitals. Thus, it is also referred to as the *self-consistent reaction field* or (*SCRF*) procedure.[102] The polarization energy G_{P} is obtained using the simplified linear form of *Poisson–Boltzmann equation* (PBE),

$$\nabla\epsilon(\mathbf{r}) \cdot \nabla V(\mathbf{r}) - \epsilon(\mathbf{r})\lambda(\mathbf{r})\kappa^2 V(\mathbf{r}) = -4\pi\rho(\mathbf{r}) \tag{1.15}$$

where $\epsilon(\mathbf{r})$ is the dielectric constant of system (varies with $\mathbf{r}$, different for solute and solvent)
$V(\mathbf{r})$ is the electrostatic potential.[i]
$\lambda(\mathbf{r})$ is the switching function. It is zero in regions not available to the electrolyte (solvent) and one otherwise.
κ is the *Debye-Hückel parameter* and ρ is the solute charge density.

Even though continuum solvation models provide a reasonable starting point for condensed-phase computations, they fail to embody specific solute-solvent interactions like hydrogen bonding at the surface. Often a cluster-continuum model is used instead where the cluster of solute with explicit solvent molecules in the first solvation shell[j] is embedded inside the continuum of the solvent. We have used this approach to model our additives - silver salts and cesium flouride - inside the solvent.

1.6 Prospectus

Chapter 2 focuses on determining the role of silver additives in the C–H activation step of the Yu's amination reaction. The active catalyst proposed in Chapter 2 is extended to other

[i]The polarization energy G_{P} is the energy required to polarize the solute under the influence of solvent's reaction field. It is related to $V(\mathbf{r})$ by the equation $G_{\text{P}} = -\frac{1}{2}\int \rho(\mathbf{r})V(\mathbf{r})d\mathbf{r}$

[j]Solvent molecules in the second, third solvation shells, etc., can also be included. However, these add to the computational cost.

steps of the amination reaction and the findings are described in Chapter 3. We have then, in Chapter 4, looked at six different reactions to see if our hypothesis can be generalized over other reactions involving silver salts as additives and palladium acetate as the primary catalyst. Chapter 5 summarizes the key conclusions from these three chapters.

Chapter 2

Non-Innocent Additives in a Palladium(II)-Catalyzed C–H Bond Activation Reaction: Insights into Multi-Metallic Active Catalysts in an amination reaction[a]

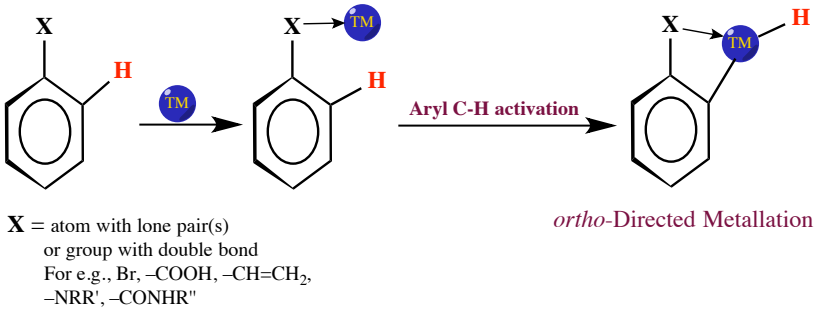
[a]This chapter is adapted from Anand, M.; Sunoj, R. B.; Schaefer III, H. F. *J. Am. Chem. Soc.* **2014**, *136*, 5535–5538.

2.1 Abstract

The role of a widely employed additive (AgOAc) in a palladium acetate-catalyzed ortho-C–H bond activation reaction has been examined using the M06 density functional theory. A new heterobimetallic [Pd(μ−OAc)$_3$−Ag] is identified as the most likely active species. This finding could have far-reaching implications with respect to the notion of the active species in palladium catalysis in the presence of other metal salt additives.

2.2 Introduction

Over the years, a broad range of methodologies has become available for making functionalized aromatic compounds using transition metal catalyzed C–H bond activation.[10,63,103–107] The approach, in general, involves the use of a suitable transition metal catalyst on substrates bearing a directing group.[12,108–110] The directing group selectively delivers the metal to the *ortho*-position of the phenyl ring and thus making the *ortho*-C–H bond more reactive (Scheme 2.1).[111] This has emerged as a promising technique for making C–C and C–heteroatom bonds in homogenous catalysis.

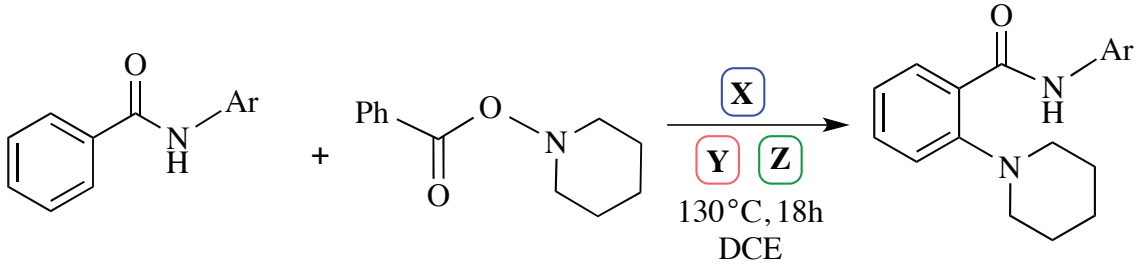


Scheme 2.1: Simple illustration of directed C–H functionalization of arenes using transition-metal (TM) catalysts.

One of the quintessential examples in this genre is the palladium acetate catalyzed *ortho*-functionalization of aryl amides as well as 2-phenyl pyridines.[112–115] A quick perusal of literature spanning over a decade reveals that several such methods resort to the use of additives to improve the efficiency of the catalytic processes.[108,116–120] Typical additives are metal salts, such as a terminal oxidant, that help regenerate the transition metal catalyst back to its native oxidation state toward the later part of the catalytic cycle.[112,114,115,121–124]

It is important to recognize that a large number of $C_{aryl}-C$ and $C_{aryl}-$heteroatom bond formation reactions for aryl functionalizations have been achieved using palladium acetate as the catalyst.[10,12,18,63,103–108,125–128] While the examples for $C_{aryl}-C$ coupling reactions are

available in abundance, reactions for $C_{aryl}-O$ and $C_{aryl}-N$ coupling remained relatively less reported until recently.[9,10,103,121,125,129–131] One of the most recent breakthroughs in direct aryl amination came from the Yu group (Scheme 2.2).[53] The resulting product aryl amines are known to be useful in many biological processes.[132]



X = $Pd(OAc)_2$; **Y** = CsF ; **Z** = AgOAc Ar = *p*-$(CF_3)C_6F_4$

X	Y	Z	Yield (%)
✓	✗	✗	~40
✓	✓	✗	~54-70
✓	✓	✓	~96

Scheme 2.2: Palladium acetate catalyzed *ortho*-Amination of *N*-arylbenzamide.[53]

The use of multiple additives under homogeneous reaction conditions is obviously expected to increase the mechanistic complexities. In particular, the nature of the catalytic species in the presence of such additives could be different from the conventionally proposed monomeric palladium acetate. Clearly, this hypothesis warrants careful scrutiny. The reaction relies on C–H functionalization where the amide acts as the directing group for *ortho*-C–H bond activation. In this chapter, we intend to capture the first molecular insights on the potential involvement of some novel multi-metallic catalytic species in the vital C–H bond activation step.

2.3 Computational Details

All stationary points such as reactants, intermediates, and transition states were fully optimized at the B3LYP/6-31G*, LANL2DZ (Pd, Cs, Ag) levels of theory[69,133–137] using Gaussian09 suite of quantum chemical programs.[138] To incorporate solvent effects these structures were re-optimized at the B3LYP/6-31G**, LANL2DZ (Pd, Cs, Ag) level of theory in the dielectric continuum of 1,2-dichloroethane using the Polarized Continuum Model (PCM).[80–100] In the recent literature, it has been demonstrated that improved treatment of non-covalent interactions in transition metal systems could be achieved by using the M06 functional.[75,139,140] Therefore, single-point energies were computed at the PCM_{DCE}/M06/6-31+G**, LANL2DZ (Pd, Cs, Ag)//PCM_{DCE}/B3LYP/6-31G**, LANL2DZ (Pd, Cs, Ag) level of theory. Such methods have been widely used in the study of mechanisms of transition metal catalyzed reactions.[141–144] Hence, the condensed phase free energies, as reported in the main text, are obtained at the M06 level of theory on the condensed phase B3LYP optimized geometries and thermal and free energy corrections at the PCM_{DCE}/B3LYP/6-31G**, LANL2DZ (Pd, Cs, Ag) level of theory.

The optimized geometries were characterized as stationary points on the potential energy surface at respective levels of theories by evaluating the vibrational frequencies. The transition states were characterized by one and only one imaginary frequency. These frequencies were identified as representing the correct reaction coordinate, first by visual inspection of the imaginary frequency. The intrinsic reaction coordinate (IRC) calculations were subsequently carried out for selected transition states (that fall within a window of 10 kcal/mol with respect to energetically the most favored transition state in each model that are presented) to further authenticate the transition states.[145,146]

Computation of Relative Energies

The energies of the transition states are computed with respect to the infinitely separated reactants. Depending on the nature of the intermediates or transition states, the reactants include palladium acetate, silver acetate, cesium fluoride and the substrate (*N*–arylbenzamide). The primary catalyst, palladium acetate, is known to exist as trimeric $Pd_3(OAc)_6$ species in several solvents, including that in 1,2-dichloroethane employed in the title reaction.[147–152] This prompted us to consider a more realistic trimeric palladium acetate as the reference point instead of a commonly used monomeric palladium acetate, which is of higher energy. When a monomeric species is considered as involved in any of the stationary points in the present study, the energy is deduced from the energy of the trimeric $Pd_3(OAc)_6$ as one third energy of the trimer.

Another key aspect relating to this reaction is that the reaction is conducted in 1,2-dichloroethane (DCE), which has a measured dielectric constant ϵ_r of 10.36. This solvent is known to behave similar to dichloromethane ($\epsilon_r = 8.93$), both of which are weakly coordinating solvent.[153–160] Hence, it is highly likely that the DCE molecules will coordinate to silver acetate to yield species of the type $[AgOAc \cdot (DCE)_n]$.[161] A monomeric silver acetate with two coordinating DCE molecules, i.e., $AgOAc \cdot (DCE)_2$, is taken as the reference point. The mass balance in relative energy computations has been done by adding the energy of a $(DCE)_2$ cluster, wherever required.

Cesium fluoride is the third additive used in this reaction and subjected to a similar treatment as that for silver acetate. For a better representation of cesium fluoride in DCE, a good understanding of the behavior of ionic salts in polar (or moderately polar) aprotic solvents is important. In terms of its dielectric constant (ϵ_r =10.36), DCE should be regarded as a borderline solvent. Hence, cesium fluoride could exist as a contact-ion pair or as solvent-shared/separated ion pair in DCE.

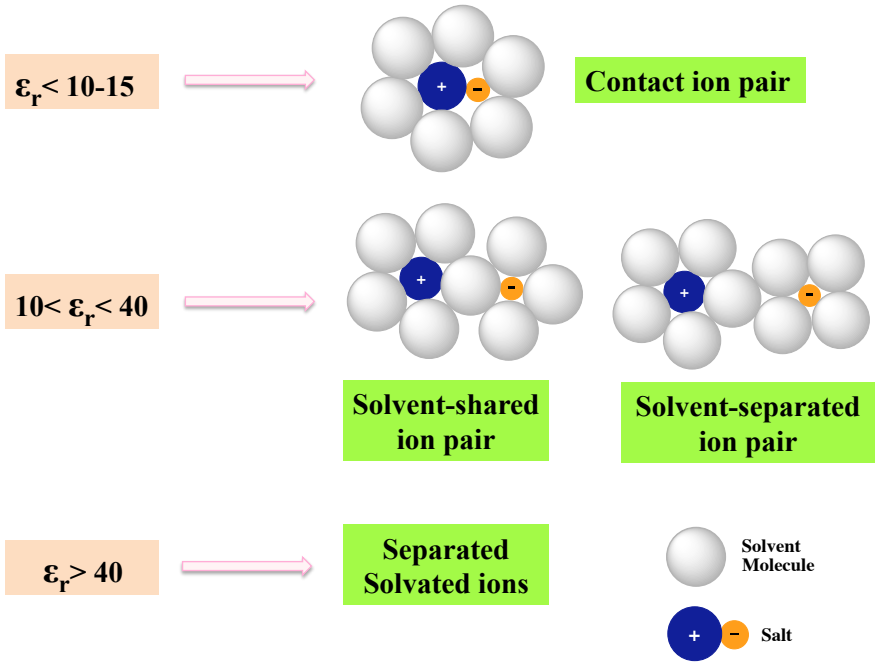


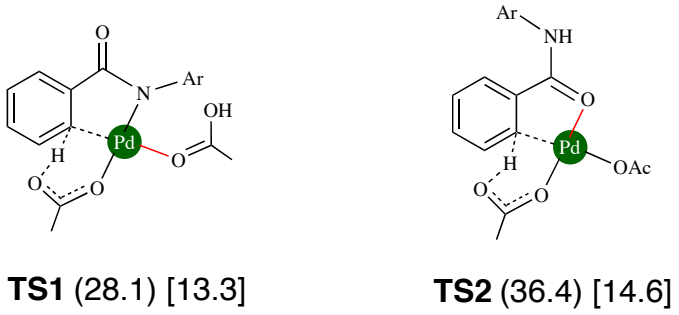
Figure 2.1: Illustration of how ionic salts behave in solvents of different dielectric strength.

Complexes of the type $CsF \cdot (DCE)_n$ were first optimized in the dielectric continuum wherein n was varied from 1 to 6. Among these solvated species, $CsF \cdot (DCE)_6$ appeared to be energetically the best possible representation with three molecules clustering around the fluorine, two around cesium and one coordinated to both cesium and fluorine.[162] Any additional solvent molecule is likely to aggregate as part of the secondary coordination sphere around the molecule. For stoichiometric balance, the energy of a cluster of six DCE molecules is included in the transition state energy calculations whenever CsF is involved.

In summary, the Gibbs free energies of transition states are computed with respect to reference points - $Pd_3(OAc)_6$, $AgOAc \cdot (DCE)_2$, $CsF \cdot (DCE)_6$, and the substrate. Our discussion is presented in terms of the Gibbs free energies computed with the M06 density functional theory in 1,2-dichloroethane (DCE) as the continuum solvent.

2.4 Results and Discussion

The reaction shown in Scheme 2.2 can be envisaged to begin with the coordination of the catalyst to the amido nitrogen.[163] The role of different additives has been probed by explicitly including them in the C–H activation transition state. Among the different possibilities considered, energetically the most preferred only are discussed whereas other alternatives are used for cogent comparisons. To begin, a conventional pathway wherein a molecule of palladium acetate functions as the sole catalyst is examined. Similar to the other known systems, the N–H activation by palladium acetate is considered as the first step after the combination of catalyst with the substrate.[164] The resulting intermediate is poised to undergo *ortho* C–H bond activation owing to the proximity between the metal and the aryl C–H bond. The ensuing acetate assisted C–H activation via **TS1** or **TS2**, as shown in Figure 2.2, will provide a palladacycle intermediate.[127,128,165]



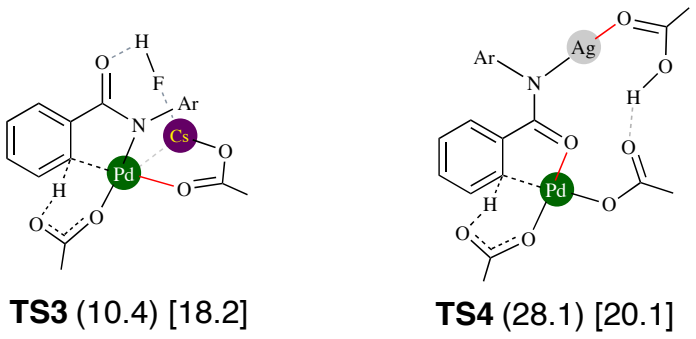
TS1 (28.1) [13.3] **TS2** (36.4) [14.6]

Figure 2.2: C–H activation transition states with a monomeric palladium acetate catalyst. The values in parentheses are the relative free energies (in kcal/mol) with respect to the separated reactants, and those in square brackets are with respect to the preceding intermediate.

Although the relative Gibbs free energy of this transition state (28 kcal/mol) appears reasonable, the participation of additives is unclear. Hence, the transition state models are refined by explicit inclusion of silver acetate and cesium fluoride. To enable comparison of the computed energetics uniform across different possible scenarios arising as a result of

inclusion of silver and cesium salts in the transition state models, the relative energies with respect to the infinitely separated reactants are provided.[166] The elementary step barriers are as well included such that the activation barriers of a given type of transition states (with identical stoichiometry) can be compared.

The inclusion of additives in the transition state is found to help in the deprotonation of the amido group. For instance, the fluoride derived from CsF can lead to the formation of HF, while the acetate of AgOAc can give rise to AcOH. Facilitating the deprotonation of the amido nitrogen may be regarded as the first likely role of CsF.[b] The resulting amidate can now interact with the cesium or the silver ion. The C–H activation in the metalamidate species is found to be energetically more favored when CsF is involved (**TS3**) as compared to that with AgOAc (**TS4**) (Figure 2.3).[c] The improved favorability of **TS3** (10.4 kcal/mol) as compared to **TS1** (28.1 kcal/mol) is in line with the experimental observation of higher efficiency of the reaction when $Pd(OAc)_2$ is used in conjunction with CsF (Scheme 2.2).



TS3 (10.4) [18.2] **TS4** (28.1) [20.1]

Figure 2.3: C–H activation transition states for cesium (**TS3**) and silver (**TS4**) amidates. The values in parentheses are the relative free energies (in kcal/mol) with respect to the separated reactants, and those in square brackets are with respect to the preceding intermediate.

[b] In TS3, we also observed a weak palladium–cesium (Pd–Cs distance is 3.81Å) interaction, and its energy is lower than the similar TS where the cesium ion is far from palladium (Figure A.2(i) in Appendix A).

[c] Interestingly, Yu and co-workers have reported an X-ray structure of a similar cesium ion-bound intermediate under similar reaction conditions. However, silver acetate was not used in this analogous reaction (See ref. 167). See Figure A.2 in the Appendix A for analogous transition states with different modes of coordination between palladium and the substrate.

A comparison worth considering at this juncture is that the energy of the transition state with silver bound to the amidate **TS4** is about 18 kcal/mol higher than for the corresponding cesium-bound **TS3** (Figure 2.3). More interestingly, however, both of these modes of C–H activation are lower in energy than the conventional transition states (**TS1** and **TS2**) with a monomeric $Pd(OAc)_2$. It is important to note that there could be alternative sites for coordination of the AgOAc to the substrate. We have therefore explored different configurations wherein the catalyst and additives are bound to the substrate while maintaining close proximity between them. Consideration of such geometric propensities can help probe the effect of multimetallic interactions, or even synergism, in the key C– H activation step.

To our surprise, a number of interesting transition-state configurations exhibiting multimetallic interactions were identified. To our knowledge, C–H activation transition states exhibiting such hetero-bimetallic interactions are seldom reported.[168] More importantly, **TS5** and **TS6** in this family are energetically lower than all the other transition-state models (Figure 3).[169]

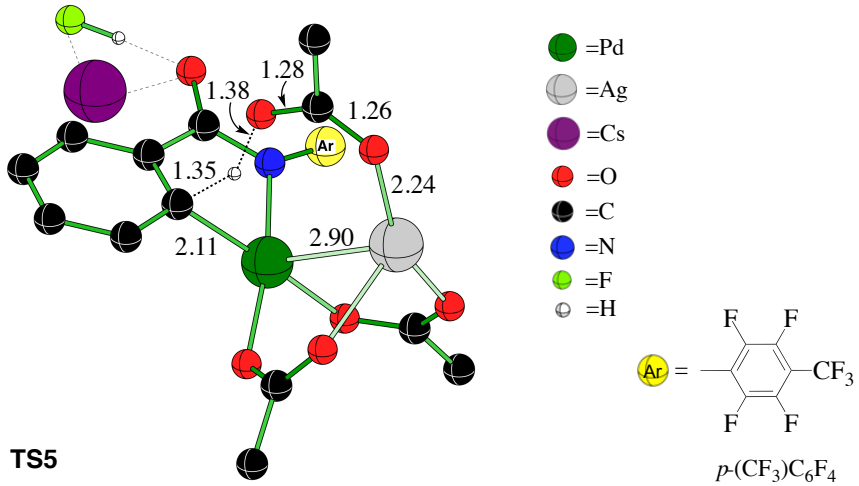


Figure 2.4: Optimized geometry of the C–H activation transition state **TS5** exhibiting Pd–Ag interaction.

For instance, **TS5**, with a Pd–Ag heterobimetallic interaction, is 30 kcal/mol lower in free energy than **TS1** (with the conventional monomeric $Pd(OAc)_2$) and 13 kcal/mol lower than **TS3** (inclusive of CsF). The geometries of these transition states indicated that the cesium ion interacts with other atoms/groups (oxygen of –CONHAr and –OAc, HF, $C_6F_5CF_3$ groups shown as Ar for improved clarity) than what is shown in the figures.[170]

The geometry of **TS5** exhibits some interesting features (Figure 2.4). First, the short contact between Pd and Ag (2.9 Å) indicates a favorable electronic communication.[171] Availability of crystal structures of d^8-d^{10} hetero-bimetallic complexes with bidentate acetate bridges provides additional credence to our hypothesis.[172,173] Besides the direct Pd(II)–Ag(I) interaction, the acetate bridges can augment the intermetallic interaction.[174–180] While the heterometallic d^8-d^{10} interaction in the Pd(II)–Ag(I) system can be viewed as similar to that in Pd(II)–Pd(0), the heterogeneity can offer different cooperative effects in catalysis.[181,182]

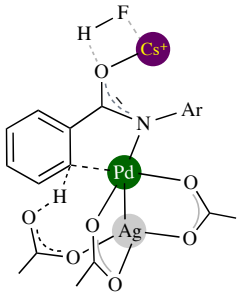
It is also interesting to note that although the C–H activation is facilitated by palladium(II), the proton abstraction is performed by the acetate bound to the silver atom. Interchanging the positions of these two metals, such that silver(I) is closer to the C–H bond while the acetate bound to the palladium abstracts the proton, results in a higher energy transition state.[d] This implies that the $Pd(OAc)_2$ acts as the primary catalyst and hence the reaction is not expected to take place in its absence.

In view of available bimetallic palladium complexes, we have also examined the efficiency of a homo-dimeric $Pd_2(OAc)_4$ as an active species for the C–H activation (**TS6**) (Figure 2.5).[e] However, the computed energies are found to be higher (∼10 kcal/mol) than those for the hetero-bimetallic [$Pd(\mu-OAc)_3Ag$] analogue (**TS5**). This suggests the existence of cooperativity between the catalyst $Pd(OAc)_2$ and the additive (AgOAc). In addition, transition

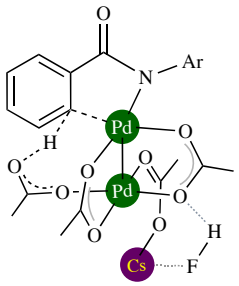
[d] See Figure A.5 in the Appendix A.

[e] See Figure A.6 in the Appendix A for other higher energy C–H activation transition states with homodimeric $Pd_2(OAc)_4$ as the active catalyst.

states consisting of more than one molecule of AgOAc and CsF are examined. These possibilities, however, are of higher free energies as compared to what has herein been presented.[f]



TS5 (-2.6) [9.1]



TS6 (7.1) [11.8]

Figure 2.5: C–H activation transition states exhibiting metal-metal interactions. The values in parentheses are the relative free energies (in kcal/mol) with respect to the separated reactants, and those in square brackets are with respect to the preceding intermediate.

In conclusion, explicit consideration of silver acetate and cesium fluoride in the key C–H activation transition states led to the identification of a new hetero-bimetallic $[Pd(\mu{-}OAc)_3{-}Ag]$ species as the most likely active catalyst in a palladium acetate catalyzed ortho-amination reaction. The results reported herein are expected to have broad mechanistic implications for other transition metal-catalyzed reactions employing metal salts as additives.

[f]See Figure A.7 in the Appendix A. Attempts to locate C–H activation TSs with two CsF failed to converge even after repeated attempts, perhaps indicating that the optimum number of CsF could just be one.

Chapter 3

Palladium–Silver Cooperativity in an Aryl Amination Reaction through C–H functionalization[a]

[a]This chapter is adapted from Anand, M.; Sunoj, R. B.; Schaefer III, H. F. *ACS Catal.* **2016**, *6*, 696–708.

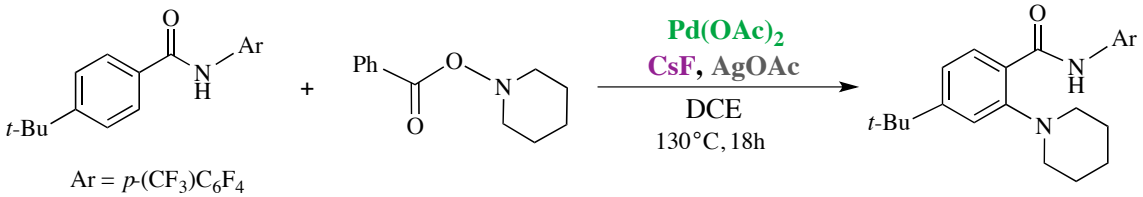
3.1 Abstract

The mechanism of palladium-acetate-catalyzed ortho-amination of *N*-arylbenzamides by using *O*-benzoyl hydroxylpiperidine [PhCOON(C_5H_{10})] has been examined by using DFT(M06, B3LYP) computational methods. Particular emphasis is placed on the role of additives such as cesium fluoride and silver acetate. The lowest-energy pathway has been identified by carefully examining 15 or more configurationally different possibilities in each important step of the reaction. The key mechanistic events include (i) the aryl C–H activation of the substrate through a cyclometalation deprotonation; (ii) N–O activation of the reactant PhCOONR_2 (where NR_2 = pypiridyl); and (iii) reductive elimination wherein the N(C_5H_{10}) substituent gets transferred to the substrate. A heterobimetallic active species [Pd(μ−OAc)$_3$Ag] is identified as catalytically superior over the conventionally proposed monometallic palladium acetate. A cooperative interaction between Pd(II) and Ag(I) is found to offer additional stabilization to the transition states and intermediates, as compared to those devoid of such an interaction. The second additive, CsF, helps in the deprotonation of the amidic nitrogen as well as offers electrostatic stabilization to intermediates and transition states, thereby influencing the energetics of the reaction. Our findings clearly suggest that refined transition-state models inclusive of additives are highly desirable toward identifying the most preferred mechanistic pathways.

3.2 Introduction

Recent developments in the domain of C–H bond activation reactions have been unprecedented.[63,105,183–188] Palladium continues to remain the most widely used catalyst, both in industry and academia.[17,21,189,190] As mentioned in the earlier chapters, most of these TM catalyzed reactions utilize a variety of reagents ranging from simple acids to complex TM salts[39–42] as additives to improve the outcome of the reaction,[35–38] whose role at molecular level is not well understood.

Transition-metal catalysts with suitable additives have been used for constructing C–C and C–X (where X = O, N, S) bonds in both aliphatic and aromatic compounds.[16,18,103,117,119,124,129,191–193] The challenges in C–heteroatom (N, O, S, etc.) bond formation reactions are greater than those in C–C bond formation reactions. The number of reports on TM-catalyzed C–N or C–O bond formation reactions are far fewer as compared to the vast experimental literature concerning carboncarbon bond formations. Directed C–H functionalization of arenes is a powerful strategy to address the issue of selectivity in TM catalyzed reactions.[12,108,110,113,194–198]



Scheme 3.1: Palladium acetate catalyzed amination of N-arylbenzamide by $PhCOON(C_5H_{10})$ reaction.[53] [a]Solvent used was 1,4-dioxane and [b]toluene in these cases, while it is DCE when both additives were used.

As a part of our continued efforts toward understanding the mechanism of TM-catalyzed C–heteroatom bond-formation reactions,[54–57] we became interested in a palladium(II)-catalyzed

ortho-C–H amination reaction of *N*–arylbenzamides reported by the Yu group (Scheme 1).[53] This reaction provides easy access to biologically significant tertiary amines.[132] The amide group in the product can easily be converted to esters, acids, and alkanes.[11] Aromatic compounds with carbon–nitrogen bonds have found applications in medicines, dyes, plastics, surfactants, and pesticides.[43–52] The wider use of nitrogen containing compounds in diverse fields underscores the importance of C–N bond-forming reactions. The yield of this reaction improves significantly upon introduction of additives such as silver acetate and cesium fluoride. For instance, the yield changes from 40% with just palladium acetate to 70% with the inclusion of cesium fluoride.10 Further improvement to 97% was noted when silver acetate is employed in conjunction with cesium fluoride. These observations hint at potential participation of the additives in the catalytic process. In view of very limited understanding on the molecular role of such metal salt additives, we are convinced that the present investigation could have broader implications in transition metal catalysis.

Yu's amination reaction, as shown in Scheme 3.1, is a prototypical "*directed C–H functionalization reaction*", where the –CONHAr group directs the Pd(II) closer to the ortho C–H bond of the aryl ring that eventually is substituted by the amine. This reaction provides access to compounds similar that of the Buchwald–Hartwig Amination (BHA) without the use of external phosphine ligands.[23,24] The mechanistic complexity of Yus reaction is expected to be higher, owing to the use of multiple additives, and hence, it warrants careful investigation. Though there are a few experimental reports on the mechanism of C–N bond formation reactions,[25,58–61] transition-state models as well as the energetics of such reactions are seldom reported.[199]

In the recent past, there have been interesting computational studies from the groups of Musaev and Houk addressing the role of additives in TM catalysis.[200,201] Our recent research has also revealed that the barrier for an aryl C–H bond activation is much lower with a heterobimetallic species [Pd(μ−OAc)$_3$Ag] as compared to the conventional monomeric

$Pd(OAc)_2$ active species.[202] Along similar lines, we continued to investigate whether or not [$Pd(\mu{-}OAc)_3Ag$] could serve as an active catalyst in various steps throughout the catalytic cycle.[203] The key objective of this work is to understand the complete mechanism of ortho-aryl amination of N-arylbenzamides using PhCOON(C_5H_{10}), with an emphasis on the role of metal salts such as cesium fluoride and silver acetate.

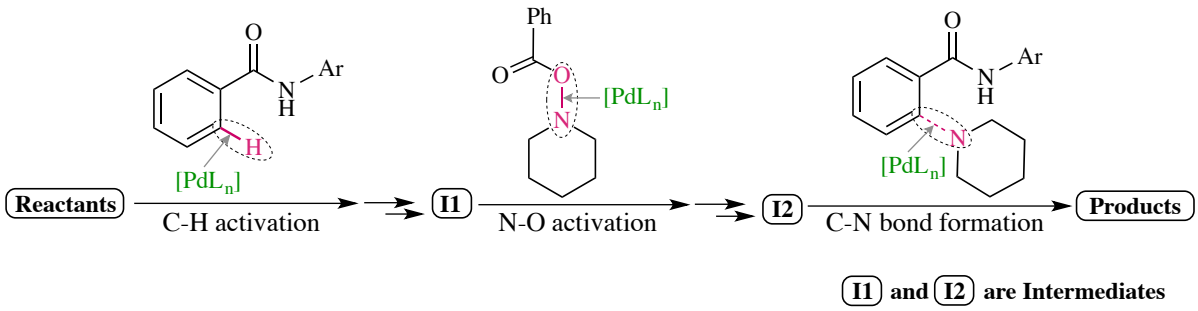
3.3 Computational Methods

All stationary points including transition states and intermediates are completely optimized using the Gaussian09 suite of programs.[138] To incorporate solvation effects, the dielectric continuum of 1,2-dichloroethane (DCE) was applied using the polarized continuum solvation model (PCM).[204] Geometries are obtained at the PCM_{DCE}/B3LYP/6-31G**, LANL2DZ(Pd, Cs, Ag) level of theory.[69,137,205] These geometries were then subjected to single-point energy computations at the PCM_{DCE}/M06/ TZVP,def2-TZVP(Pd,Ag,Cs) level of theory.[75,139,140,206,207] All the transition states were characterized as having only one imaginary frequency and intermediates (minima) by zero imaginary frequencies. Intrinsic reaction coordinate (IRC) computations were done for important transition states to ensure that they corresponded to the desired reaction coordinate.[145,146] Unless otherwise stated, all energies in this chapter are the Gibbs free energies computed at the PCM_{DCE}/M06/TZVP,def2-TZVP(Pd,Ag,Cs)//PCM_{DCE}/B3LYP/6- 31G**,(LANL2DZ) with respect to the infinitely separated reactants[166] that comprise $[Pd(OAc)_2]_3$, $AgOAc \cdot (DCE)_2$, $CsF \cdot (DCE)_6$, PhCONHAr (model system for the experimentally used p$-(^tBu)$PhCONHAr) and PhCOON(C_5H_{10}).[201,208–211] Since we intend to compare the effect of no additive, inclusion of one and more additive(s) in sequence, the corresponding pre-reacting complex or the preceding intermediate would remain nonuniform in each such scenario. On the other hand, the use of infinitely separated reactants would provide a reasonable global reference point. This reference point

can readily provide adequate mass balance when different pathways are compared. These reference points were chosen in order to be closer to the likely scenario in the condensed phase. Palladium acetate is known to exist as trimer in several solvents including 1,2-dichloroethane.[148–152,212] Since 1,2-DCE is a weakly coordinating solvent, it is likely to bind to silver acetate and cesium fluoride.[153–160] Hence, microsolvated $AgOAc \cdot (DCE)_2$ and $CsF \cdot (DCE)_6$ are taken as more realistic representations of these additives in the solvent. The primary coordination spheres of silver acetate and cesium fluoride can, respectively, accommodate 2 and 6 solvent molecules. To ensure stoichiometric balance in the evaluation of energetics, the energies of the solvent clusters, $(DCE)_2$ and $(DCE)_6$, have been included, as required.

3.4 Results and Discussion

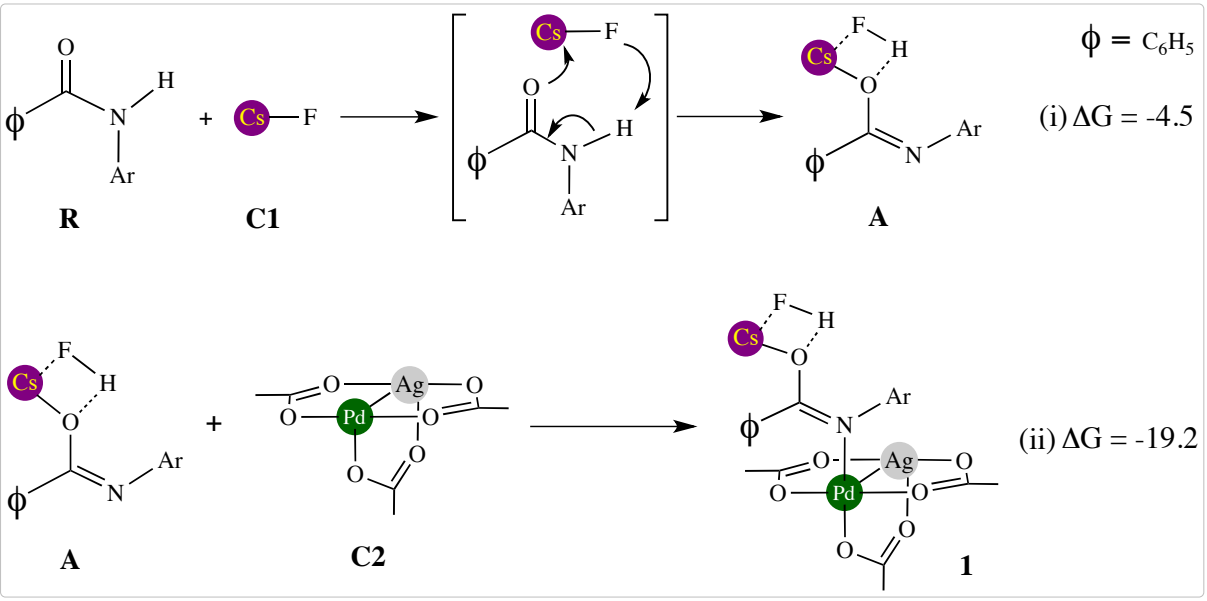
The mechanism of reaction between *N*–arylbenzamide and *O*–benzoyl hydroxylpiperidine can be considered as involving three key steps: (i) C–H activation, (ii) N–O activation, and (iii) reductive elimination, as shown in Scheme 3.2. Due to the presence of two additives, in addition to the catalyst and substrates, a richly diverse set of possible pathways can be envisaged.



Scheme 3.2: A succinct illustration of three important mechanistic events involved in palladium catalyzed ortho-amination of N-arylbenzamide.

3.4.1 Catalyst–Substrate Combination

The substrate, PhCONHAr, can combine with the catalyst and the additives in different possible ways. An interaction between CsF and the substrate (N–arylbenzamides) is considered first, wherein CsF abstracts the amidic proton as shown in Scheme 3.3.



Scheme 3.3: Computed Gibbs free energies (in kcal/mol) of formation of (i) the cesium amidate intermediate (A) and (ii) the catalyst substrate pre-reacting complex (1).

In fact, such a deprotonation was earlier observed by Yu and coworkers under an identical reaction conditions.[167] The proton abstraction by CsF in the present case is found to be exoergic by -4.5 kcal/mol. The resulting cesium amidate intermediate **A** readily binds to the active catalyst [Pd(μ−OAc)$_3$Ag] to give rise to a catalyst–substrate complex **1**. The formation of **1** is fairly exoergic (ΔG = -19.2 kcal/mol), suggesting the likely involvement of such species that consists of both the additives in the mechanistic events.[213] In other words, a significantly lower-energy pathway appears to open up through the explicit involvement of CsF and silver acetate. Palladium maintains a square-pyramidal geometry in **1**, with

the silver atom occupying the apical (or axial) position.[b] The complete catalytic cycle commencing with **1** is shown in Scheme 3.4.

3.5 C–H Activation

Though the C–H activation has been discussed earlier in the previous chapter, for sake of completeness we will briefly introduce few points on this step in the context of the Scheme 3.4 in this section.

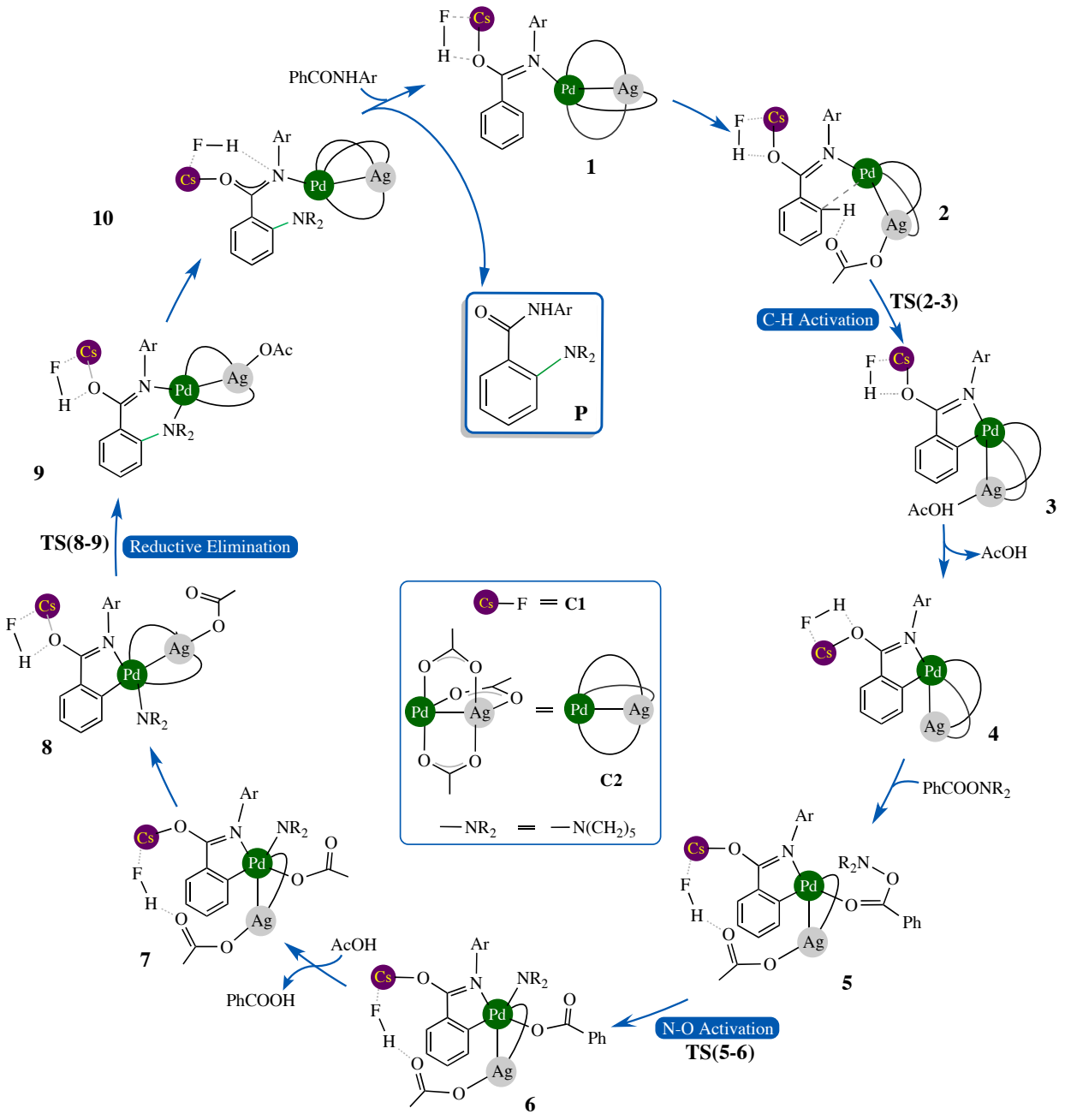
The catalyst–substrate complex **1** can undergo a minor structural change to give another intermediate **2** wherein palladium gets closer to the *ortho*-C–H bond of the phenyl ring. In **2**, one of the bridging acetates of [Pd(μ−OAc)$_3$Ag] opens up to create a partial coordinative unsaturation on palladium. This situation facilitates a weak agostic interaction between Pd(II) and the *ortho*-aryl C–H bond (Pd–C = 2.346 Å), leading to the C–H bond activation. The C–H bond distance increases from 1.085 Å in **1** to 1.092 Å in **2**.[c] In the next step, i.e., **2** → **3** conversion, the proton of the activated C–H bond is abstracted by the pendent acetate bound to the silver atom. After an exhaustive search, spread over 32 configurations and conformations for the C–H activation **TS(2–3)**, the lowest-energy transition state is identified (ΔG = 1.1 kcal/mol).[214] A comprehensive representation of these different possibilities, arising due to the presence and absence of additives in the C–H activation transition state, is provided in Figure 3.1.[d]

It may be readily noticed that the relative energies of the transition states devoid of any additives are much higher. While the inclusion of cesium fluoride or silver acetate results in additional stabilization, the presence of both additives is certainly the most effective mode of stabilization. In the next section, a discussion of a select set of C–H activation

[b]Other intermediates with same stoichiometry as **1** were also identified to learn that those are of higher energy. See Figure B.1 in the appendix A for more details.

[c]More geometric details of **2** is discussed in Figure B.2

[d]See Figure B.3 in the appendix A for structures of each of the transition states in Figure 3.1



Scheme 3.4: Catalytic cycle for $[Pd(\mu{-}OAc)_3Ag]$ catalyzed *ortho*-amination of *N*-arylbenzamide.

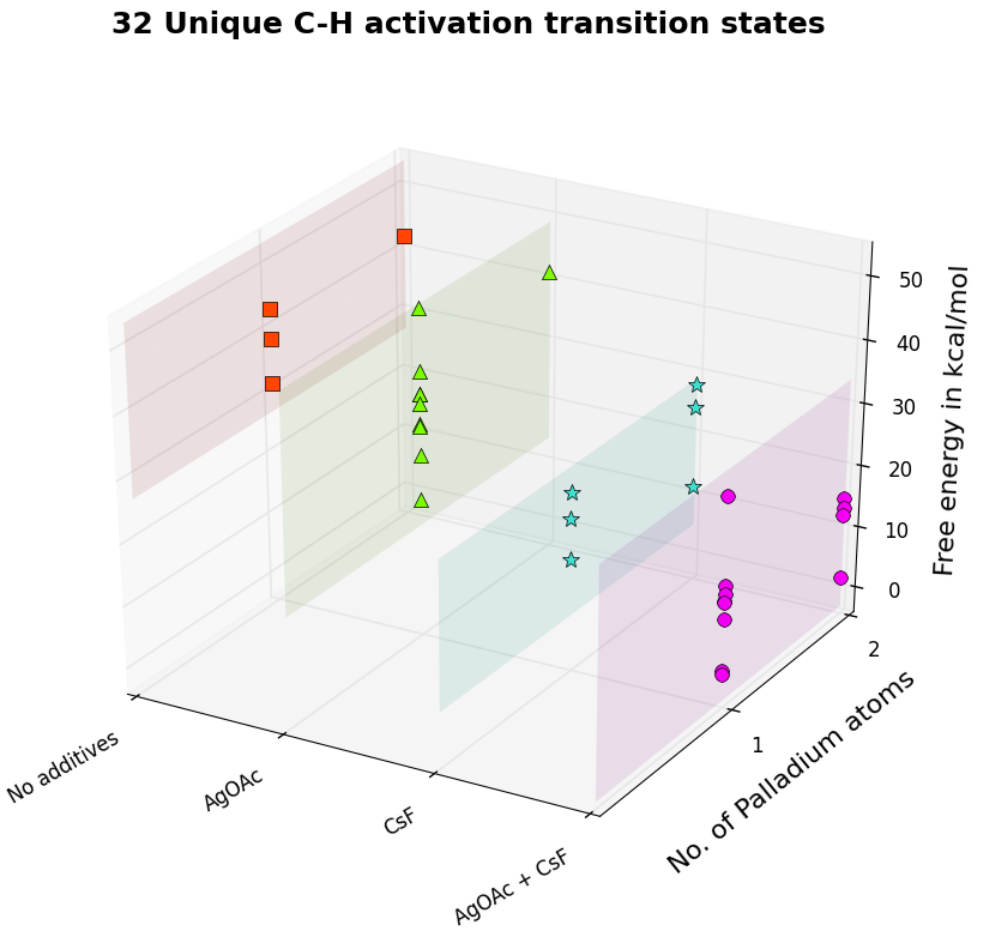


Figure 3.1: 3D plot of Gibbs free energies for C–H activation transition states as a function of the number of additives (X-axis) and the nuclearity of the palladium catalyst[215,216](Y-axis).

transition states are provided. It should be noted that a broad and general comparison is provided in the following sections on the basis of the relative energies of the transition states with respect to the separated reactants. With due consideration of mass balance, this approach will help compare pathways of differing stoichiometric compositions arising due to the presence of differing number of explicit additives. Adequate attention is also paid to the activation barrier, computed with respect to the preceding intermediate (as obtained through the intrinsic reaction coordinate calculations and further geometry optimization to the nearest minimum) for each of transition states involved in different pathways.

Some of the lower-energy CMD transition states, with and without the inclusion of additives, are provided in Figure 3.2.

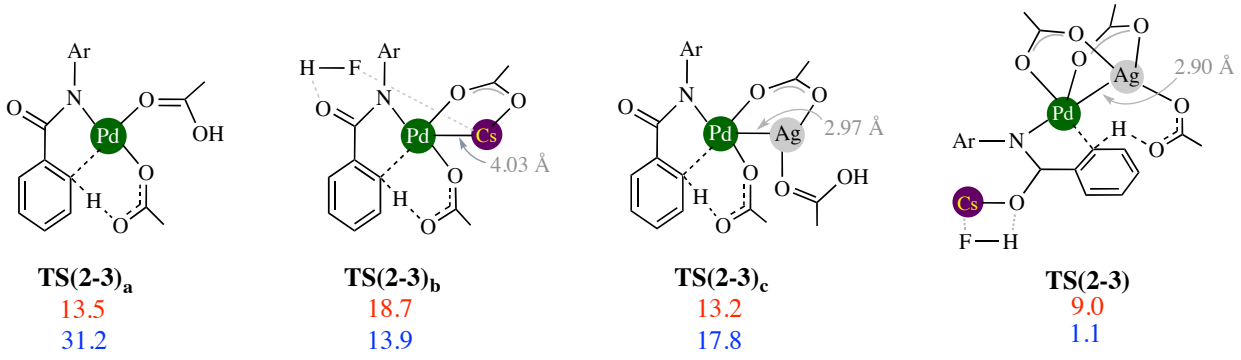


Figure 3.2: C–H activation transition states with and without additives. The numbers in red are the elementary step barriers, whereas those in blue color are the relative free energies (in kcal/mol) with respect to the infinitely separated reactants. The alphabetical subscripts denote transition states of different configurations. The most preferred transition state is denoted without any subscript.

It can be noticed that all transition-state geometries, except **TS(2–3)**, are archetypal 6-membered cyclometalation deprotonation transition states.[127,217–221] These transition states connect to the corresponding 5-membered palladacycles, similar to intermediate **3** (shown in Scheme 3.4). The *ortho*-aryl proton in all these transition states is abstracted by the acetate (palladium-bound acetate **TS(2–3)$_a$** or the silver-bound acetate **TS(2–3)$_c$**), resulting in

the formation of acetic acid. It is evident that the transition state without any additive is of higher-energy (**TS(2–3)$_a$**, 31.2 kcal/mol) than those involving explicit additives (**TS(2–3)$_b$**, 13.9 and **TS(2–3)$_c$**, 17.8 kcal/ mol). Akin to that with the transition states, explicit inclusion of additives results in stabilization of intermediates involved in the catalytic cycle. It is interesting to note that the elementary step barriers computed with respect to the corresponding preceding intermediates in each case, also exhibited a similar trend as that noted with the relative energies. For instance, the lowest activation barrier for CMD is noted for **TS(2–3)**, which is 10.9 kcal/mol lower than **TS(2–3)$_a$** devoid of any explicit additives. The barriers in the case of **TS(2–3)** and **TS(2–3)$_a$** can be computed with respect to the nearest exoergic intermediate **1** and the separated reactants, respectively. A direct comparison of the elementary step barriers with respect to the preceding intermediates (**2** and **2$_a$** which are corresponding intermediates respectively with and without the additives) in both these pathways (as obtained through intrinsic reaction coordinate calculations) indicates a lowering of 4.5 kcal/mol due to the presence of additives in the transition state. In the absence of cesium fluoride, one of the bound acetates would have to deprotonate the amidic hydrogen first. However, the inclusion of cesium fluoride helps in the initial deprotonation of the amidic hydrogen, as well as renders significant electrostatic stabilization in the subsequent C–H activation step.[222] In **TS(2–3)$_b$** an interesting Pd–Cs intermetallic interaction is identified. An alternative C–H activation mode with an explicit molecule of CsF but without any direct Pd–Cs interaction is found to be less favorable than **TS(2–3)$_b$**.[e] A similar Pd–Cs contact was earlier observed in the crystal structure of $Cs_2[Pd(NO_3)_4]$.[223] Thus, it appears that an additive such as cesium fluoride could influence the energetics of the reaction by providing additional stabilization to different transition states involved in the reaction.

Further interesting features are found by including silver acetate in the C–H activation transition states. In the lower energy transition states belonging to this group, i.e., in **TS(2–**

[e]See Figure B.3 in the appendix A.

3)$_c$ and **TS(2–3)**, the intermetallic Pd–Ag contacts are,[f] respectively, found to be 2.97 and 2.90 Å, indicating a metal–metal bond with acetate as the bridging ligand.[171,224,225] Ag(I) lowers the relative energies of these TSs through intermetallic cooperativity, which has also been suggested in the case of other heterobimetallic complexes.[176,182,226–234] Analogous to Pd(II)–Ag(I), other d^8–d^{10} interactions between two transition metals have also been noted in both experimental and computational studies.[177,235–242] Furthermore, we have identified orbital interaction between palladium- and silver-centered orbitals as well as bond critical point between the metals using Atoms-In- Molecule (AIM) analysis.[242] **TS(2–3)$_c$** benefits only through the cooperativity effect of silver acetate whereas **TS(2–3)** appears to combine the best of both additives. Such cooperativity between two metals has also been noted in some gas phase reactions,[243] as well as in homogeneous catalysis.[244–247] These structural and energetic features clearly suggest that refined transition state models inclusive of additives are highly desirable toward identifying the most preferred mechanistic pathway.

As a result of the acetate-assisted C–H activation, the pendent acetate bound to silver in intermediate **2** is converted to acetic acid in **3** (Scheme 3.4). Acetic acid being a labile ligand, it can be displaced by the incoming aminating reagent ($PhCOONR_2$). The expulsion of acetic acid leads to intermediate **4**, which in turn, can take up $PhCOONR_2$ to give intermediate **5** ($\Delta G(\mathbf{3} \rightarrow \mathbf{4})$ = 0.5 kcal/mol; $\Delta G(\mathbf{4} \rightarrow \mathbf{5})$ = 2.9 kcal/mol). The incoming $PhCOONR_2$ can coordinate either to the silver or the palladium center. One of the bridging acetates in **4** opens up due to the binding of $PhCOONR_2$ to the palladium center. In the resulting intermediate **5**, this silver bound acetate is seen to develop an interaction with the HF. The acetate is thus prevented from recoordinating to palladium. Such distortions in the geometry around the palladium makes **4** → **5** conversion mildly endoergic, by 2.9 kcal/mol. The Pd–Ag bond distance shows an interesting variation from 2.96 Å in intermediate **3** to

[f]AIM ananlysis of **TS(2–3)** showing the bond critical point between Pd and Ag atoms is shown in Figure B.4.

2.90 Å in **4**.[g] When other ligands coordinate to silver, its ability to accept electrons from palladium is expected to be lower. All these features point to the existence of an intermetallic communication that can influence the energetics of the reaction. The discussions up until now have been on the formation of a palladacycle intermediate with a bound $PhCOONR_2$ (**5**). In the next section, different modes for the N–O bond activation in $PhCOONR_2$ are presented.

3.6 N–O Activation

N–O bond cleavage is the second vital step of the reaction that provides the $-NR_2$ moiety to be used for *ortho*-amination of the phenyl ring. Along the similar lines to that with the C–H activation step, we have sampled as many as 15 different transition state possibilities in this step to identify the most preferred one. Some of the important transition states are shown in Figure 3.3.[h]

In general, the N–O activation transition states exhibit a five membered geometry as shown in Figure 3.3. Note that the N–O bond of the incoming substrate ($PhCOONR_2$) cleaves at the palladium center in the case of **TS(5–6)$_\mathbf{a}$**, **TS(5–6)$_\mathbf{b}$**, and **TS(5–6)**, while in **TS(5–6)$_\mathbf{c}$** and **TS(5–6)$_\mathbf{d}$**, it occurs at the silver center. **TS(5–6)$_\mathbf{a}$** without any of the additives is evidently the least favored transition states in this group of possibilities.

Inclusion of additives results in considerable stabilization of the corresponding transition states as well as the preceding intermediates. For instance, **TS(5–6)$_\mathbf{b}$** with cesium fluoride and **TS(5–6)$_\mathbf{c}$** with silver acetate, are, respectively, about 12– 15 kcal/mol lower than **TS(5–6)$_\mathbf{a}$** devoid of these additives. A comparison of the activation barriers also indicates that the pathway inclusive of both additives via **TS(5–6)** offers the lowest barrier. In **TS(5–6)$_\mathbf{b}$**,

[g] See Figure B.6 in the appendix A for geometric details of **3** and **4**

[h] Details of the additional transition states, from the group of 15 TSs examined in this study are provided in Figure B.7 in the appendix A.

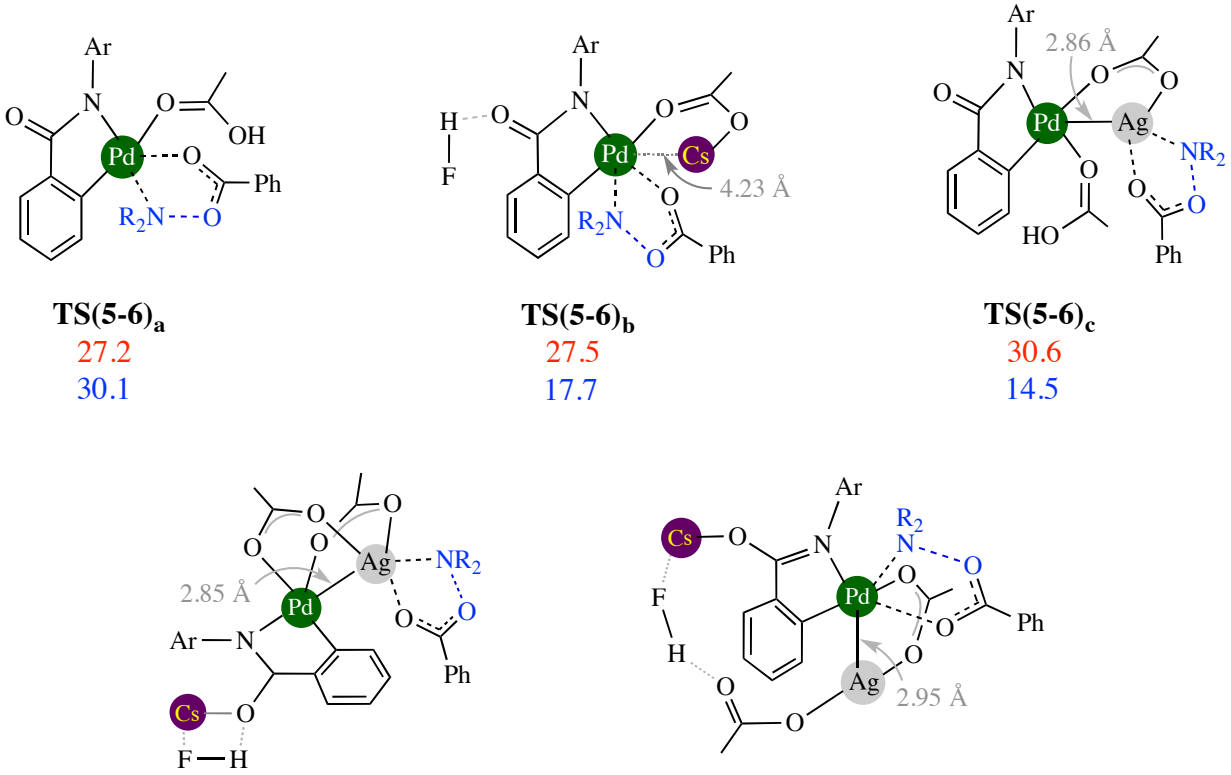


Figure 3.3: N–O activation transition states with and without additives. The numbers in red are the elementary step barriers, whereas those in blue color are the relative free energies (in kcal/mol) with respect to the infinitely separated reactants. The alphabetical subscripts denote transition states of different configurations. The most preferred transition state is denoted without any subscript.

the presence of a Pd–Cs interaction (4.23 Å) similar to what was found earlier in the case of C–H activation (**TS(2–3)$_b$**) is also noticed (Figure 3.2 and Figure 3.3).[248] **TS(5–6)$_b$** also enjoys a F−H$\cdots$O hydrogen-bonding contributing to its additional stabilization. In the lower-energy transition state **TS(5–6)$_c$** for this step, the cooperativity effect of palladium and silver (Pd–Ag distance of 2.86 Å) is evident.[249]

Of the five low-energy possibilities summarized in Figure 3.3, **TS(5–6)$_d$** and **TS(5–6)** have both additives and thus incorporate the favorable features of both **TS(5–6)$_b$** and **TS(5–6)$_c$**. In these TSs, the amidic nitrogen is deprotonated by the fluoride of cesium fluoride and the Pd–Ag interaction is modulated by the bridging acetate ligands. The substrate $PhCOONR_2$ is bound, respectively, to silver and palladium in **TS(5–6)$_d$** and **TS(5–6)**. The N–O activation at the palladium (**TS(5–6)**, ΔG = 4.2 kcal/mol) is energetically more preferred over that on the silver center (**TS(5–6)$_d$**, ΔG = 9.3 kcal/ mol).[250]

A comparison of the optimized geometries of **TS(5–6)$_d$** and **TS(5–6)**, as given in Figure 3.4, reveals some interesting features of the intermetallic interaction. Both **TS(5–6)** and **TS(5–6)$_d$** are late transition states with N–O distances of 2.60 and 2.24 Å, respectively (N–O bond length in the preceding intermediate **5** is 1.47 Å). The Pd–Ag distance reduces to 2.79 Å in the ensuing intermediate, as identified using the intrinsic reaction coordinate computations toward the product side, starting from **TS(5–6)**d.[i] On the contrary, the Pd–Ag distance increases to 2.95 Å in **TS(5–6)** and further to 2.98 Å in intermediate **6**. This bond lengthening in **TS(5–6)** (as well as **6**) may be regarded as a manifestation of reduced electron donation from Pd(IV) to Ag(I). This is opposite to what was observed above in the context of **TS(5–6)$_d$** and the forward intermediate obtained from the corresponding IRC calculation.

[i]See Figure B.8 in the appendix A for further structural details of **6** and the product obtained from the IRC of **TS(5–6)$_d$**

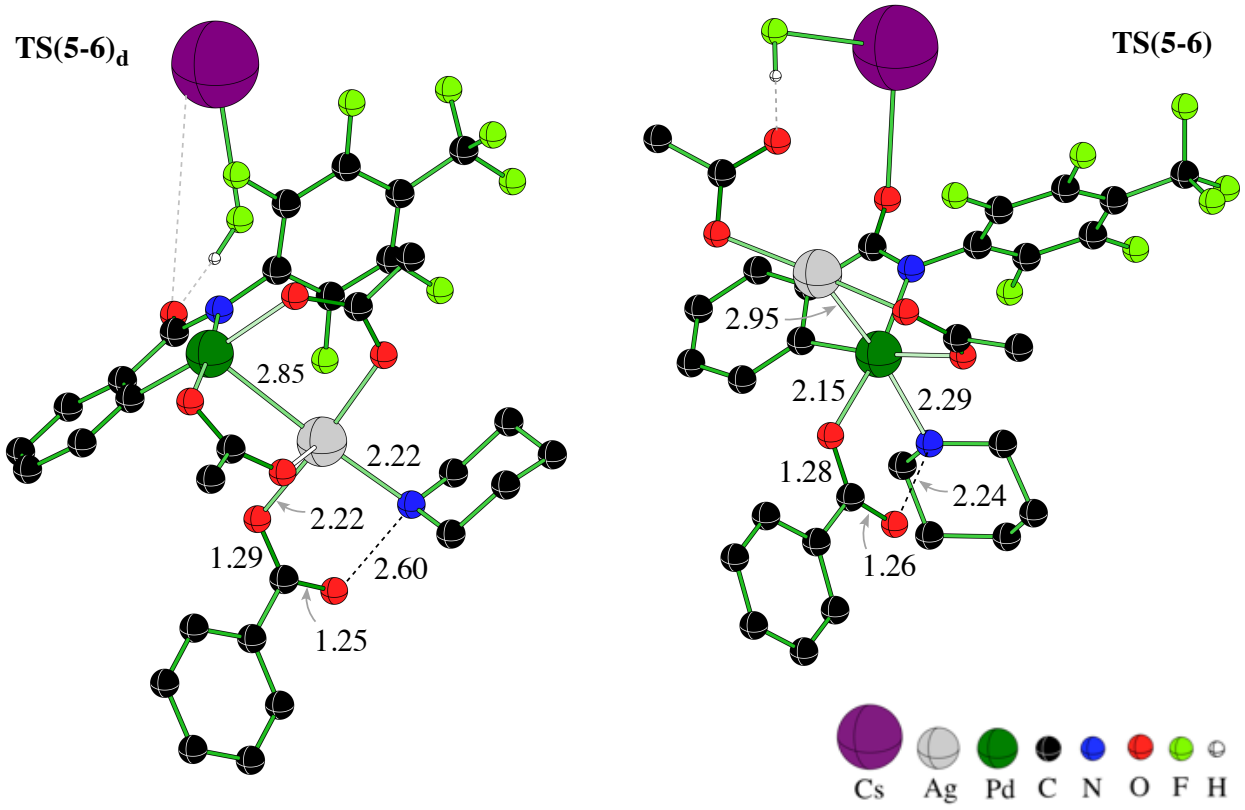


Figure 3.4: Optimized geometries of **TS(5–6)** and **TS(5–6)d** at the PCM_{DCE}/B3LYP/6-31G**, LANL2DZ(Pd, Cs, Ag) level of theory. Hydrogen atoms are omitted for improved clarity. The bond distances are in angstrom.

The computed energetics presented in this section makes it evident that the N–O bond cleavage is preferred at the Pd(II) center rather than Ag(I). The Pd–Ag interaction is maintained through this process, indicating that [Pd(μ−OAc)$_3$Ag] continues to serve as the active species in the N–O activation step of the title reaction. However, the Pd–Ag bimetallic distances are expected to be longer in Pd(IV) intermediates (such as the one formed as a result of the N–O activation (**6**)) than that in Pd(II) species (such as in intermediate **5**), due to the diminished electron-donating ability of the former.

3.7 Conversion from Intermediate 6 → 7 → 8

The important mechanistic step that follows N–O bond cleavage is the introduction of the $-NR_2$ moiety to the *ortho*-carbon of the phenyl ring. It is important to recollect that in the C–H activation step, leading to the formation of a palladacycle intermediate, a molecule of acetic acid was released (Scheme 3.4). Herein, the palladium-amidate intermediate **6** first converts to another intermediate **7** through a barrierless ligand exchange process, wherein the incoming acetic acid protonates the Pd bound benzoate, which in turn, departs as benzoic acid. This step is essential to the regeneration of the active catalyst toward the later phase of the reaction. Once the aminated product is produced, the triacetate bridged active catalyst [Pd(μ−OAc)$_3$Ag] can be regenerated for subsequent catalytic cycles.

The palladium amidate **7** is not the best of the possible species for further steps of the reaction leading to amination of the *ortho* aryl carbon. The minor structural change converts intermediate **7** to **8** with a better orientation of the $-NR_2$ group, suitable for the C–N bond formation (Figure 3.5).

In addition, the orientation of the acetate groups in **8** makes it easier for the subsequent catalyst regeneration following the reductive elimination. Hence, the intermediate **7** → **8** conversion is considered as an important step in this study. In intermediate **8**, palladium

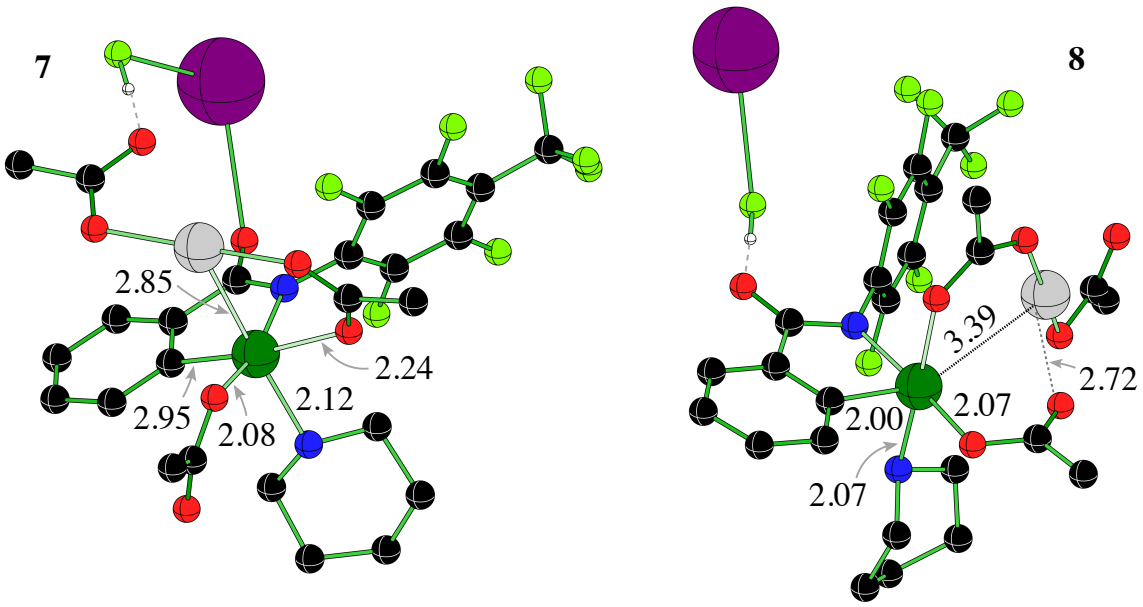


Figure 3.5: Optimized geometries of intermediate **7** and **8** at the PCM_{DCE}/B3LYP/6-31G**, LANL2DZ(Pd, Cs, Ag) level of theory. Hydrogen atoms are omitted for improved clarity. The bond distances are in angstrom.

adopts a penta-coordinate geometry with an additional weak interaction with the silver atom, which offers two minor advantages (Figure 3.5): (a) The penta-coordinate geometry around the Pd(IV) in intermediate **8** makes it more reactive,[251,252] (b) it would be easier to accommodate the expected distortion in the ensuing transition state **TS(8–9)** for the C–N bond formation. Another interesting feature is that the Pd–Ag interaction is weaker in intermediate **8** (3.39 Å) as compared to that in **7**. With this reactive Pd(IV) intermediate, the stage is set for the next major steps in the catalytic cycle, as described below.

3.8 Reductive Elimination

The reductive elimination step parallels a C–H activation step in terms of it relevance in TM-catalyzed reactions. As a result of the reductive elimination, the oxidation state of palladium

is lowered by two and the carbon–nitrogen bond is formed. The catalyst thus gets regenerated for its participation in the next catalytic cycle. Analogous to the C–H activation step, a large number of possibilities for the C–N bond formation has been considered in an effort to identify the most preferred transition state. Two types of reductive elimination transition states can be envisaged. The amino group can either be considered as bound to the palladium, leading to an inner-sphere reductive elimination (ISRE), or it could remain without a direct interaction with the palladium, resulting in an outer-sphere reductive elimination (OSRE). We have located both the ISRE and OSRE transition states for the CN bond formation (Figure 3.6).[j]

The Pd $\cdots$ NR_2 distances in the OSRE transition states are around 3.10–3.02 Å, whereas the corresponding distances in the ISRE transition states are between 2.01–2.10 Å. In the OSRE pathway, the N–O bond breaking and the C– N bond formation take place simultaneously. This would imply that the N–O activation step can be avoided if the OSRE pathway is followed. Interestingly, the Pd(II) outer-sphere $\mathbf{TS(8–9)_b}$ is of comparable energy to an equivalent Pd(IV) inner-sphere alternative $\mathbf{TS(8–9)_a}$. To identify the most preferred RE transition state, we have considered the role of explicit additives. Figure 3.6 provides five such transition states for the reductive elimination, of which $\mathbf{TS(8–9)_c}$ includes only cesium fluoride, while $\mathbf{TS(8–9)_d}$ and $\mathbf{TS(8–9)_e}$ have silver acetate as the exclusive additive. In $\mathbf{TS(8–9)_e}$, the deprotonated amidic nitrogen is bound to palladium, although in $\mathbf{TS(8–9)_d}$, it is the carbonyl oxygen that is coordinated to the palladium center.[k]

Similar to the C–H and N–O activation steps, we anticipated that there could be additional stabilization by explicit inclusion of both additives in the transition states. Two such representative RE transition states, with both silver acetate and cesium fluoride, are

[j]Other possible TSs for this step with palladium acetate as the only reagent is discussed in Figure B.9 in the appendix A.

[k]Similar higher-energy transition states with varying ligand combinations are provided in Figure B.9 of the appendix A.

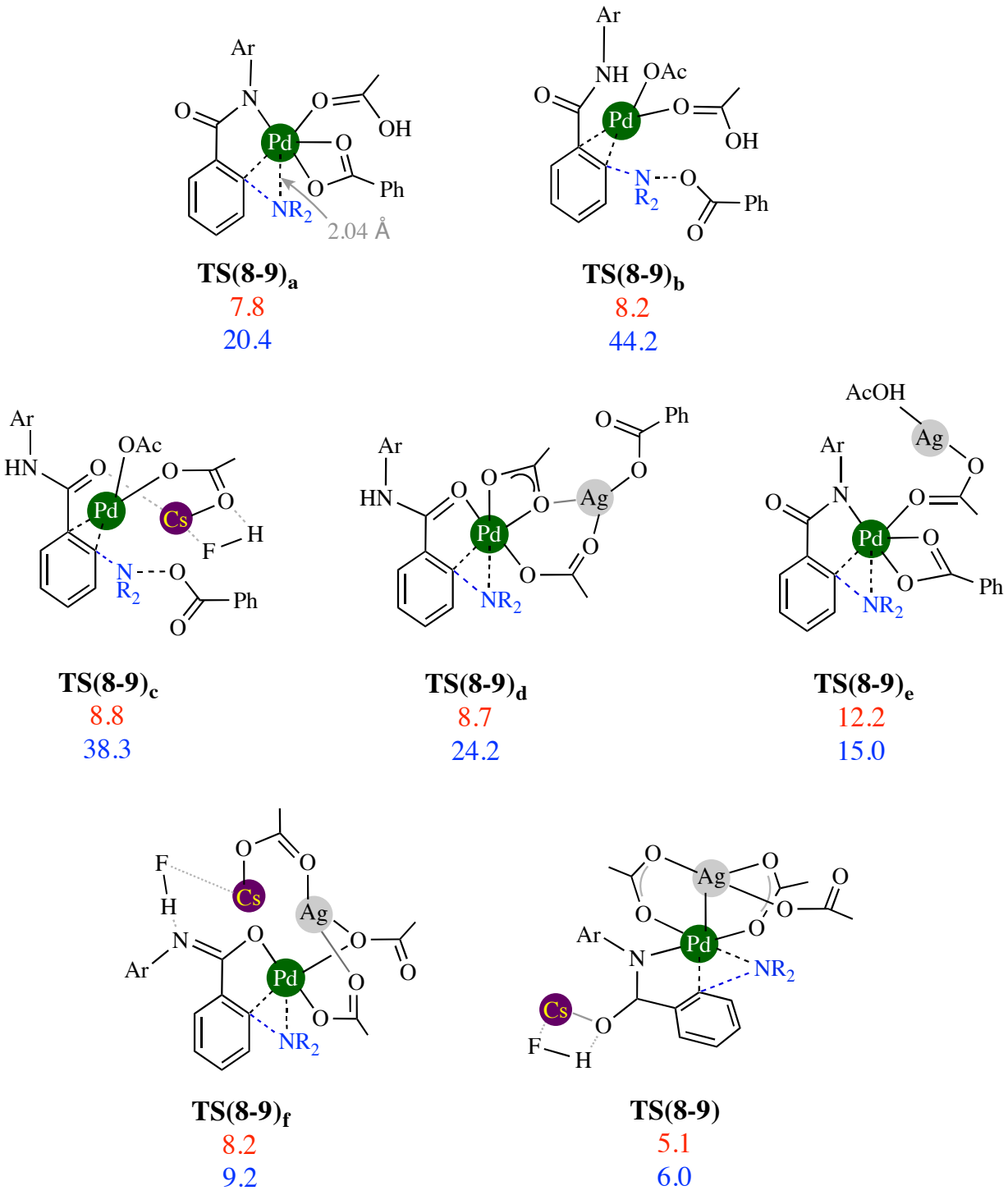


Figure 3.6: Reductive elimination transition states with and without additives. The numbers in red are the elementary step barriers, whereas those in blue color are the relative free energies (in kcal/mol) with respect to the infinitely separated reactants. The alphabetical subscripts denote transition states of different configurations. The most preferred transition state is denoted without any subscript.

provided in Figure 3.6.[1] These possibilities belong to the ISRE pathway involving a Pd(II) Pd(IV) couple. Unlike the C–H and N–O activation TSs discussed in the earlier sections, **TS(8–9)$_\mathbf{f}$** does not have any Pd–Ag interaction, although it is connected via a bridging acetate ligand.[253] The free energies of the pertinent TSs, as given in Figure 3.6, make it evident that the inclusion of both silver acetate and cesium fluoride additives can offer significant stabilization to the corresponding RE transition states. For instance, the free energies of **TS(8–9)** and **TS(8–9)$_\mathbf{f}$** that includes both additives are much lower than the other alternatives. Furthermore, the activation barrier for the RE is the lowest for **TS(8–9)**. The most preferred mode **TS(8–9)** involves the participation of [Pd(μ−OAc)$_3$Ag] heterobimetallic species in the C–N bond formation (Figure 3.7).

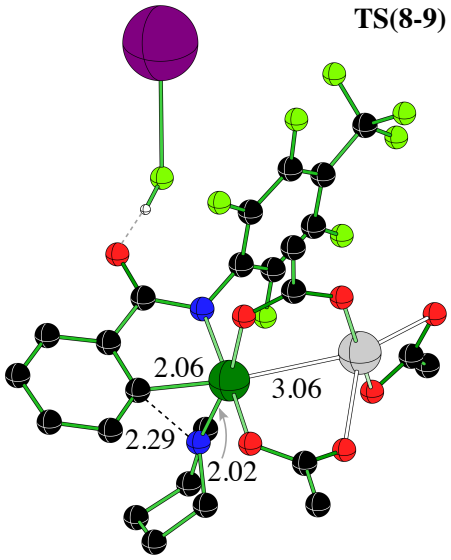


Figure 3.7: Optimized geometries of reductive elimination transition state leading to C–N bond formation at the PCM$_{\mathrm{DCE}}$/B3LYP/6-31G**, LANL2DZ(Pd, Cs, Ag) level of theory. Hydrogen atoms are omitted for improved clarity. The bond distances are in angstrom.

Although the Pd–Ag interaction in this transition state is weaker, both the metals are held together by one of the bridging acetate ligands. It is important to note that the strong Pd–

[1]See Figure B.9 in the appendix A for other higher energy transition states for the reductive elimination step.

Ag interaction is an undesirable feature in the RE step. However, the reasonable proximity facilitated by the bridging ligands appears to be good.[m] A closer perusal of the transition-state geometries raises a few pertinent questions on the coordination environment of cesium. Although cesium interacts with the aromatic π-face of the *N*-aryl group of the substrate, we have examined alternative possibilities with one or two explicitly included solvent molecules (DCE) as summarized in Figure 3.8. An increase in free-energy barrier is noticed in the case of C–H activation step as compared to the other lower-energy transition states devoid of explicit DCE molecules. The comparison of the relative free energies of **TS(2–3)** with $\mathbf{TS(2–3)_{DCE}}$ and $\mathbf{TS(2–3)_{2DCE}}$, given in the first row of Figure 3.8, indicates a free-energy penalty associated with the inclusion of explicit solvent molecules in the C–H activation step.

In the N–O activation step, no major change in energetics is noticed with the inclusion of DCE molecules. Interestingly, a modest increase in the activation barrier in the reductive elimination is likely by introducing explicit DCE molecules in the transition states. The Gibbs free energies of these microsolvated transition states suggest that the intramolecular coordination of cesium with the substrate offers a reasonably good model that satisfies its coordination environment.

3.9 Conversion of Intermediate 9 → 10

The intrinsic reaction coordinate, beginning from the key RE transition state **TS(8–9)** toward the product side, connects to an aminated product complex **9** with the -NR_2 group at the *ortho*-carbon (Scheme 3.4). The Pd–Ag distance of 3.06 Å in **TS(8–9)** reduces to 2.82 Å in the ensuing intermediate **10**. Interestingly, the triacetate bridge is restored in **10**, which similar to that in intermediate **1** at the beginning of the catalytic cycle (Pd–Ag distance in **1** is 2.84 Å). The catalyst is released at this stage of the reaction as the formation of the

[m]Another lower-energy transition state in this group has been located, without a Pd–Ag bond. See Figure B.9 in the appendix A for more details.

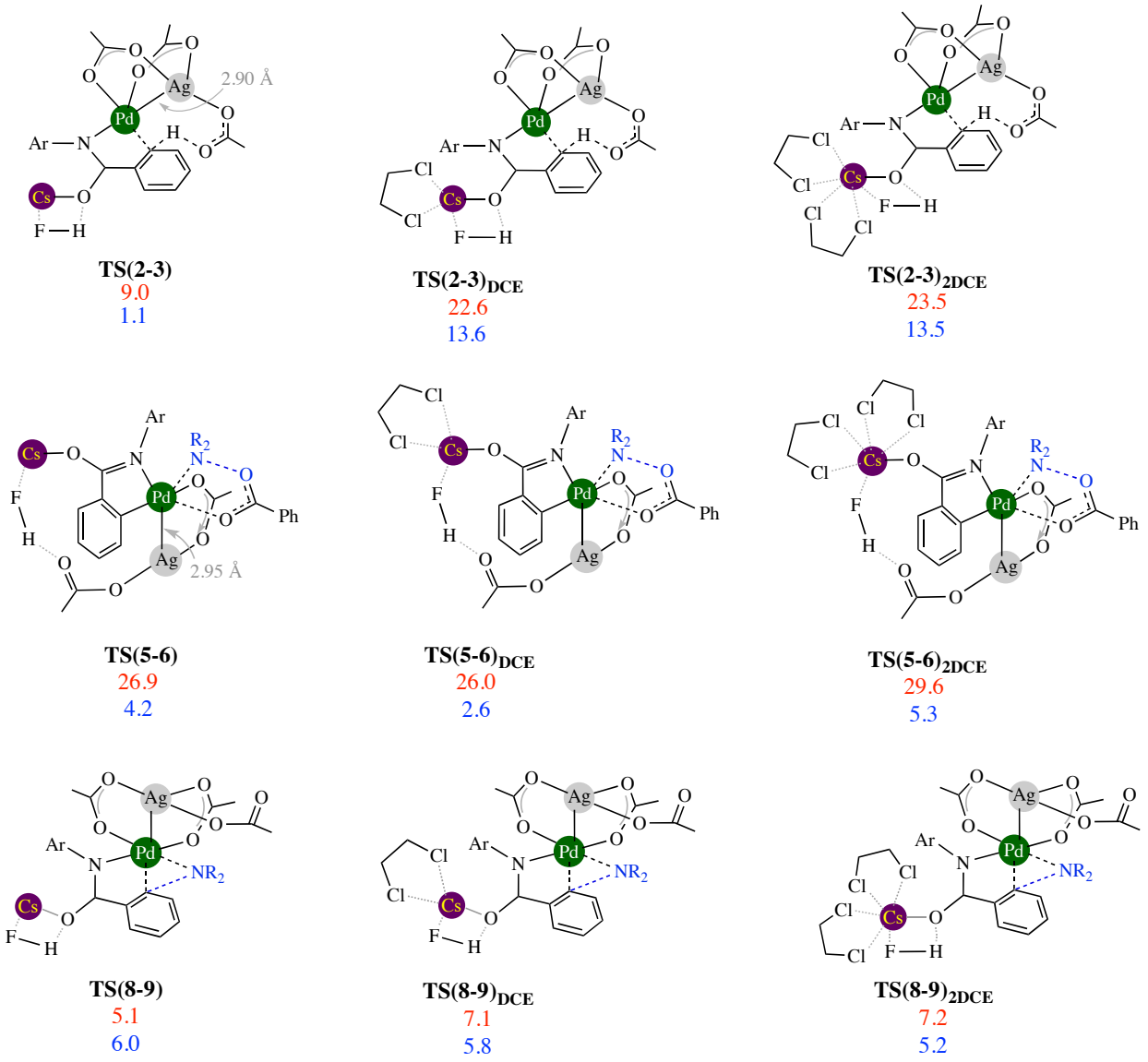


Figure 3.8: Transition states with zero, one and two DCE molecules bound to the cesium in the CH activation, NO activation, and the reductive elimination steps. The numbers in red are the elementary step barriers with respect to the respective intermediates, whereas those in blue are relative Gibbs free energies (in kcal/mol) with respect to the infinitely separated reactants. The alphabetical subscripts denote transition states of different configurations. The most preferred transition state is denoted without any subscript.

aminated product is complete. The [Pd(μ−OAc)$_3$Ag] and cesium fluoride are now ready for uptake of another substrate molecule to continue the catalytic cycle. The Gibbs free-energy profile of the complete reaction (with an explicit cesium fluoride and silver acetate) is shown in Figure 3.9. The reaction is found to be overall exoergic by about 31 kcal/mol, computed as the difference in energies between the reactants and the product. It should be noted that intermediate **10**, as shown in the Gibbs free-energy profile, is a product complex between the aminated arene and the active catalyst, namely, [Pd−(μ−OAc)$_3$−Ag], and a bound cesium fluoride. The complete release of the aminated product is then facilitated by the uptake of another molecule of the substrate. The Gibbs free energy for the product release is exoergic by 12 kcal/mol, which is calculated as **10** + substrate → **1** + product.

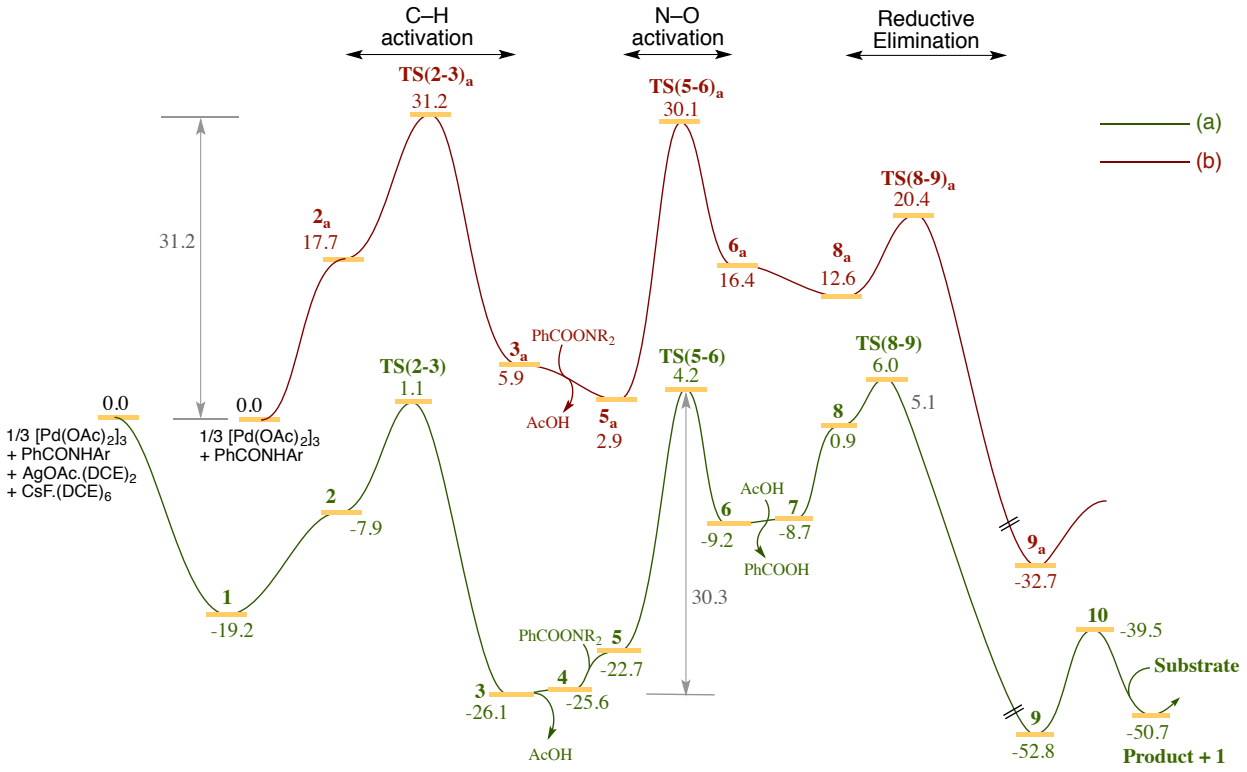


Figure 3.9: Gibbs free-energy profile of the overall reaction (a) with an explicit molecule of silver acetate and cesium fluoride shown in green color and (b) without any additive in red color. The energies are reported with respect to the separated reactants.

3.10 Comparison of Gibbs Free Energy Profiles with and without the Participation of Additives

Through the earlier sections, a comprehensive description of all the lower energy transition states, with and without the inclusion of explicit additives for three major mechanistic steps of the reaction has been provided. It would be most appropriate at this stage to highlight some of important features by comparing the Gibbs free-energy profiles in these two scenarios. The similarities and differences between the energetic features of the catalytic cycle, with and without explicit additives, can be understood with the help of the Gibbs free-energy profiles provided in Figure 3.9.

One of the most noticeable general features is that the inclusion of additives results in a lower-energy pathway, as depicted using the green color curve in Figure 3.9. While a specific comparison appears difficult due to the differing stoichiometric compositions of various intermediates and the transition states involved in these two pathways, a broad and general comparison with the experimental observations is possible. First, the computed highest barriers in both situations are in line with the high reaction temperature. Second, at the same reaction temperature, the catalysis is more efficient with the use of additives, as indicated by the higher yield. This observation is comparable to the lowering of the activation barriers for the pathway involving additives (the lower-energy profile shown in green color). The highest barrier to overcome without any additive is between the starting point and $\mathbf{TS(2–3)_a}$ with a value of 31.2 kcal/mol. However, the highest barrier with additives, appears to be between **3** and **TS(5–6)** with a barrier of 30.3 kcal/mol. If the activation barrier for the reductive elimination is calculated as the energy difference between intermediate **3** and **TS(8–9)**, it is about 32.1 kcal/mol. Although the mass balance is implicitly taken into account by including the energies of appropriate species in the respective equations, modest differences in energies between these key steps in the mechanism makes definitive conclusions

rather difficult. Since the number of species involved is not identical in these steps, it would be more appropriate to suggest that the difference between the activation energies, with and without the inclusion of additives, is in line with the experimental observation (Scheme 3.1), irrespective of which one of the steps in the catalytic cycle is most directly affected.

3.11 Conclusions

We have studied the mechanism of the palladium acetate catalyzed *ortho*-amination of *N*-arylbenzamides with a focus on the role of additives: cesium fluoride and silver acetate. There are three key steps in the reaction: (i) C–H activation, (ii) N– O activation, and (iii) reductive elimination. The lowest-energy pathway for the reaction has been identified after considering a large number of intuitively attractive transition states for each of these steps. Other important results are the following:

1. $[Pd(\mu{-}OAc)_3Ag]$ is identified as the active catalyst that offers a cooperative effect between Pd and Ag throughout the catalytic cycle.

2. Cesium fluoride helps in deprotonation of the substrate as well as provides additional stabilization to the transition states.

3. The reaction proceeds through a Pd(II)–Pd(IV) cycle.

4. N–O activation at the palladium center is preferred over that of silver. This step results in the coordination of the -NR_2 group to Pd(IV). The -NR_2 is eventually transferred to the *ortho*-carbon of the phenyl ring.

5. The Pd–Ag interaction weakens prior to the reductive elimination step.

Our study provides molecular insights into the role of additives such as cesium fluoride and silver acetate in palladium-acetate-catalyzed reactions. The most putative active catalyst,

monomeric palladium acetate, results in higher-energy transition states than the proposed heterobimetallic [Pd(μ−OAc)$_3$Ag] species. The results offer a different perspective on the role of silver salts. The identification of the most likely mechanism by considering various pathways and configurations within each of intermediates and transition states suggest that silver salt additives have a direct impact on the relative energies of different stationary points. This research will not only encourage future experiments to establish the potential participation of heterobimetallic Pd–Ag species in homogeneous catalysis but also provides an impetus to the burgeoning area of multimetallic cooperative catalysis.

Chapter 4

New Insights on C–H Activation and Reductive Elimination in a dual C–H activation reaction[a]

[a]This chapter is adapted from Malakar, S.; Anand, M.; Verma, P.; Bhaskararao, B.; Prakash, P.; Schaefer III, H. F. and Sunoj, R. B. *(manuscript in preparation)*.

4.1 Abstract

Transition metal catalysis, embraced by both industry and academic researchers, involves a few fundamental mechanistic steps. In the contemporary practice of palladium catalysis, silver salt additives are the most frequently used. The molecular understanding of the role of additives in traditional transition metal catalysis continues to remain rather vague. In this report, we disclose an intriguing new and a potentially general role for silver salts, discovered through rigorous computational investigations on the two key mechanistic steps across six different reaction types. The C-H activation (sp^3 alkyl and sp^2 aryl C–H bonds) and reductive elimination steps in the mechanisms, with and without the explicit inclusion of silver additives in the respective transition states, have been examined. The inter-metallic Pd–Ag interaction is found to provide additional stabilization to the transition states for the C–H activation via a cyclometallation deprotonation (CMD) and for the reductive elimination steps. The pivotal role of silver salts in homogeneous catalysis is likely to manifest in the form of a Pd–Ag hetero-bimetallic species that facilitates an intermetallic electronic communication. The subtle and desirable change in the electronic features of the palladium center, where the reaction occurs, is ably modulated by the proximal silver atom. The findings could have very broad practical implications in the mechanism of transition metal catalysis and the current perceptions on the same.

4.2 Introduction

There have been many endeavors toward activating relatively inert C–H bonds in an aryl or an alkyl group of organic molecules by using transition metal catalysts.[188,254] This domain, popularly known as C–H activation, has witnessed an unprecedented growth in the last two decades.[255,256] Although converting inert hydrocarbons, aromatic or aliphatic, into more useful compounds through transition metal catalyzed C–H functionalization appeared a distant goal in the early days, it has became increasingly more amenable in recent times.[29,257] Today, transition metal catalysis pervades both academia and industry and is capable of providing difficult-to-access compounds as well as improved catalytic efficiency.[105,258] One of the most widely used transition metals in catalysis is palladium,[259] which offers significant versatility in its catalytic attributes.

The commonly found examples of homogeneous catalysis involving palladium are proposed to follow a few general mechanistic steps, such as oxidative insertion (as in a coupling reaction) and reductive elimination.[63,260] Although there could be other steps such as migratory insertion, depending on the nature of the reaction, the ones that are vital and of inherent interest are oxidative insertion and reductive elimination. It is equally important to consider that a C–H activation might as well go through a ligand assisted cyclometallation deprotoation (CMD) pathway.[217,261] In most cases, terminal oxidants are used in homogeneous transition metal catalysis to regenerate the catalyst or its active species. While a whole range of oxidants such as molecular oxygen, benzoquinone, potassium bisulphate are in use,[125,262–264] the most dominant oxidants are silver salts like silver acetate or silver triflate.[265,266]

An important question that continues to remain unanswered is the timing and mode of action of these silver salts in the catalytic cycle, especially on the catalyst itself. In a typical scenario wherein a Pd(0)/Pd(II) catalytic cycle is invoked, the action of oxidant is suggested

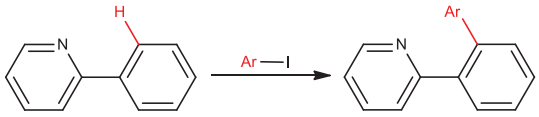
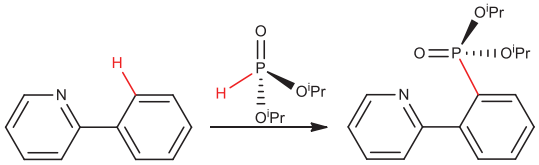
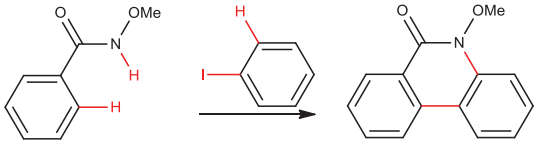
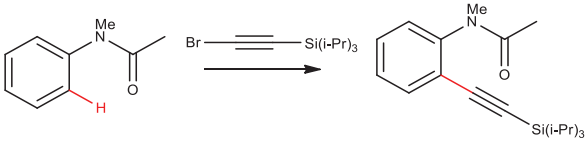
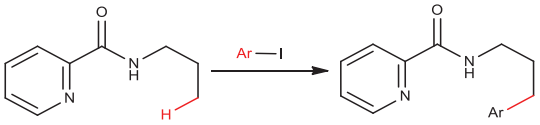
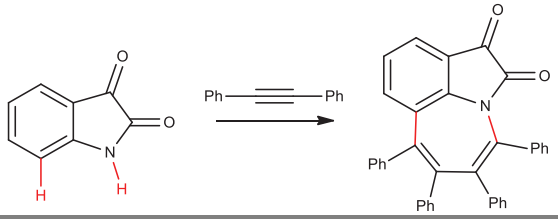
to occur in the catalyst regeneration step.[12] This premise would naturally imply a rather passive, or even no role, for such additives until the end of a given catalytic cycle, when the catalyst acquires a lower oxidation state through the reductive elimination step. Motivated by these serious lacunae, the fundamental question we wish to address through this study is whether the silver salts can be envisaged to play a more active role in the catalytic cycle than merely acting as a terminal oxidant. If so, how does it differ from the earlier or conventional mechanistic pathways in palladium catalysis?

In order to examine the molecular origin of how silver salt additives influence the vital steps in palladium catalysis, we have chosen a rich and diverse set of reactions, as shown in Table 4.1. Herein, we use modern computational tools to probe the role of silver by establishing the associated energetics of the reactions. Over the last couple of decades, computational studies have become an integral part of mechanistic investigations on transition metal catalysis. We use density functional theory computations using an appropriate solvent continuum relevant to each reaction, to locate the intermediates and transition states involved in the most important mechanistic events of these reactions. Further details of the computational methods is provided in the next section.

4.3 Computational Methods

Computations were performed using Gaussian09 suite of quantum chemical program.[138] The geometries were optimized by using the M06 hybrid density functional theory,[75] using Poples 6-31G** basis set for all atoms except for the heavy atoms. Los Alamos pseudopotential (LANL2DZ) basis set consisting of an effective core potential (ECP) for 28 core electrons and a double-ζ quality valence basis set for 18 valence electrons was employed for Pd atom, 28 core electrons and a double-ζ quality valence basis set for 19 valence electrons was employed for Ag atom, 46 core electrons and a double-ζ quality valence basis set for 7 valence electrons

Table 4.1: Palladium Acetate Catalyzed Reactions Involving C–H Activation and Reductive Elimination in the Presence Various Silver Salt Additives.

Sr.No.	Reaction	Silver Additive	Solvent	Temp.(°C)
1		AgOAc	AcOH	110
2		AgOAc	t-AmylOH	120
3		Ag_2O	AcOH	120
4		AgOTf	Toluene	70
5		AgOAc	Neat	130
6		AgOAc	DMF	120

was employed for I atom and 28 core electrons and a double-ζ quality valence basis set for valence electrons was employed for Br atom.[267–269] All the stationary points were characterized, as minima or a first-order saddle point (transition states) by evaluating the corresponding Hessian indices. The transition states were verified by examining whether it has a unique imaginary frequency representing the desired reaction coordinate. Intrinsic reaction coordinate (IRC) calculations were additionally carried out to further ascertain the true nature of the transition states that it connects to the reactants and products.[145,146] The geometries obtained as the end-points on the either side of the IRC trajectories were subjected to further optimization using a more stringent criteria by using opt = calcfc (as implemented in Gaussian09 program). This exercise enabled us to obtain the reactant and product such that their connection to the transition state could be established. All the stationary points were optimized at the $SMD_{(Solvent)}$/M06/6-31G**,LANL2DZ(Pd, Ag, I, Br) level of theory. The effect of a solvent continuum, was evaluated using the Cramer–Truhlar SMD continuum solvation model that employs quantum mechanical charge densities of solutes. The discussions in the text are presented by using the $SMD_{(Solvent)}$/M06/6-31G**,LANL2DZ (Pd, Ag, I, Br) level of theory.

4.3.1 Computation of Relative Energies

The energies of the transition states are computed with respect to the infinitely separated reactants. Depending on the nature of the intermediates or transition states, the reactants include palladium acetate, silver acetate, the substrates and other additives. The primary catalyst, palladium acetate, is known to exist as trimeric $Pd_3(OAc)_6$ species in several solvents employed in the title reactions. This prompted us to consider a more realistic trimeric palladium acetate as the reference point instead of a commonly used monomeric palladium acetate, which is of higher energy. When a monomeric species is considered as involved in any of the stationary points in the present study, the energy is deduced from the energy of

the trimeric $Pd_3(OAc)_6$ as one third energy of the trimer. The silver salt additive, silver acetate, is known to exist as polymeric $[Ag_2(OAc)_2]_n$ species in its solid state crystallographic structure. In summary, the Gibbs free energies of transition states are computed with respect to reference points - $Pd_3(OAc)_6$, $[Ag_2(OAc)_2]$.nX(Solvent/Additive) and the substrate. For the reaction **3**, silver acetate has been modeled as $Ag(OAc) \cdot 2\,AcOH$ because acetic acid is a polar solvent and has high dipole moment. Thus, it is highly likely that the polymeric structure of silver acetate and solvent molecules would coordinate to the silver center.

4.4 Results and Discussion

These reactions can broadly be classified as belonging to directed C–H activations, wherein the directing group helps bring the transition metal closer to the site of reaction. The choice of reactions **1** – **6**, as listed in Table 4.1, are guided by certain vital similarities, such as the use of palladium acetate and silver salt additives, and some interestingly desirable diversity in the reaction type. The prototypical directing groups such as pyridine, amide, and anilide are present in the substrates in reactions **1** – **3** and involve aryl sp^2(C–H) activations. A remote sp^3(C–H) activation in reaction **5**, dual aryl C–H activations in **3**, and cyclization in **6** are other notable features. These reactions can be chemically classified as alkenylation (**1**), phosphorylation (**2**), sp^2 arylation (**3**), alkynylation (**4**), sp^3 arylation (**5**), and oxidative cycloaddition (**6**). In addition, most of the final products or their variants has its own practical significance, either due to its potential biological activity or other importance. For example, the derivatives of product phenanthridinone obtained from reaction **3** are commonly found in quinoline, quinazoline, and acridone alkaloids (Figure 4.1).[47,270,271]

While the mechanisms of these reactions are of inherent interest and could present different levels of complexities, herein we focus on two of the most important steps in these

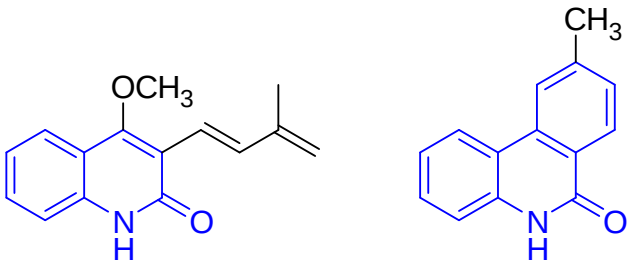
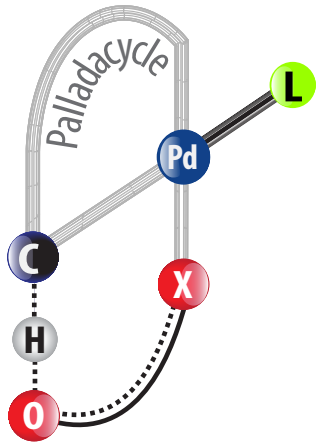


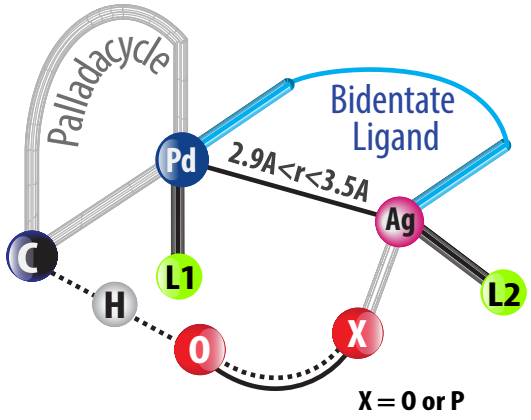
Figure 4.1: Natural products containing phenanthridinone moeity.

reactions, namely, cyclometallation deprotonation (CMD) and reductive elimination.[272,273] In a CMD process, one of the ligands bound to the transition metal assists in C–H deprotonation and results in a concomitant formation of a cyclometallated intermediate, as illustrated in Figure 4.2. Furthermore, both CMD and RE are often considered as capable of being the rate determining steps in catalytic reactions.[201,274] First, the catalytic action of palladium acetate in each of these steps is examined by locating the corresponding transition states, all in the absence of the silver additive. Then, silver acetate or silver triflate is explicitly included in the respective transition states to probe whether the additive could participate more actively in dictating the energetic course of the reaction.

As the silver salt could interact with different binding sites of the substrate, a rigorous sampling of different configurations in the transition states is performed so as to identify the most preferred pathway. The discussions in this chapter employ only the lowest energy intermediates and transition states thus obtained. During the course of geometry optimizations, performed as part of the configuration sampling, we noticed a systematic tendency for the silver atom to drift closer to the palladium across all these reaction types (**1**–**6**). Further sampling of the lower energy transition states helped us identify an interesting Pd–Ag hetero-bimetallic interaction, as shown in Figure 4.2 and Figure 4.3. Although the catalytic attributes of d^8-d^{10} hetero-bimetallic complexes are only rarely documented,[202,275] crystal

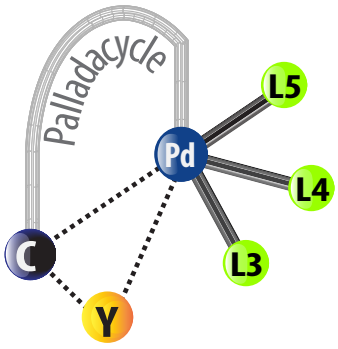


Rxn	L	O...X
1	AcO^-	AcO^-
2	$(OMe)_2PO^-$	$(OMe)_2PO$
3	AcOH	AcO^-
4	$CF_3SO_3^-$	AcO^-
5	AcO^-	$-CC_4H_4N$
6	$\eta^2(C{=}C)$	AcO^-



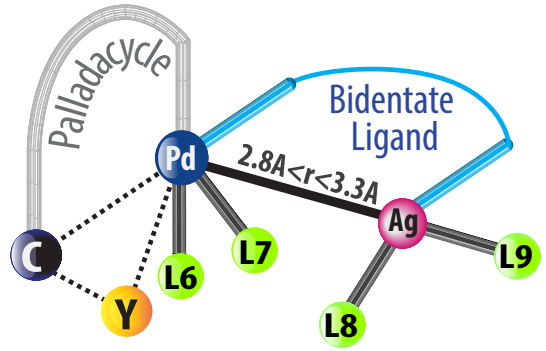
Rxn	L1	L2	O...X	$\cap$
1	AcO^-	Pyridine	AcO^-	CO_3^{2-}
2	$(OMe)_2PO^-$	AcOH	$(OMe)_2PO^-$	$(OMe)_2PO^-$
3	AcO^-	AcOH	AcO^-	AcO^-
4	AcO^-	AcO^-	$CF_3SO_3^-$	$CF_3SO_3^-$
5	AcO^-	AcOH	AcO^-	AcO^-
6	$\eta^2(C{=}C)$	AcOH	AcO^-	AcO^-

Figure 4.2: A generalized representation of cyclometallation deprotonation (CMD) transition states with a monometallic and a hetero-bimetallic catalysts.



$Y = CR_2, PR'_3$

Rxn	L3	L4	L5
1	AcO^-	–	–
2	BQ	–	–
3	AcOH	AcOH	I^-
4	AcOH	$CF_3SO_3^-$	Br^-
5	–	–	I^-
6	AcOH	AcOH	–



$Y = CR_2, PR'_3$

Rxn	L6	L7	L8	L9	
1	AcO^-	–	AcO^-	–	HCO_3^-
2	–	–	$(OMe)_2P(OH)$	–	$(OMe)_2PO^-$
3	I^-	–	AcOH	AcOH	AcO^-
4	Br^-	AcOH	$CF_3SO_3^-$	–	AcO^-
5	–	–	I^-	–	AcO^-
6	–	–	AcOH	AcOH	AcO^-

Figure 4.3: A generalized representation of reductive elimination (RE) transition states with a monometallic and a hetero-bimetallic catalysts.

structures of related compounds have earlier been reported.[173,224,276] The energetic comparison between the conventional and the refined transition states with Pd–Ag hetero-bimetallic interaction are presented in the following sections.

The initial catalyst-substrate complex in all these reactions helps bring the palladium center to a suitable orientation such that the palladium-bound acetate engages in a cyclometallation deprotonation (CMD). The catalyst–substrate complexes are found to be of much lower energy in the case of hetero-bimetallic species as compared to the corresponding complexes with the monomeric palladium acetate.[b] Such an energetic advantage can be regarded as offering a thermodynamic impetus toward a lower energy pathway involving hetero-bimetallic Pd-Ag species.

An important question is whether the key transition states enjoy any advantage through a hetero-bimetallic interaction. A generalized representation of the CMD and RE transition states is provided in Figure 4.2 and Figure 4.3. The energetics between the conventional monometallic and the refined hetero-bimetallic pathways for the reactions **1**-**6** are compared by using the graphical summary of the relative energies of the CMD and RE transition states (Figure 4.4). It can be noticed that the presence of Pd–Ag interaction generally leads to lower energy transition states compared to their mono-metallic analogue. Depending on the nature of the reaction, the extent of transition state stabilization for the CMD and RE steps is different. For instance, the largest stabilization to a CMD transition state is noticed in the case of the phosphorylation reaction (**2**) whereas the alkenylation reaction (**1**) shows the most pronounced effect in the RE step.

The details on how the most preferred transition states were identified in this study are vital at this juncture. Under the reaction condition, several ligand combinations around palladium and silver are likely, in addition to the nature of the bimetallic bridging ligand. In Figure 4.5, we provide a subset of such ligand combinations around the metal, chosen from

[b]See Figure C.1 in the Appendix C.

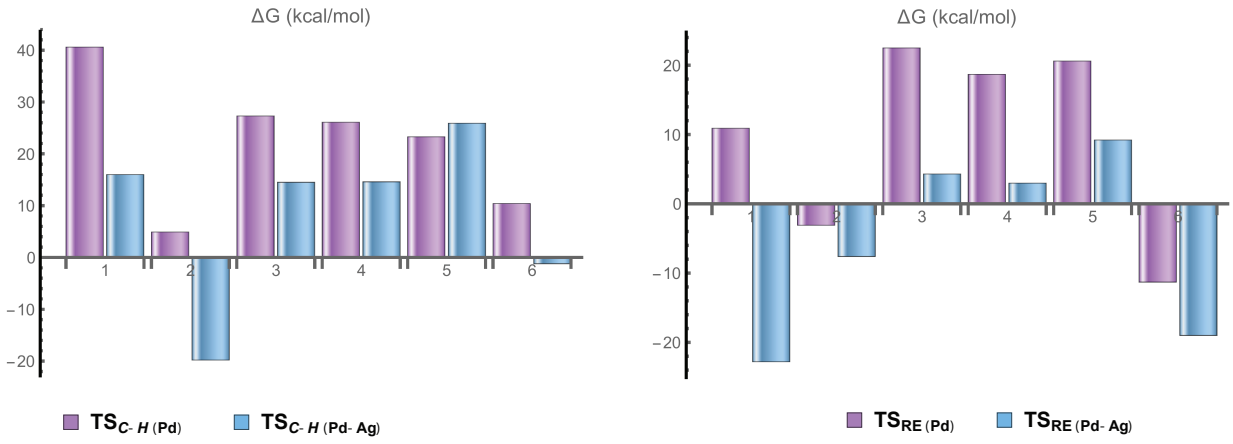


Figure 4.4: Relative Gibbs free energies of monometallic (in purple) and hetero-bimetallic pathways (blue) for C–H activation (via cyclometallation deprotonation) and reductive elimination computed with respect to the infinitely separated reactants. The numbers **1** to **6** refer to different reactions as shown in Table 4.1.

a larger set of such possibilities, by using the dual *aryl* C–H activation (**3**) as an illustrative example. As shown in Table 4.1, the reaction involves the use of phenyl iodide, silver oxide, and acetic acid as the solvent. Silver oxide combines with acetic acid to give silver acetate and water.[277] It may be noticed that the acetate bridged Pd–Ag is the most preferred ligand combination for the CMD step (Figure 4.5) with the acetate bound to palladium abstracting the *ortho*-hydrogen of the phenyl ring. In the lowest energy RE transition state palladium and silver are bridged by an acetate and an iodide ligand (Figure 4.6). We have also carried out similar analyses for other reactions and find that the results are of general applicability.

After identifying the most preferred transition states, we became more interested in rationalizing the predicted trends. In an effort to identify the origin of the transition state stabilization with the Pd–Ag bimetallic species, the structural and electronic features are analyzed. The comparison of the transition state geometries between the mono-metallic and the hetero-bimetallic situations for the CMD pathway points to a diminished strain in

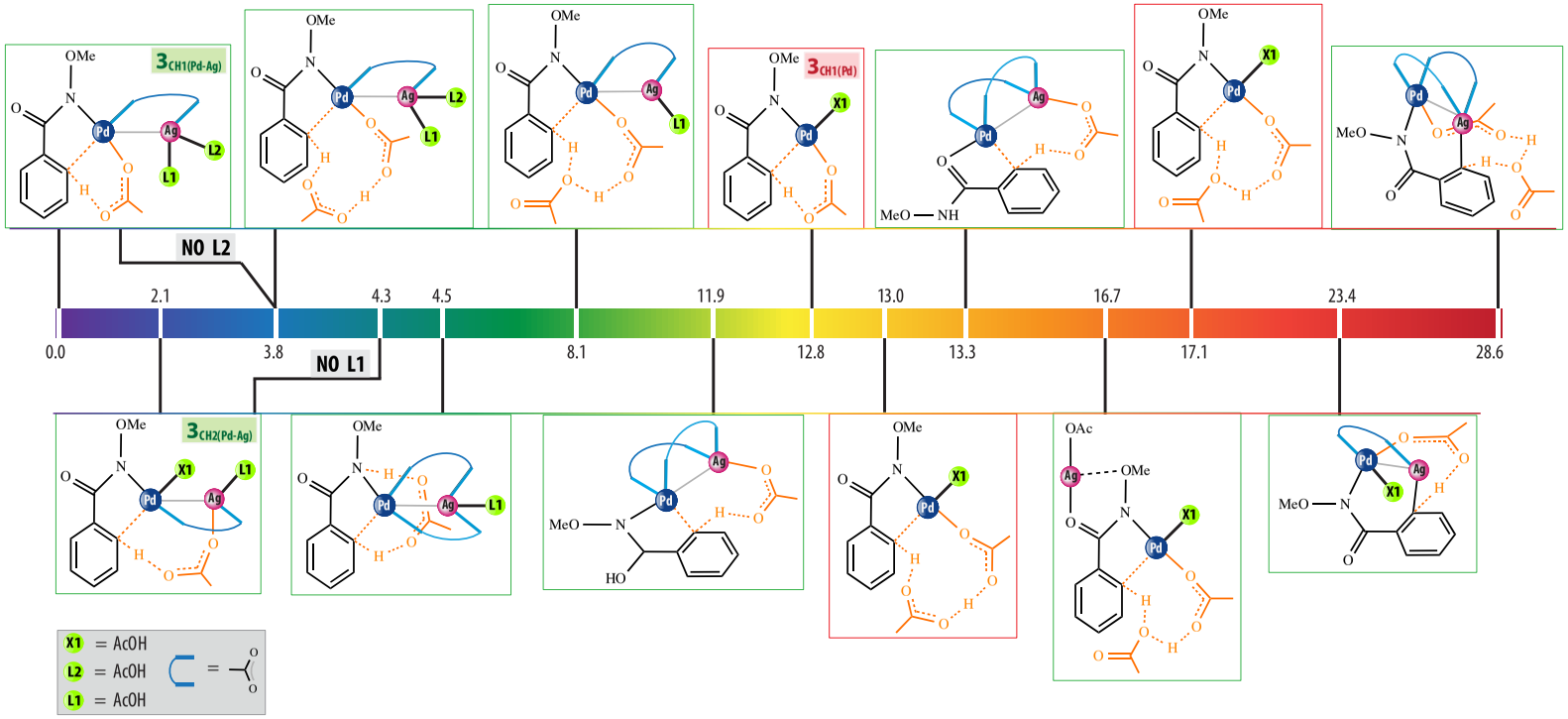


Figure 4.5: Important ligand combinations considered in the CMD transition states in the case of dual aryl C–H activation reaction (**3**). The relative energies of transition states shown in the stacking are in kcal/mol. Note that it is the carbonyl oxygen of **X1**, **L1**, and **L2** that coordinates to the metal.

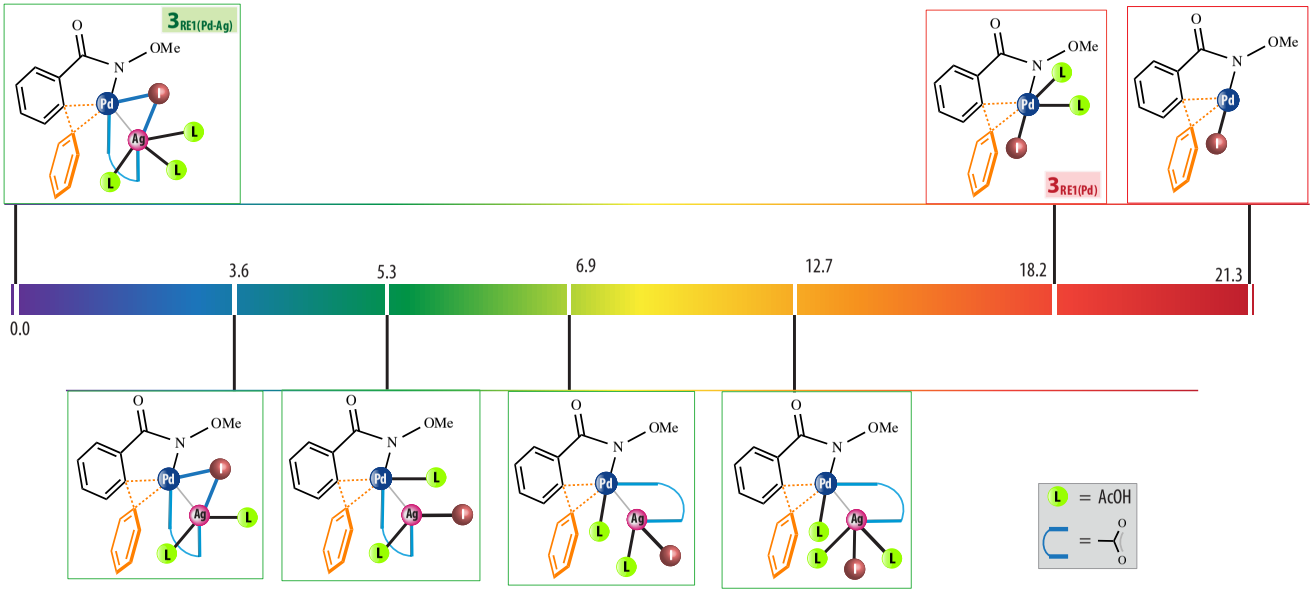


Figure 4.6: Important ligand combinations considered in the CMD transition states in the case of dual aryl RE activation reaction (**3**). The relative energies of transition states shown in the stacking are in kcal/mol. Note that it is the carbonyl oxygen of **X1**, **L1**, and **L2** that coordinates to the metal.

the latter. This is presumably due to the fact that a distant silver-bound ligand facilitates the CMD in the hetero-bimetallic case, whereas in the mono-metallic analogue a proximal palladium-bound ligand is the one that is responsible for the CMD through a relatively more strained transition state (Figure 4.2). This is more vivid if we compare the seven-membered transition state $\mathbf{3_{CH2(Pd\text{-}Ag)}}$ about 10.7 kcal/mol lower in energy than the six-membered transition state $\mathbf{3_{CH1(Pd)}}$ (Figure 4.5).

Without the premise of relative free energies of transition states (with and without silver additive), the logical way of lowering the energy of transition state $\mathbf{3_{CH1(Pd)}}$ (Figure 4.6) would be to bring structural (or electronic) changes that would facilitate the abstraction of *ortho*-hydrogen of the phenyl ring. This can be done by further weakening the *ortho*-C–H bond, and thereby improving the interaction of palladium with the σ^* (C–H) bond. Fallout of this would reduce the distance between the *ortho*-hydrogen and the oxygen of the pendent acetate. The transition state $\mathbf{3_{CH1(Pd\text{-}Ag)}}$ precisely displays such structural changes when compared to $\mathbf{3_{CH1(Pd)}}$ where the Pd···H and O···H distances reduce by 0.035 Å and 0.023 Å units (Figure 4.7). Since the transition state $\mathbf{3_{CH1(Pd\text{-}Ag)}}$ shows reduced strain compared to $\mathbf{3_{CH1(Pd)}}$ in spite of being six-membered, it alludes that the Pd–Ag electronic interaction may also contribute to the geometric relaxation of the transition state. We next looked at the palladium *d*-orbital occupancies and charges on it under these two scenarios.

The comparison of the electronic features between these two major modes of CMD and RE transition states offers additional insights. In general, the proton of the C–H bond that is being activated acquires more protic character as compared to the corresponding monometallic counterpart. Additionally, the aryl carbon tends to be more nucleophilic in both CMD and RE transition states. The data in Table 4.2 and Table 4.3 for the representative dual aryl C–H activation reaction **3** demonstrates the same. In fact, occupancies of palladium *d*-orbitals of $\mathbf{3_{CH1(Pd\text{-}Ag)}}$ and $\mathbf{3_{RE1(Pd\text{-}Ag)}}$ also get influenced in the presence of silver when compared with $\mathbf{3_{CH1(Pd)}}$ and $\mathbf{3_{RE1(Pd)}}$ respectively (Table 4.4 and Table 4.5).

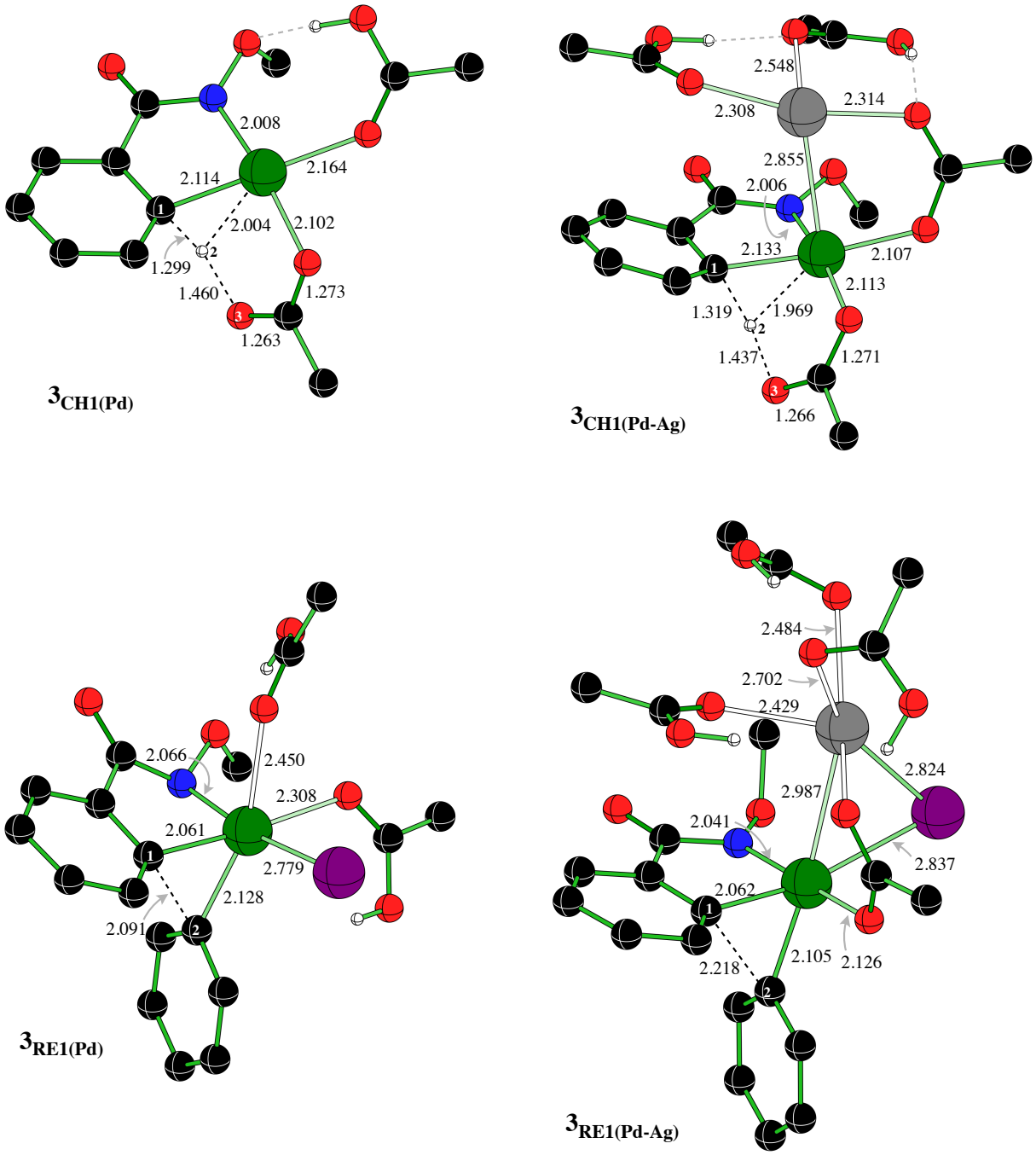


Figure 4.7: Optimized geometries of CMD and RE transition states for dual aryl C–H activation (reaction-**3**), respectively, without (a) and with (b) the involvement of silver salt in the transition state. The relative Gibbs free energies (in kcal/mol) are provided in parentheses.

Table 4.2: Natural population analysis (NPA) charges on the carbon, hydrogen, and oxygen atoms involved in the reaction coordiante of the CMD transition states for reaction **3**.

TS	Atom	Charge on center	Relative Charge on center
$\mathbf{3}_{\mathbf{CH1(Pd)}}$	C1	-0.374	0.000
	H2	0.404	
	O3	-0.720	
$\mathbf{3}_{\mathbf{CH1(Pd—Ag)}}$	C1	-0.356	+0.018
	H2	0.405	+0.001
	O3	-0.726	-0.006

Table 4.3: Natural population analysis (NPA) charges on the carbon, hydrogen, and oxygen atoms involved in the reaction coordiante of the CMD transition states for reaction **3**.

TS	**Reductively Eliminating Center**	**Charge on Center**	**Relative Charges**
$\mathbf{3}_{\mathbf{RE1(Pd)}}$	C1	-0.042	0.000
	C2	-0.028	
$\mathbf{3}_{\mathbf{RE1(Pd—Ag)}}$	C1	-0.031	-0.003
	C2	0.009	+0.051

Table 4.4: Electron occupancies in palladium *d*-orbitals in the CMD transition states.

TS	**Orbitals Involved**	**Occupancy**	**Relative Occupancy**	**Overall occupancy**
$\mathbf{3}_{\mathbf{CH1(Pd)}}$	d(xy)	1.961	0.000	8.931
	d(yz)	1.971		
	d(xz)	1.963		
	$d(x^2-y^2)$	1.101		
	$d(z^2)$	1.935		
$\mathbf{3}_{\mathbf{CH1(Pd—Ag)}}$	d(xy)	1.921	-0.040	8.925
	d(yz)	1.943	-0.028	
	d(xz)	1.680	-0.283	
	$d(x^2-y^2)$	1.445	+0.344	
	$d(z^2)$	1.936	-0.001	

Table 4.5: Electron occupancies in palladium *d*-orbitals in the RE transition states evaluated on SMD_{AcOH}/M06/6-31G**,LANL2DZ(Pd,Ag,Br,I).

TS	Orbitals Involved	Occupancy	Relative Occupancy	Overall occupancy
$\mathbf{3}_{\mathbf{RE1(Pd)}}$	d(xy)	1.779	0.000	8.913
	d(yz)	1.647		
	d(xz)	1.864		
	$d(x^2-y^2)$	1.789		
	$d(z^2)$	1.834		
$\mathbf{3}_{\mathbf{RE1(Pd—Ag)}}$	d(xy)	1.937	+0.158	8.870
	d(yz)	1.417	-0.230	
	d(xz)	1.972	+0.108	
	$d(x^2-y^2)$	1.701	-0.088	
	$d(z^2)$	1.843	-0.009	

The topological analysis of the electron density using Baders theory of Atoms-In-Molecule (AIM) indicates the presence of an intermetallic interaction.[c] The bond critical points were identified between Pd and Ag for the lowest energy transition states of all the 6 reactions with electron densities (ρ) in the range of 1.59 to 3.55 (x 10^{-2} a.u.), comparable to other known weak interactions.[278–281] Figure 4.8(a) shows the bond critical point between palladium and silver in $\mathbf{3}_{\mathbf{CH1(Pd\text{-}Ag)}}$ and compared with that of a known palladium silver complex bridged by acetate ligands (Figure 4.8(b)).[173] Similarly, an important Kohn-Sham molecular orbital that corresponds to the primary interaction between the Pd and Ag atoms is also identified (Figure 4.9). Thus, an electronic communication between the metal centers is conspicuous in the Pd–Ag hetero-bimetallic transition states.

[c]See section **C.1** in appendix **C** for detailed description of AIM analysis.

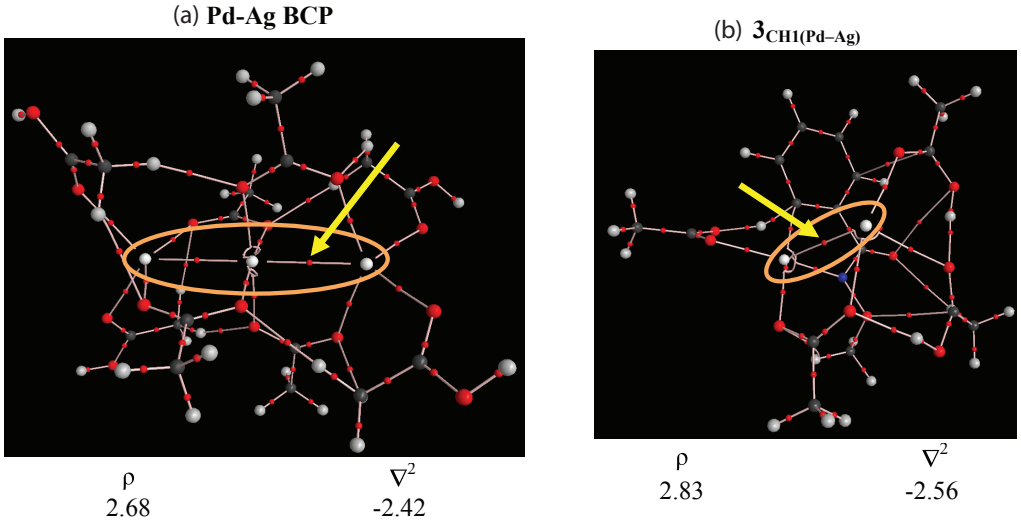


Figure 4.8: Identification of Pd-Ag bond critical points at the M06/6-31G**(LANL2DZ=Pd, Ag) level of theory (a) using the geometry as noted in the crystal structure obtained from the CCDC[173] and (b) the $\mathbf{3}_{\mathbf{CH1(Pd\text{-}Ag)}}$ transition state.

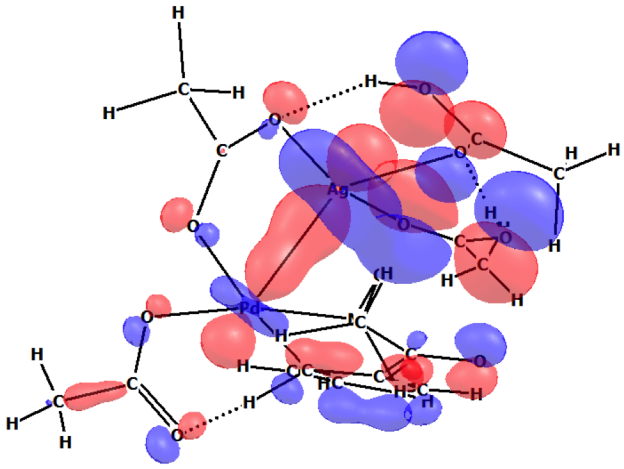


Figure 4.9: Kohn-Sham orbitals depicting the Pd–Ag interaction in the most preferred CMD transition states for the dual aryl C–H activation reaction **2**.

4.5 Conclusions

We have identified a molecular interaction between the catalyst and the silver salt additives in the critical transition states for a set of six different palladium acetate catalyzed sp^3-alkyl and sp^2-aryl C–H bond activation reactions. An intermetallic Pd–Ag interaction is identified as vital in the most preferred mechanistic pathway, suggesting that silver salts are involved throughout in the catalytic cycle, not just as terminal oxidants. While the diminished strain helps stabilize the cyclometallation deprotonation transition states, the improved electronic communication between Pd and Ag is concluded to be as responsible for a relatively more favorable reductive elimination via the bimetallic transition states. The insights obtained through a set of six different C-H activation reactions are expected to have a broader and general applicability in transition metal catalysis.

Chapter 5

Conclusions

We have investigated detailed mechanisms of seven catalytic reactions conducted in different solvents using palladium acetate as the primary TM catalyst and silver salts as additives. The primary focus of this study is to find the plausible role of silver additives at the molecular level. Density functional theory is employed to locate the transition states and the intermediates for each of these reactions. The C–H activation and the reductive elimination steps are recognized as the most relevant steps in the reaction. The chapters 2 and 4, emphasize mainly on these two sections of the overall reactions mechanism.

In chapter 2, we have reported an extensive study on possible C–H activation transition states of the palladium acetate catalyzed Yu's amination reaction[53] between *N*–arylbenzamide and *O*–benzoyl hydroxylpiperidine with DCE as the solvent and additives - AgOAc and CsF. The lowest energy transition state (**TS5**) was identified to have a Pd–Ag bond where the silver bound acetate in the active catalyst [Pd(μ−OAc)$_3$Ag] abstracts the *ortho*-hydrogen from the substrate (*N*–arylbenzamide). Cesium flouride deprotonates the nitrogen of the substrate to form activated metal amidate species in the beginning of the reaction.

Interestingly, the heterobimetallic Pd–Ag interaction is maintained throughout the catalytic cycle in this amination reaction. This forms the basis for our discussion in chapter 3. We located all conceivable transition states for other steps (15 for N–O activation and 17 for RE) and proposed a plausible lowest energy pathway for the reaction with [Pd(μ−OAc)$_3$Ag] as the active catalyst. The breaking of N–O bond of the *O*–benzoyl hydroxylpiperidine is preferred at the palladium center while maintaining the palladium–silver bond using one acetate bridging ligand.

Encouraged by these findings, we tested our hypothesis on 6 other reactions to understand if the Pd–Ag interaction is a general phenomena in catalytic reactions where palladium acetate and silver salts are used as the main catalyst and additives, respectively (chapter 4). We performed an exhaustive search for all imaginable transition states for C–H activation and reductive elimination steps of each of these reactions. The discussion of this chapter is built on the final results of dual C–H activation reaction **3** resulting in the formation of phenanthridinones.[277] The computed relative free energies unequivocally demonstrate the existence of Pd–Ag interaction in the energetically most favored transition states for the C–H activation and RE steps of these reactions. The structural analysis of these TSs reveal reduced strain in the presence of silver additive.

To the best of our knowledge, even though complexes containing Pd–Ag bonds are well known, their role in homogenous catalysis, as proposed in this study has never been considered. Our results advocate the existence of hetero-bimetallic (Pd–Ag) cooperativity in reactions using palladium acetate and silver salts as additives. These findings could have direct implications toward the design of newer catalysts with improved efficiency which can give better yield with low catalyst loading under mild conditions and less number of additives. Some of the future directions where this idea can be extended would involve studies with different combinations of TMs, and other bridging ligands such as triflate, carbonate, iodide, bromide, etc.

Appendices

Appendix A

For Chapter 2

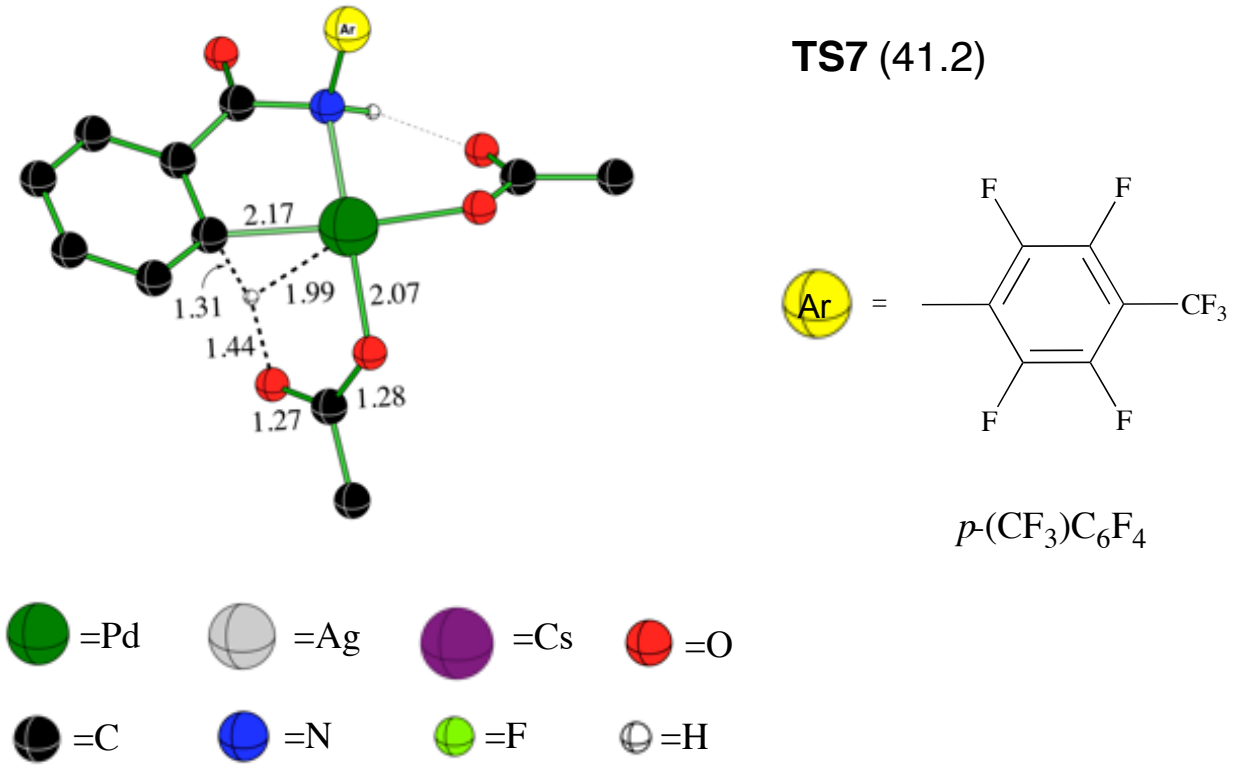


Figure A.1: C-H activation transition state without N-H activation. The values in parenthesis are Gibbs free energies (in kcal/mol). The numbers in parentheses is the Gibbs free energies in kcal/mol at PCM_{DCE}/M06/6-31+G**,LANL2DZ(Pd,Ag,Cs)//PCM_{DCE}/B3LYP/6-31G**(LANL2DZ) with respect to the infinitely separated reactants.

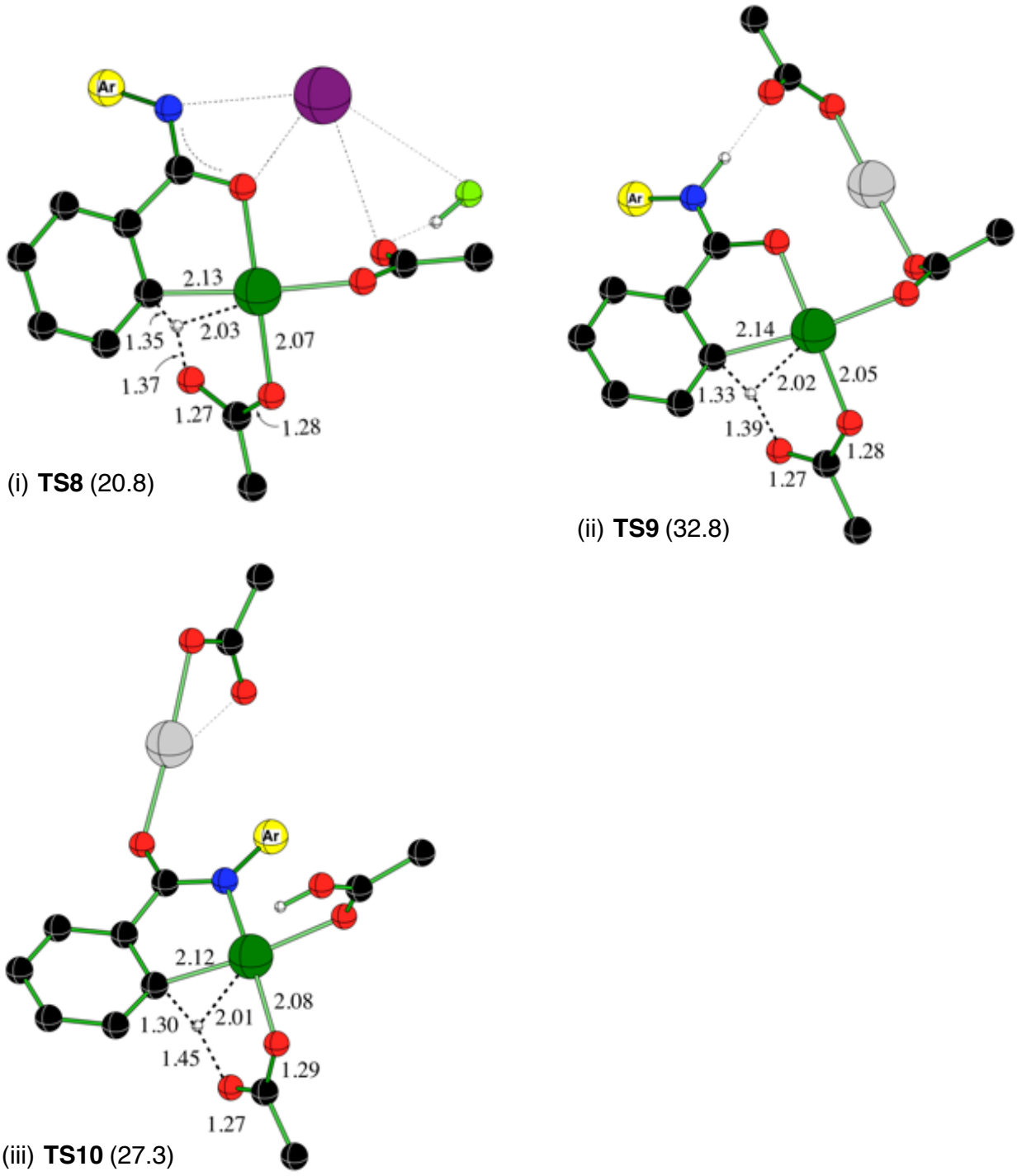
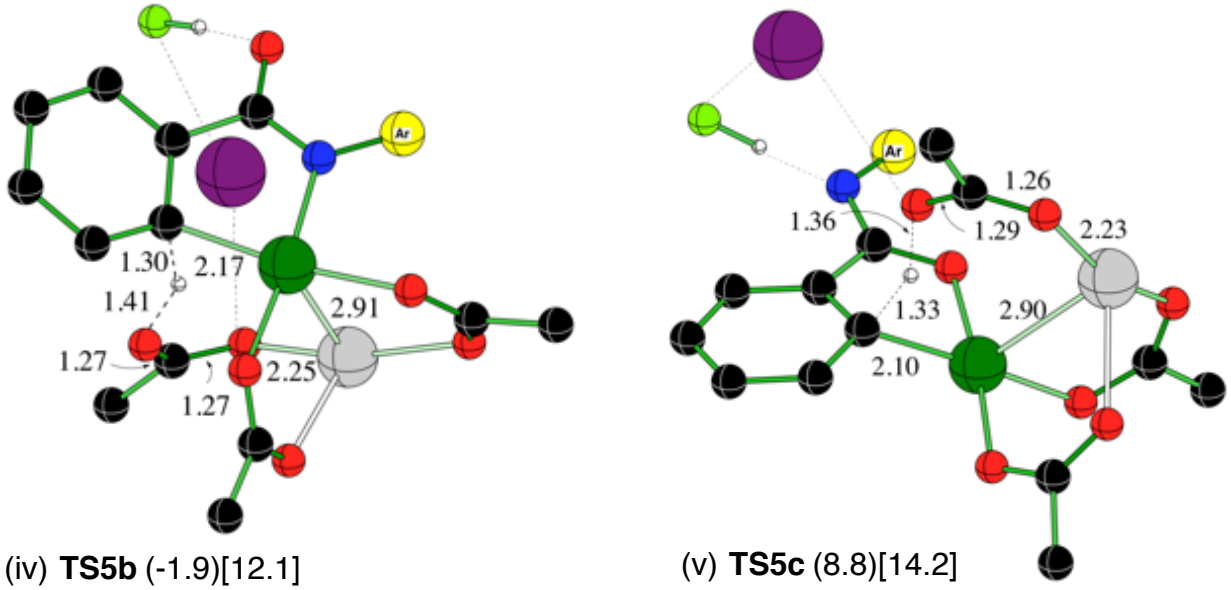
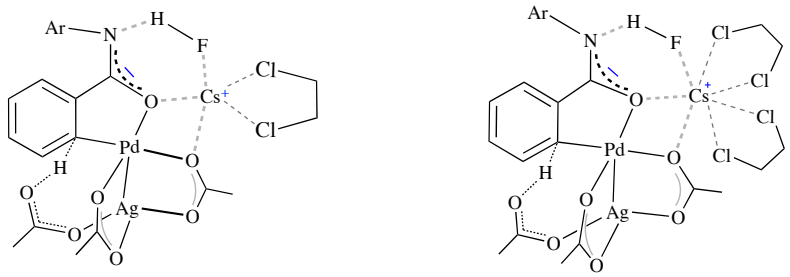


Figure A.2: (i-iii) Alternative higher energy C–H activation transition states wherein only one of the additives (either CsF or AgOAc) along with the primary catalyst palladium acetate is involved.



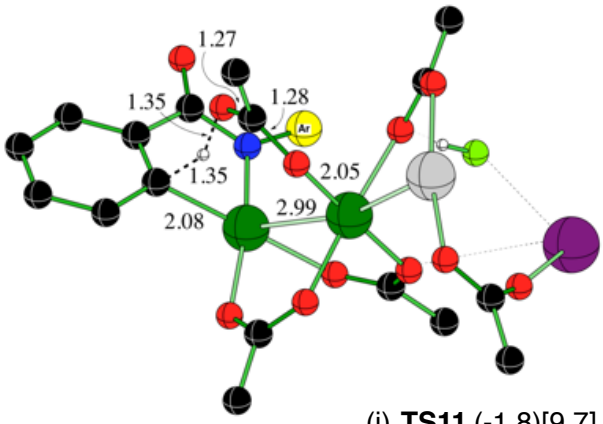
(iv) **TS5b** (-1.9)[12.1] (v) **TS5c** (8.8)[14.2]

Figure A.2: (iv-v) **TS5b** and **TS5c** are higher energy transition states involving palladium acetate and both additivies. [Pd(μ−OAc)$_3$Ag] is the active catalyst in (iv) and (v). The values in parentheses are Gibbs free energies (in kcal/mol). For **TS5b** and **TS5c**, the free energy barriers, with respect to the preceding intermediates, are also provided (in kcal/mol) in square brackets.

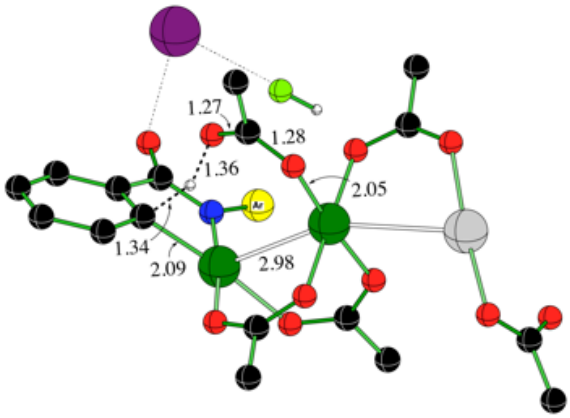


(i) **TS5$_{1DCE}$** (11.9) (ii) **TS5$_{2DCE}$** (18.9)

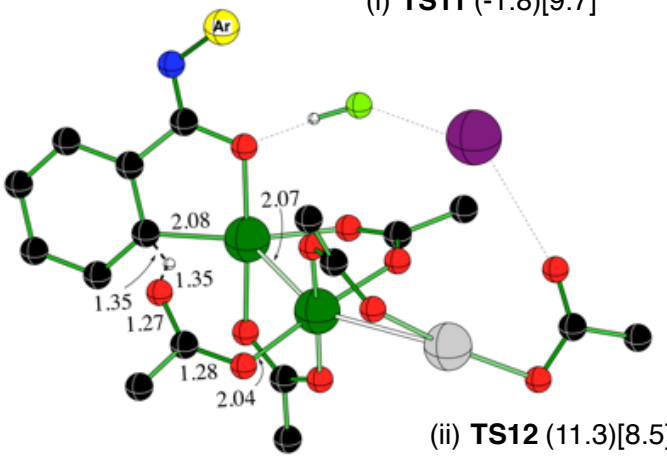
Figure A.3: Representative C–H activation transition states with (i) 1, and (ii) 2 solvent (1,2-Dichlororethane) molecules. The numbers in parentheses are relative free energies in kcal/mol with respect to the infinitely separated reactants



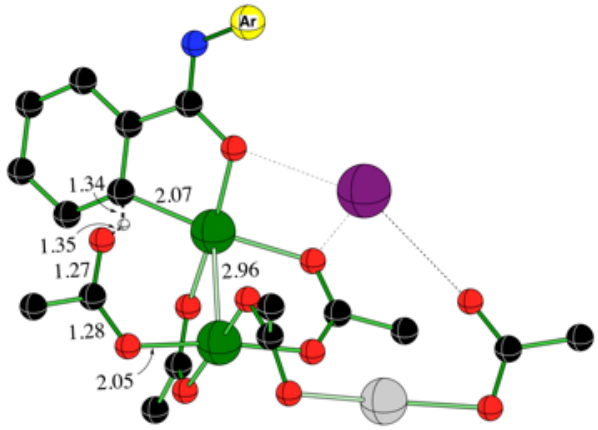
(i) **TS11** (-1.8)[9.7]



(iv) **TS14** (9.7)[10.7]



(ii) **TS12** (11.3)[8.5]



(iii) **TS13** (12.5)[14.1]

Figure A.4: C-H activation transition state with hetero-trimeric (Pd-Pd-Ag) complex as the catalyst. The values in parentheses are Gibbs free energies (in kcal/mol). The free energy barriers with respect to the corresponding preceding intermediates are provided (in kcal/mol) in square brackets.

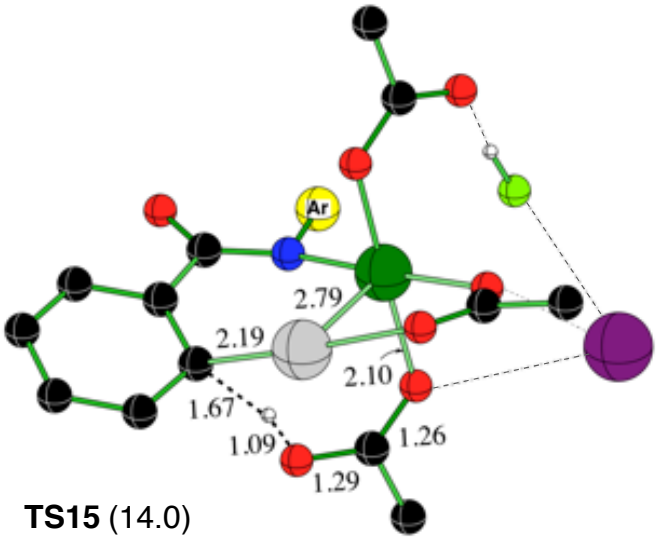


Figure A.5: C-H activation transition state with the position of palladium and silver interchanged such that the silver is closer to the ortho carbon and acetate bound to palladium abstracts the proton.

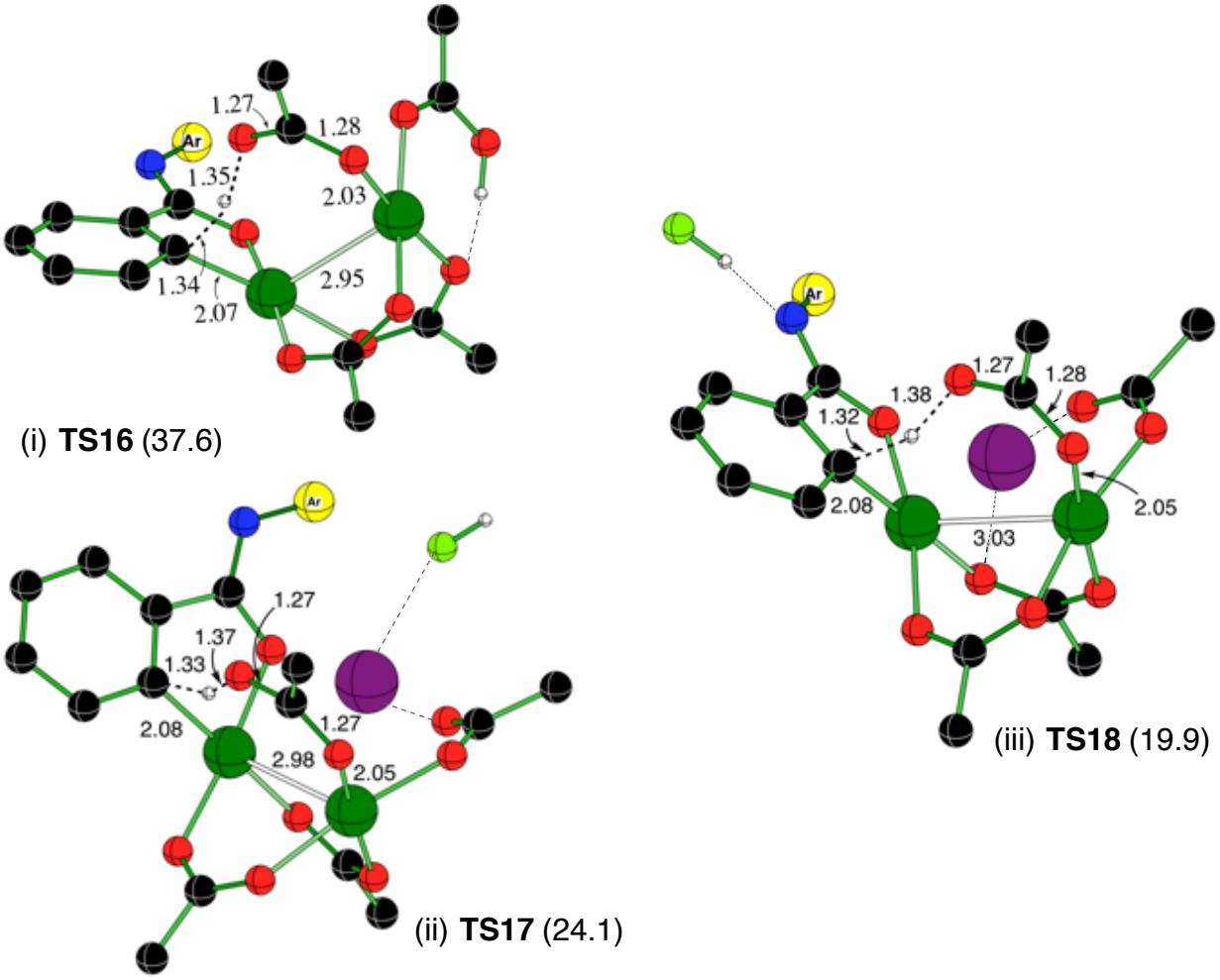


Figure A.6: (i) C–H activation transition state with homodimer $Pd_2(OAc)_4$ as the catalyst. (ii) C-H activation transition state with homodimer $Pd_2(OAc)_4$ as the catalyst in presence of cesium fluoride.

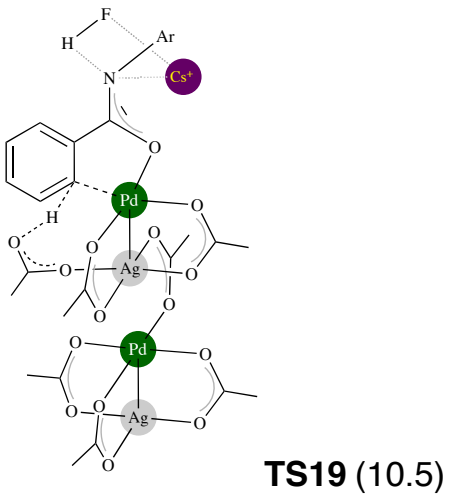


Figure A.7: A transition state involving two Pd-Ag species.

Appendix B

For Chapter 3

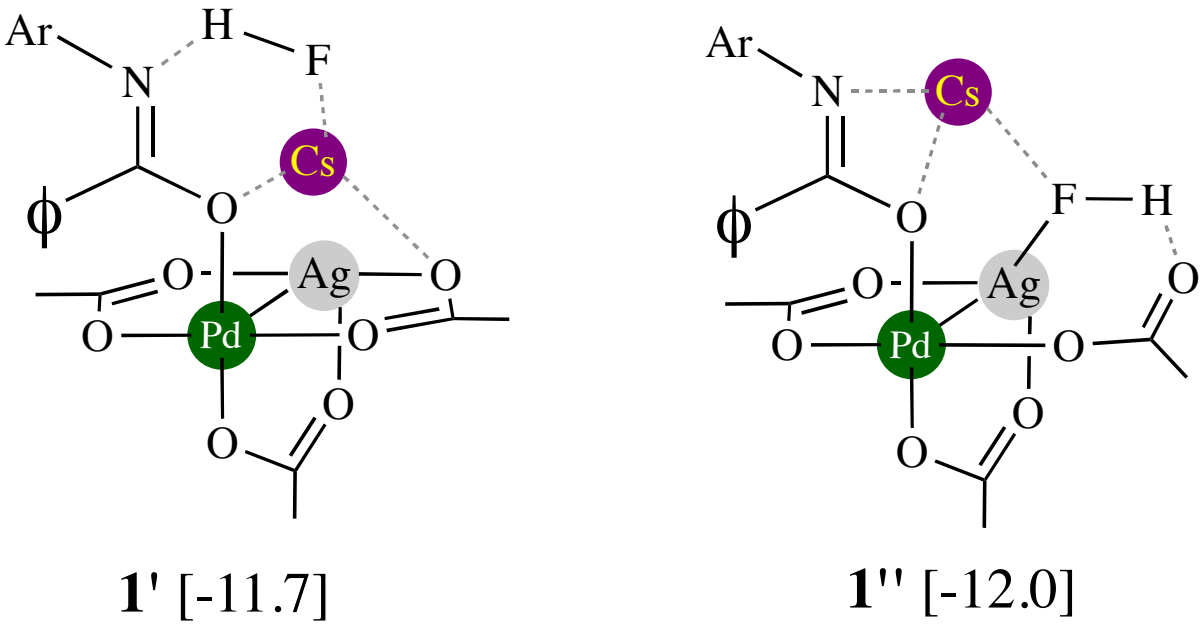


Figure B.1: Higher energy catalyst substrate adducts with same stoichiometry as intermediate **1**. The numbers in brackets are relative free energies in kcal/mol at PCM_{DCE}/M06/TZVP,def2-TZVP(Pd,Ag,Cs)//PCM_{DCE}/B3LYP/6-31G**(LANL2DZ) with respect to the infinitely separated reactants.

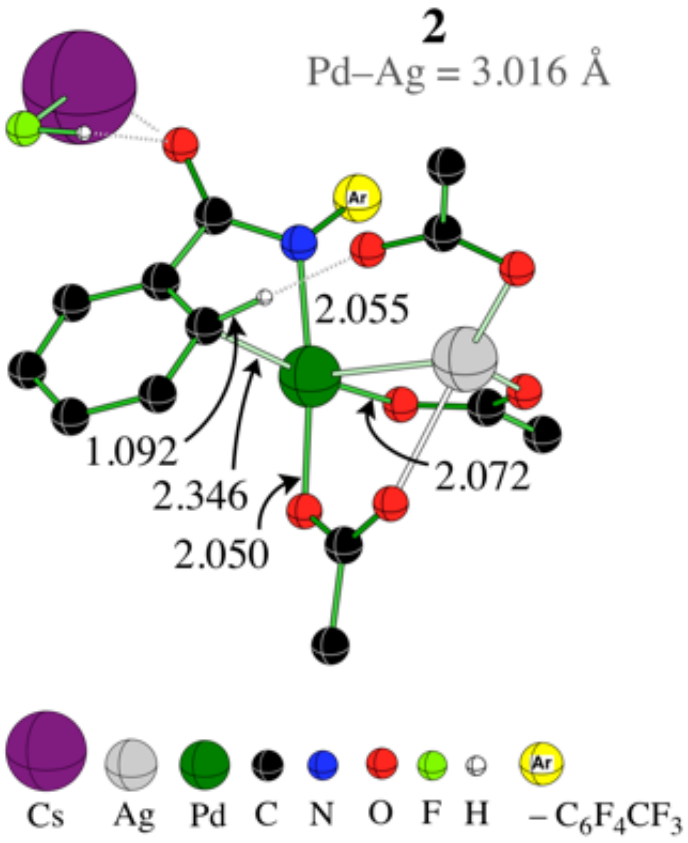


Figure B.2: Geometric details of intermediate **2**. All the bond distances are in angstroms. Most hydrogen atoms are removed for clarity.

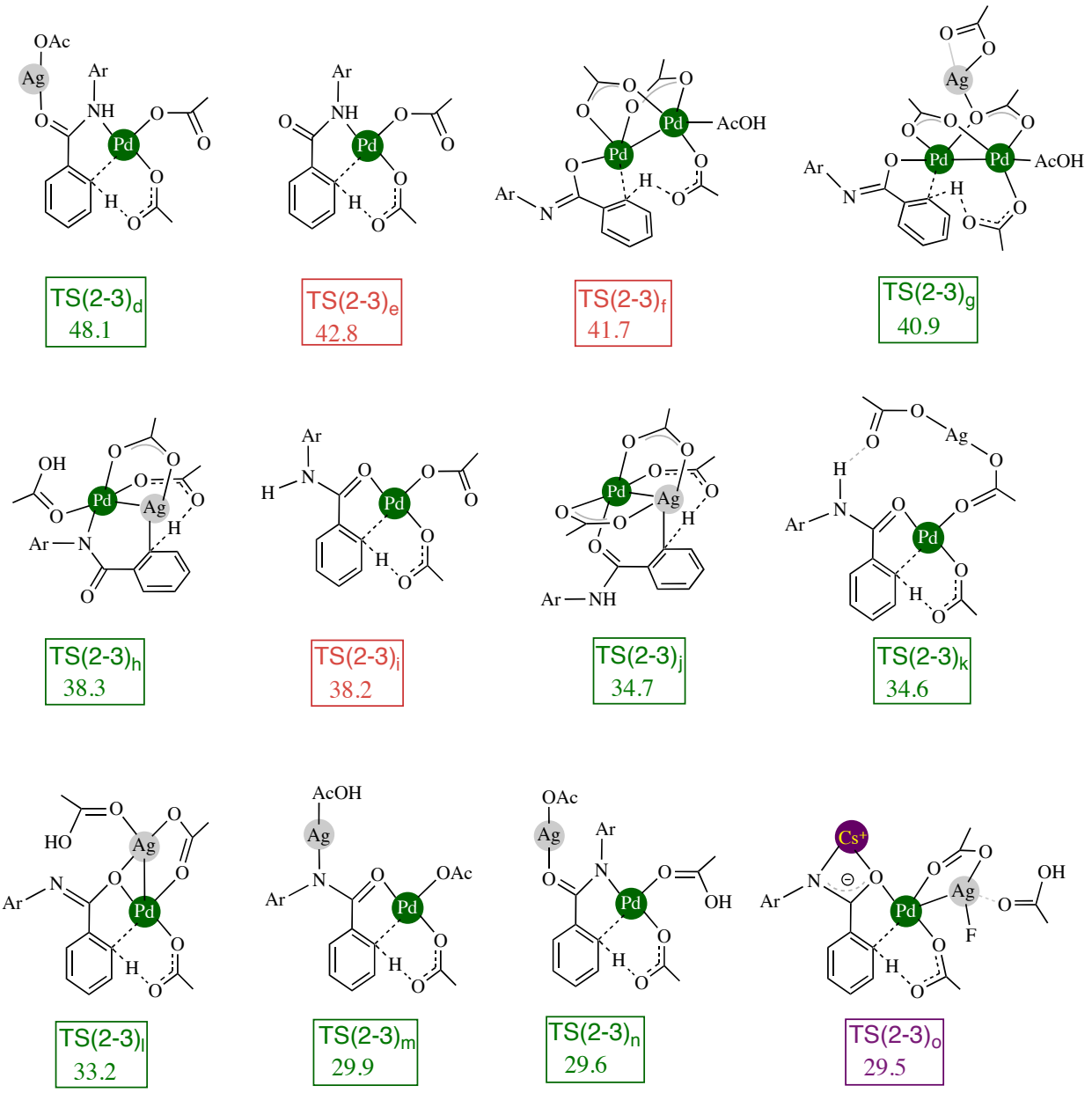


Figure B.3: C–H activation transition states plotted in Figure 3.1. The boxes with red, green, and blue colors indicate TSs with no additives, silver acetate, and cesium fluoride, respectively as additives. Pink colored boxes are for TSs with both - silver acetate and cesium fluoride as additives. The number in boxes are relative free energies of transition states with respect to infinitely separated reactants at PCM_{DCE}/M06/TZVP (def2-TZVP)//PCM_{DCE}/B3LYP/6-31G**(LANL2DZ)

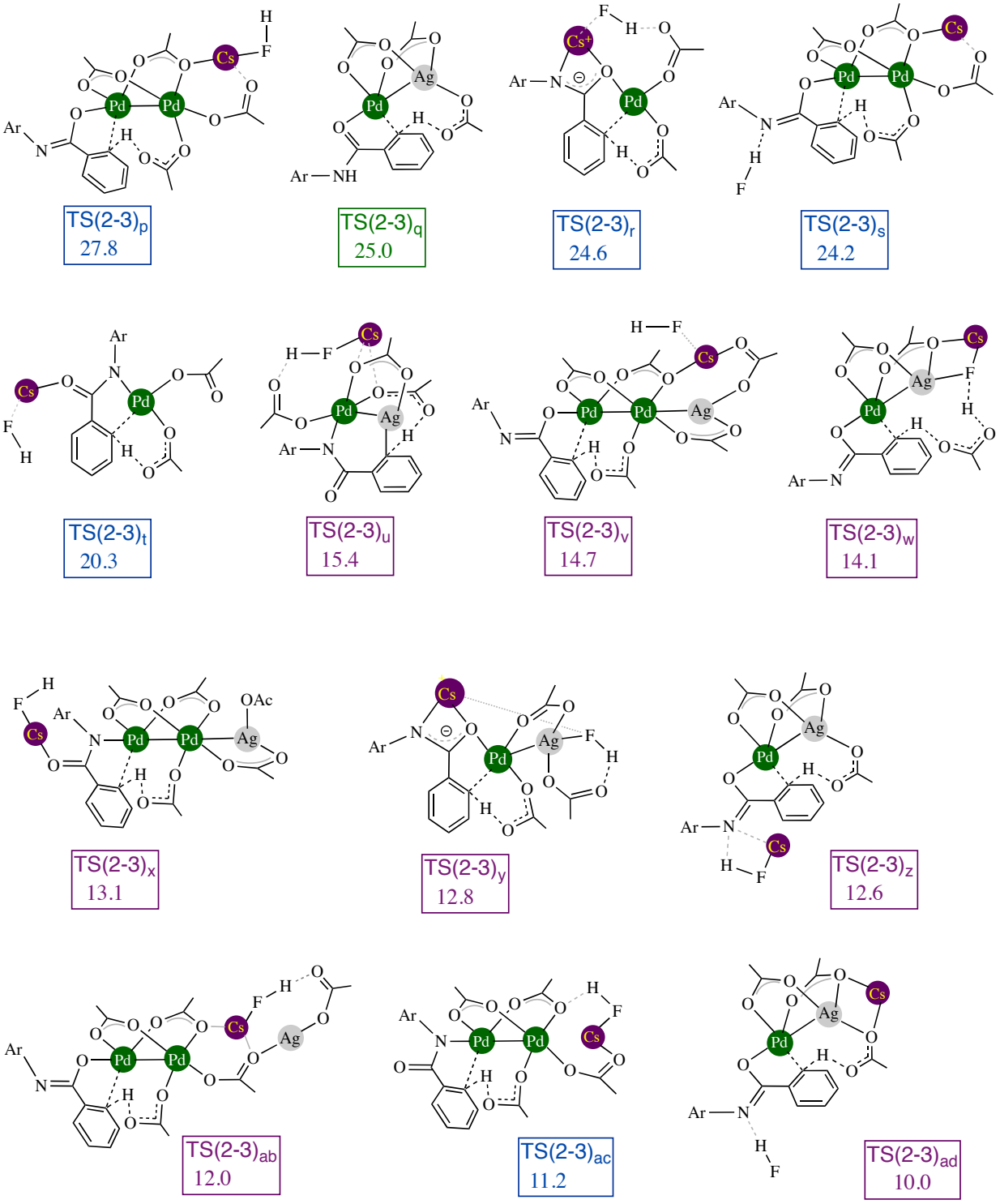


Figure B.3: Other C–H activation transition states plotted in Figure 3.1.



Figure B.3: Other C–H activation transition states plotted in Figure 3.1.

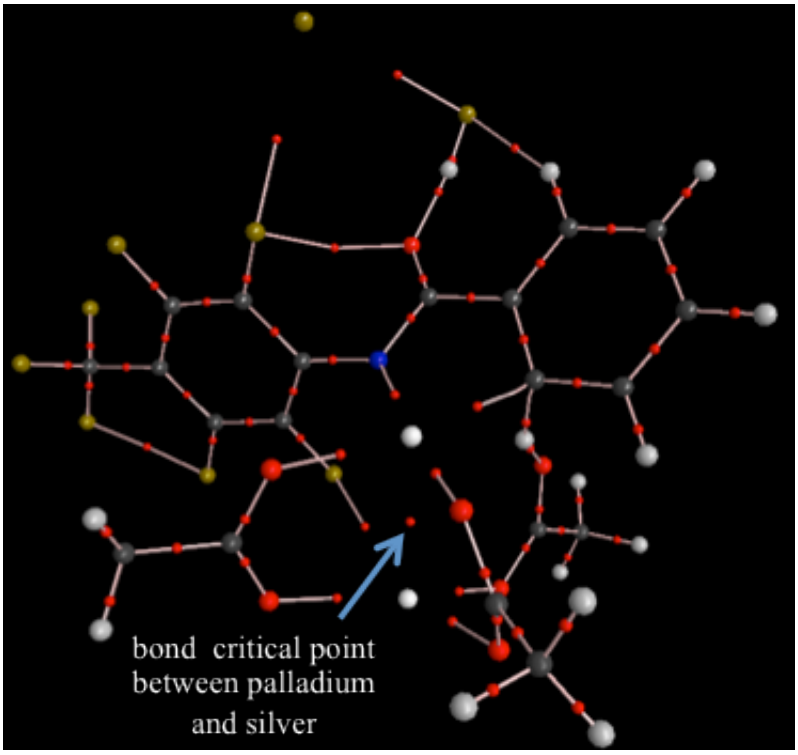


Figure B.4: Atoms-in-Molecules analysis of **TS(2–3)** showing the bond critical point between Pd and Ag atoms. [(a) AIM2000 Version 2.0; Buro fur Innovative Software, SBK-Software: Bielefeld, Germany, **2002**. (b) Biegler-Konig, F.; Schonbohm, J.; Bayles, D. *J. Comput. Chem.* **2001**, *22*, 545–559. (c) Biegler-Konig, F.; Schonbohm, J. *J. Comput. Chem.* **2002**, *23*, 1489–1494.]

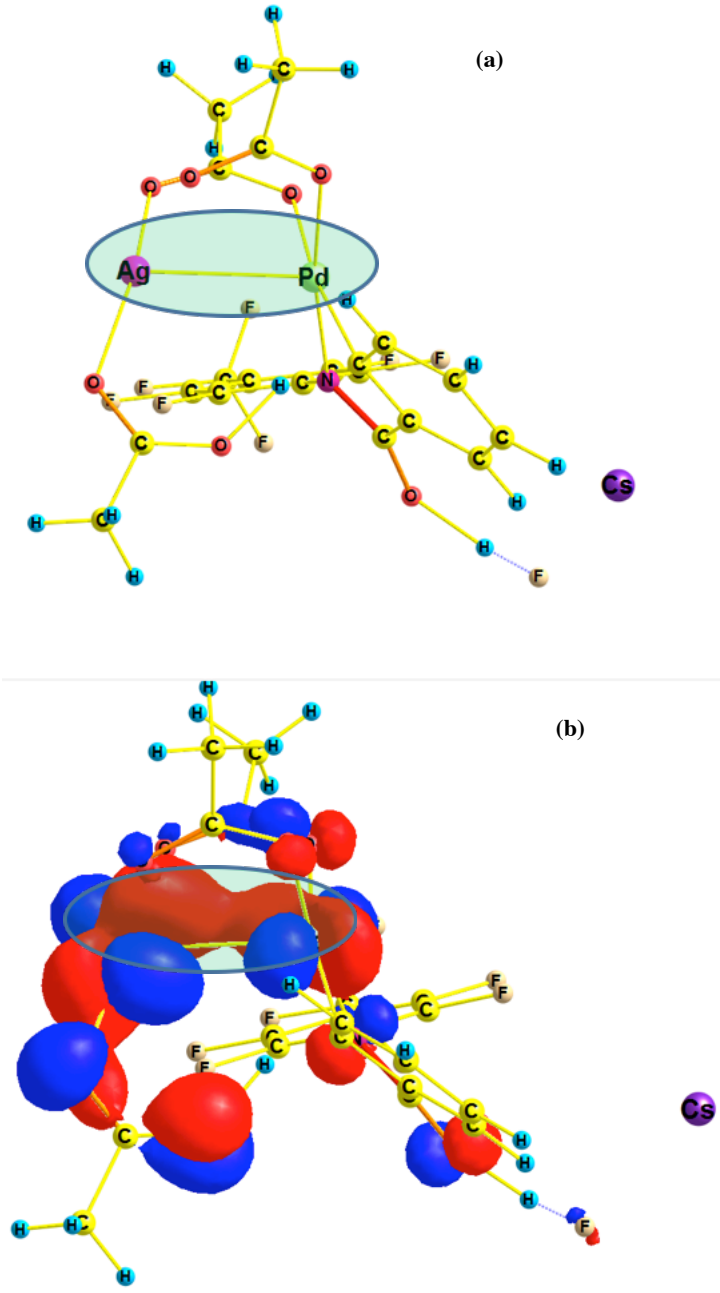


Figure B.5: (a) Optimized geometry of **TS(2–3)** and (b) molecular orbital exhibiting favorable palladium silver interaction.

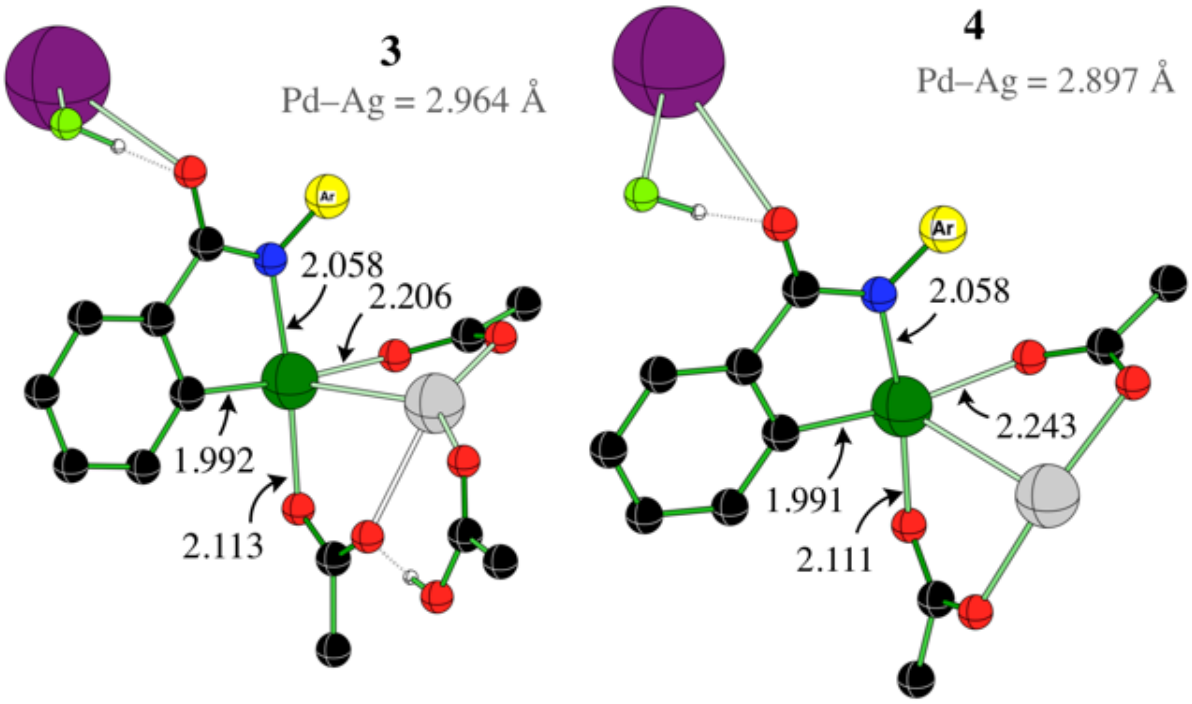


Figure B.6: Geometric details of intermediate **3** and **4**. All the bond distances are in angstroms. Most of the hydrogen atoms are removed for clarity.

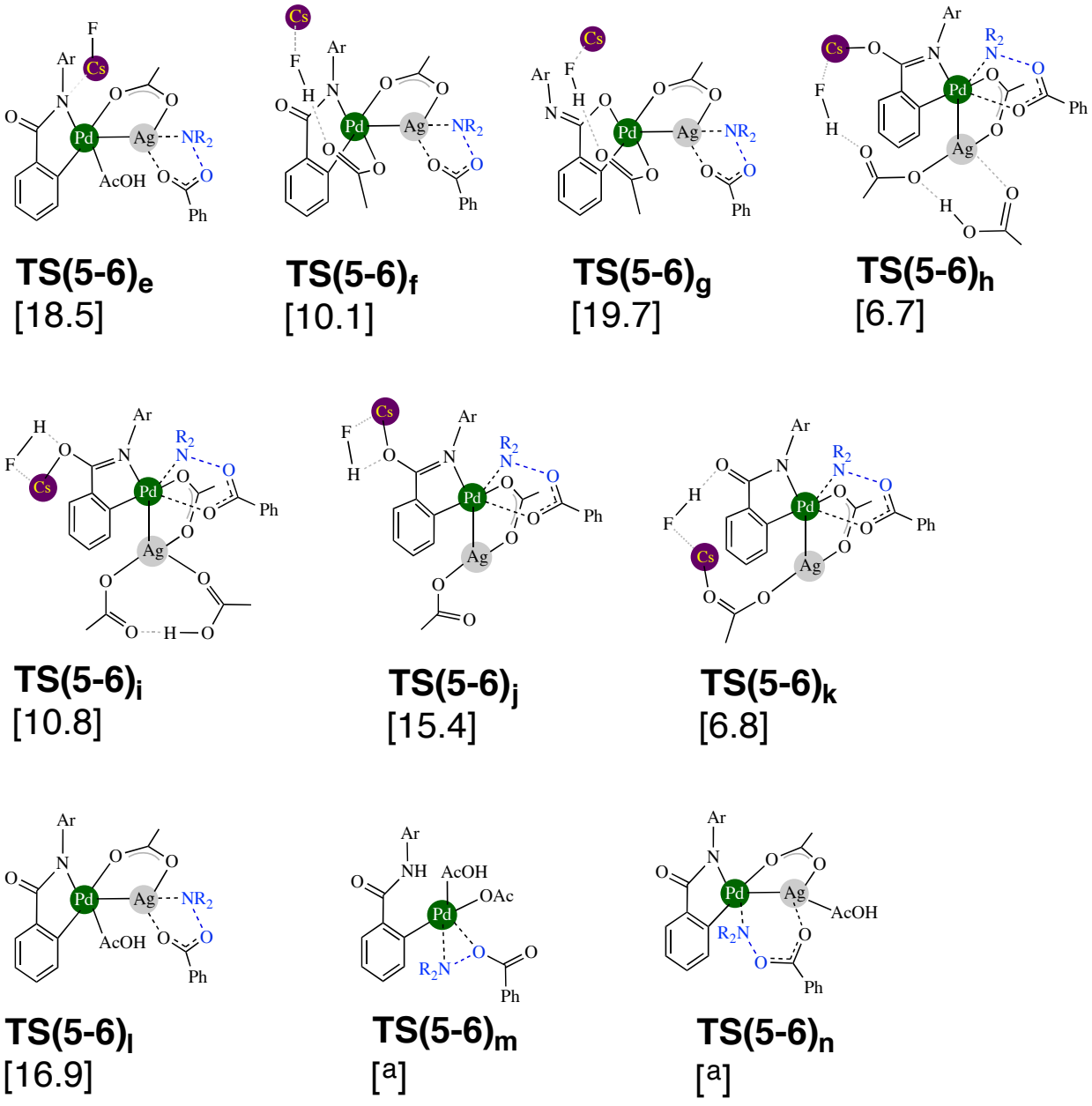


Figure B.7: N–O activation transition states with relative energies higher than **TS(5–6)**. The numbers in bracket are relative energies of transition states in kcal/mol. [a]Multiple attempts to locate these transition states in the condensed phase failed.

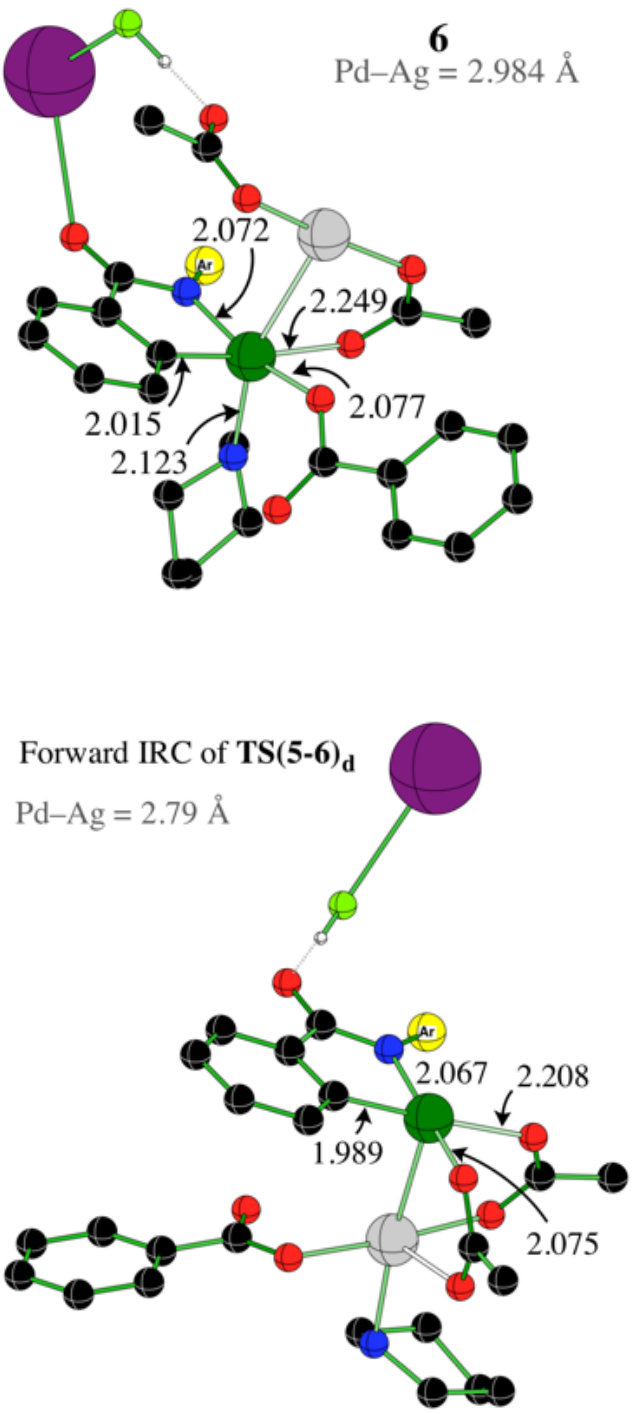


Figure B.8: Geometric details of intermediate **6** and forward IRC of $\mathbf{TS(5–6)_d}$. All the bond lengths are in angstroms. Most of the hydrogen atoms are removed for clarity.

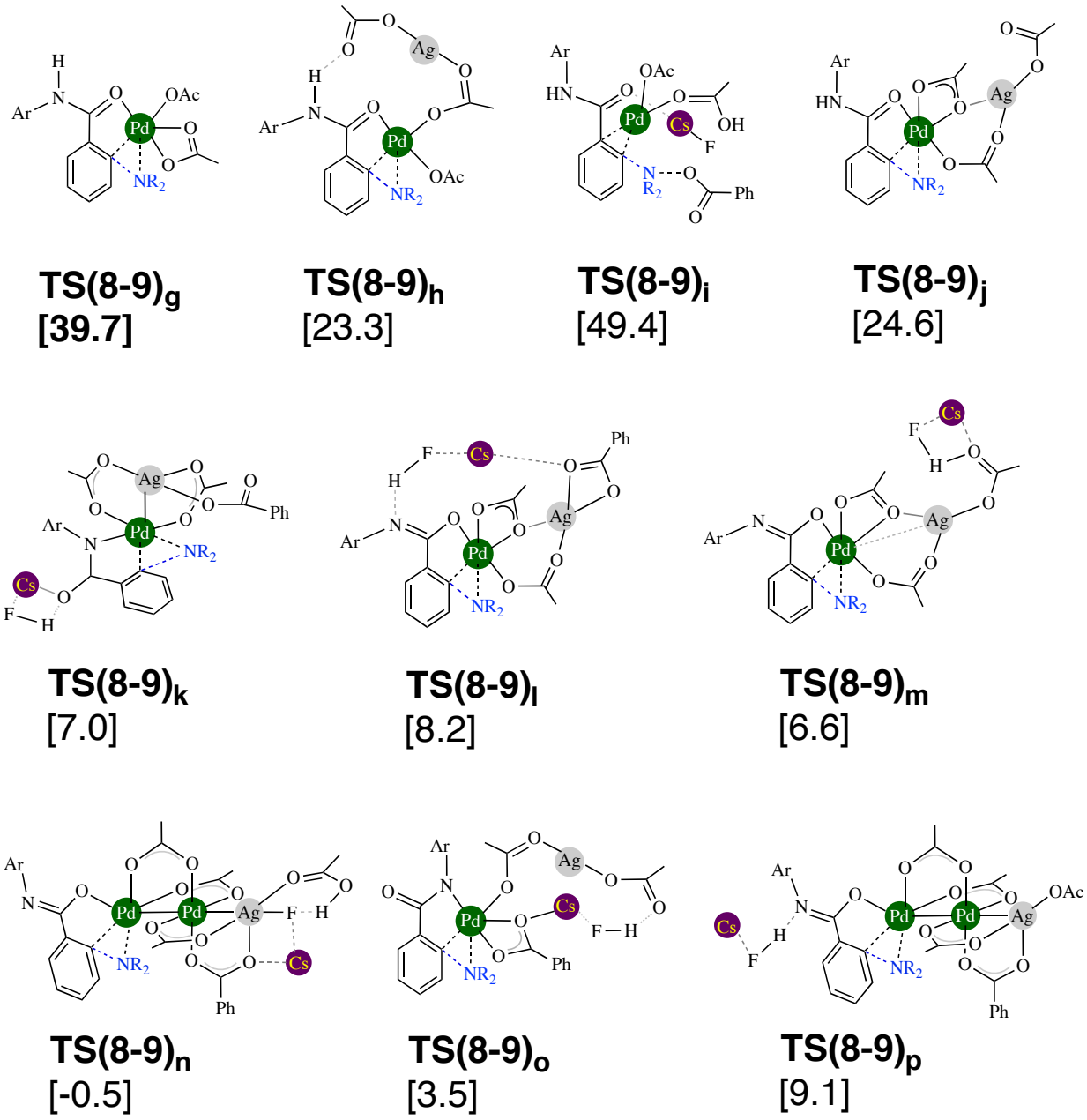


Figure B.9: Additional reductive elimination transition states. The numbers in bracket are relative free energies of TSs in kcal/mol.

Appendix C

For Chapter 4

C.1 Atoms In Molecules (AIM) Analysis

Baders theory of "Atoms in Molecules" has offered a valuable tool to analyze the nature of chemical bonds and interatomic interactions. Electron densities at the bond critical points ρ_{bcp} (a point along the bond path at the interatomic surface, where the shared electron density reaches a minimum) are calculated by using electronic wave function of the system.[282] Along with ρ, and its Laplacian (∇^2_ρ), we have calculated other topological properties such as the potential electron energy density (V), the kinetic electron energy density (G), and the total electron energy density (H) at those important BCPs. By using these parameters, we analyzed the nature of interatomic interaction between Pd and Ag metals.[283]

Initially, we have evaluated AIM properties of an experimentally reported hetero-bimetallic Pd-Ag crystal structure.[173] The wave function of this molecule was generated by using the geometry as seen in the crystal structure. AIM properties were then evaluated using this wave function. We have compared the ρ and ∇^2_ρ values for this crystal structure with all the transition states of CMD and RE steps to ascertain the presence of Pd-Ag interaction. It shows a similar trend to what we have found in the crystal structure. All wave functions of

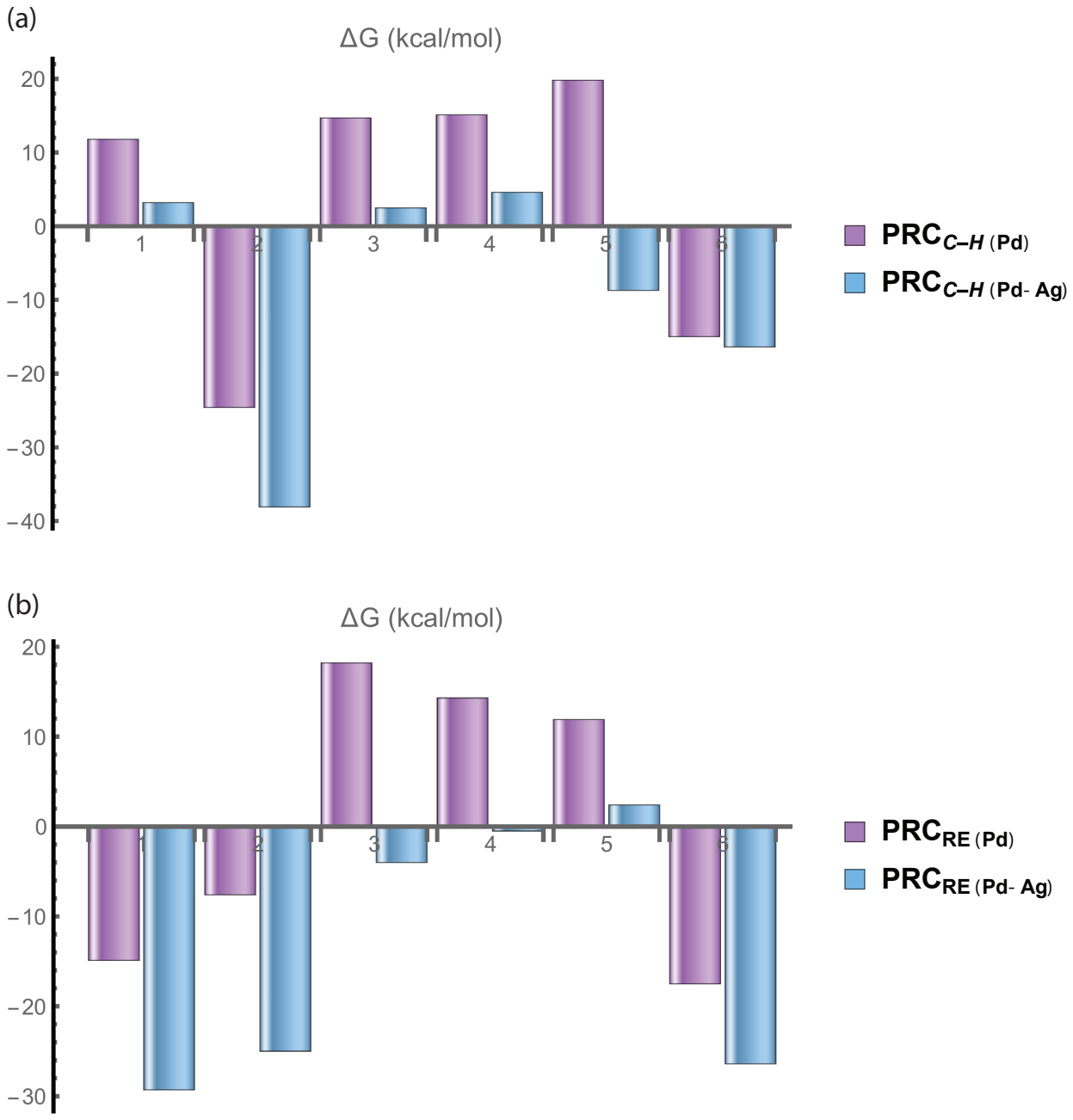


Figure C.1: Relative free energies (in kcal/mol) of preceding intermediates (or pre-reacting complex, PRC) of (a) C–H activation and (b) reductive elimination transition states for reactions **1**–**6**.

transition states are generated using the $SMD_{(solvent)}$/M06/6-31G**,LANL2DZ(Pd,Ag,Br,I) level of theory.

Bibliography

[1] Schultz, M. J.; Sigman, M. S. *Tetrahedron* **2006**, *62*, 8227–8241.

[2] Lee, J. C. H.; McDonald, R.; Hall, D. G. *Nat. Chem.* **2011**, *3*, 894–899.

[3] Behenna, D. C.; Liu, Y.; Yurino, T.; Kim, J.; White, D. E.; Virgil, S. C.; Stoltz, B. M. *Nat. Chem.* **2011**, *4*, 130–133.

[4] Lavallo, V.; Grubbs, R. H. *Science* **2009**, *326*, 559–562.

[5] Sergeev, A. G.; Hartwig, J. F. *Science* **2011**, *332*, 439–443.

[6] Lee, D.-H.; Kwon, K.-H.; Yi, C. S. *Science* **2011**, *333*, 1613–1616.

[7] Halpern, J. *Disc. Faraday Soc.* **1968**, 7–19.

[8] McNally, a.; Prier, C. K.; MacMillan, D. W. C. *Science* **2011**, *334*, 1114–1117.

[9] Hartwig, J. F. *Acc. Chem. Res.* **2012**, *45*, 864–873.

[10] Ritleng, V.; Sirlin, C.; Pfeffer, M. *Chem. Rev.* **2002**, *102*, 1731–1770.

[11] Smith, M. B.; March, J. *Advanced Organic Chemistry: Reactions, Mechanisms, and Structure*; Wiley Interscience: New York, 2001.

[12] Lyons, T. W.; Sanford, M. S. *Chem. Rev.* **2010**, *110*, 1147–1169.

[13] Wu, X. F.; Neumann, H.; Beller, M. *Chem. Eur. J.* **2012**, *18*, 419–422.

[14] Chan, K. S. L.; Wasa, M.; Wang, X.; Yu, J. Q. *Angew. Chem. Int. Ed.* **2011**, *50*, 9081–9084.

[15] Izawa, Y.; Pun, D.; Stahl, S. S. *Science* **2011**, *333*, 209–213.

[16] Mei, T.-S.; Kou, L.; Ma, S.; Engle, K.; Yu, J.-Q. *Synthesis* **2012**, *44*, 1778–1791.

[17] Chen, X.; Engle, K. M.; Wang, D. H.; Jin-Quan, Y. *Angew. Chem. Int. Ed.* **2009**, *48*, 5094–5115.

[18] Li, H.; Li, B.-J.; Shi, Z.-J. *Cat. Sci. Tech.* **2011**, *1*, 191–206.

[19] Poli, G.; Giambastiani, G.; Heumann, A. *Tetrahedron* **2000**, *56*, 5959–5989.

[20] Schlummer, B.; Scholz, U. *Adv. Synth. Cat.* **2004**, *346*, 1599–1626.

[21] Dupont, J.; Consorti, C. S.; Spencer, J. *Chem. Rev.* **2005**, *105*, 2527–2572.

[22] Selander, N.; J Szabó, K. *Chem. Rev.* **2011**, *111*, 2048–76.

[23] Guram, A. S.; Buchwald, S. L. *J. Am. Chem. Soc.* **1994**, *116*, 7901–7902.

[24] Paul, J., Frederic and; Hartwig, J. F. *J. Am. Chem. Soc.* **1994**, *116*, 5969–5970.

[25] Louie, J.; Hartwig, J. F. *Tetrahedron Lett.* **1995**, *36*, 3609–3612.

[26] Davies, H. M. L.; Manning, J. R. *Nature* **2008**, *451*, 417–424.

[27] Gutekunst, W. R.; Baran, P. S. *Chem. Soc. Rev.* **2011**, *40*, 1976–1991.

[28] Yamaguchi, J.; Yamaguchi, A. D.; Itami, K. *Angew. Chem. Int. Ed.* **2012**, *51*, 8960–9009.

[29] Wencel-Delord, J.; Glorius, F. *Nat. Chem.* **2013**, *5*, 369–375.

[30] Liu, Y.-J.; Xu, H.; Kong, W.-J.; Shang, M.; Dai, H.-X.; Yu, J.-Q. *Nature* **2014**, *515*, 389–393.

[31] Zatolochnaya, O. V.; Gevorgyan, V. *Nat. Chem.* **2014**, *6*, 661–663.

[32] Wang, X.-C.; Gong, W.; Fang, L.-Z.; Zhu, R.-Y.; Li, S.; Engle, K. M.; Yu, J.-Q. *Nature* **2015**, *519*, 334–338.

[33] Leow, D.; Li, G.; Mei, T.-S.; Yu, J.-Q. *Nature* **2012**, *486*, 518–522.

[34] McMurray, L.; O'Hara, F.; Gaunt, M. J. *Chem. Soc. Rev.* **2011**, *40*, 1885–1898.

[35] Chen, Y.; Wang, D.; Duan, P.; Ben, R.; Dai, L.; Shao, X.; Hong, M.; Zhao, J.; Huang, Y. *Nat. Commun.* **2014**, *5*, 4610.

[36] Iglesias, Á.; Álvarez, R.; deLera, Á. R.; Muñiz, K. *Angew. Chem. Int. Ed.* **2012**, *51*, 2225–2228.

[37] Collet, F.; Lescot, C.; Dauban, P. *Chem. Soc. Rev.* **2011**, *40*, 1926–1936.

[38] Pan, J.; Su, M.; Buchwald, S. L. *Angew. Chem. Int. Ed.* **2011**, *50*, 8647–8651.

[39] Torisawa, Y.; Nishi, T.; Minamikawa, J.-i. *Bioorg. Med. Chem. Lett.* **2000**, *10*, 2493–2495.

[40] Shulpin, G. B. *J. Mol. Cat. A: Chemical* **2002**, *189*, 39–66.

[41] Mee, S. P. H.; Lee, V.; Baldwin, J. E. *Angew. Chem. Int. Ed.* **2004**, *43*, 1132–1136.

[42] Fairlamb, I. J. S.; Taylor, R. J. K.; Serrano, J. L.; Sanchez, G. *New J. Chem.* **2006**, *30*, 1695–1704.

[43] Czarnik, A. W. *Acc. Chem. Res.* **1996**, *29*, 112–113.

[44] Horton, D. A.; Bourne, G. T.; Smythe, M. L. *Chem. Rev.* **2003**, *103*, 893–930.

[45] Leroux, F.; Jeschke, P.; Schlosser, M. *Chem. Rev.* **2005**, *105*, 827–856.

[46] Bruhn, D.; Madhura, D. B.; Maddox, M.; Lee, R. B.; Trivedi, A.; Yang, L.; Scherman, M. S.; Gilliland, J. C.; Gruppo, V.; McNeil, M. R.; Lenaerts, A. J.; Meibohm, B.; Lee, R. E. *Bioorg. Med. Chem.* **2012**, *20*, 6063–6072.

[47] Corbet, J.-P.; Mignani, G. *Chem. Rev.* **2006**, *106*, 2651–2710.

[48] D'Aprano, G.; Leclerc, M.; Zotti, G.; Schiavon, G. *Chem. Mat.* **1995**, *7*, 33–42.

[49] Hayes, K. *Appl. Catal., A* **2001**, *221*, 187–195.

[50] Bradshaw, J. S.; Krakowiak, K. E.; Izatt, R. M. *Tetrahedron* **1992**, *48*, 4475–4515.

[51] Turesky, R. J.; Le Marchand, L. *Chem. Res. Toxicol.* **2011**, *24*, 1169–1214.

[52] Weiss, T.; Angerer, J. *J. Chromatogr. B* **2002**, *778*, 179–192.

[53] Yoo, E. J.; Ma, S.; Mei, T.-S.; Chan, K. S. L.; Yu, J.-Q. *J. Am. Chem. Soc.* **2011**, *133*, 7652–7655.

[54] Anand, M.; Sunoj, R. B. *Org. Lett.* **2011**, *13*, 4802–4805.

[55] Anand, M.; Sunoj, R. B. *Organometallics* **2012**, *31*, 6466–6481.

[56] Kisan, H. K.; Sunoj, R. B. *J. Org. Chem.* **2015**, *80*, 2192–2197.

[57] Kisan, H. K.; Sunoj, R. B. *Chem. Comm.* **2014**, *50*, 14639–14642.

[58] Driver, M. S.; Hartwig, J. F. *J. Am. Chem. Soc.* **1997**, *119*, 8232–8245.

[59] Hamann, B. C.; Hartwig, J. F. *J. Am. Chem. Soc.* **1998**, *120*, 7369–7370.

[60] Alcazar-Roman, L. M.; Hartwig, J. F.; Rheingold, A. L.; Liable-Sands, L. M.; Guzei, I. A. *J. Am. Chem. Soc.* **2000**, *122*, 4618–4630.

[61] Müller, T. E.; Berger, M.; Grosche, M.; Herdtweck, E.; Schmidtchen, F. P. *Organometallics* **2001**, *20*, 4384–4393.

[62] Some of the computational studies on C–N bond forming reactions are the following: (a) Kretschmer, R.; Schlangen, M.; Schwarz, H. *Angew. Chem. Int. Ed.* **2012**, *5*, 3483–3488. (b) Guimond, N.; Gorelsky, S. I.; Fagnou, K. *J. Am. Chem. Soc.* **2011**, *133*, 6449–6457. (c) Ke, Z.; Cundari, T. R. *Organometallics* **2010**, *29*, 821–834. (d) Senn, H. M.; Blo chl, P. E.; Togni, A. *J. Am. Chem. Soc.* **2000**, *122*, 4098–4107.

[63] Balcells, D.; Clot, E.; Eisenstein, O. *Chem. Rev.* **2010**, *110*, 749–823.

[64] Hohenberg, P.; Kohn, W. *Phys. Rev. B* **1964**, B864–B871.

[65] Parr, R. G. *Density functional theory of atoms and molecules*; Springer, 1980.

[66] Hohenberg, P.; Kohn, W. *Phys. Rev.* **1964**, *136*, B864–B871.

[67] Kohn, W.; Sham, L. J. *Phys. Rev.* **1965**, *140*, A1133–A1138.

[68] In real systems, electrons interact and single determinant causes errors due to neglect of the electron correlation.

[69] Becke, A. D. *J. Chem. Phys.* **1993**, *98*, 5648–5652.

[70] Becke, A. D. *Phys. Rev. A* **1988**, *38*, 3098.

[71] Lee, C.; Yang, W.; Parr, R. G. *Phys. Rev. B* **1988**, *37*, 785.

[72] Slater, J. C. *Phys. Rev.* **1951**, *81*, 385.

[73] Vosko, S.; Wilk, L.; Nusair, M. *Can. J. Phys.* **1980**, *58*, 1200–1211.

[74] Zhao, Y.; Truhlar, D. G. *J. Phys. Chem. A* **2006**, *110*, 13126–13130.

[75] Zhao, Y.; Truhlar, D. G. *Theor. Chem. Acc.* **2008**, *120*, 215–241.

[76] R, D.; Hehre, W.; Pople, J. *J. Chem. Phys.* **1971**, *54*, 724.

[77] Hehre, W. J.; Ditchfield, R.; Pople, J. A. *J. Chem. Phys.* **1972**, *56*, 2257–2261.

[78] Cramer, C. J.; Truhlar, D. G. *Acc. Chem. Res.* **2008**, *41*, 760–768.

[79] Cramer, C. J.; Truhlar, D. G. *Chem. Rev.* **1999**, *99*, 2161–2200.

[80] Miertuš, S.; Scrocco, E.; Tomasi, J. *Chem. Phys.* **1981**, *55*, 117–129.

[81] Pascual-ahuir, J.-L.; Silla, E.; Tunon, I. *J. Comp. Chem.* **1994**, *15*, 1127–1138.

[82] Cossi, M.; Barone, V.; Cammi, R.; Tomasi, J. *Chem. Phys. Lett.* **1996**, *255*, 327–335.

[83] Barone, V.; Cossi, M.; Tomasi, J. *J. Chem. Phys.* **1997**, *107*, 3210–3221.

[84] Miertus, S.; Tomasi, J. *Chem. Phys.* **1982**, *65*, 239–245.

[85] Cances, E.; Mennucci, B.; Tomasi, J. *J. Chem. Phys.* **1997**, *107*, 3032–3041.

[86] Mennucci, B.; Tomasi, J. *J. Chem. Phys.* **1997**, *106*, 5151–5158.

[87] Mennucci, B.; Cances, E.; Tomasi, J. *J. Phys. Chem. B* **1997**, *101*, 10506–10517.

[88] Barone, V.; Cossi, M. *J. Phys. Chem. A* **1998**, *102*, 1995–2001.

[89] Cossi, M.; Barone, V.; Mennucci, B.; Tomasi, J. *Chem. Phys. Lett.* **1998**, *286*, 253–260.

[90] Barone, V.; Cossi, M.; Tomasi, J. *J. Comp. Chem.* **1998**, *19*, 404–417.

[91] Cammi, R.; Mennucci, B.; Tomasi, J. *J. Phys. Chem. A* **1999**, *103*, 9100–9108.

[92] Cossi, M.; Barone, V.; Robb, M. A. *J. Chem. Phys.* **1999**, *111*, 5295–5302.

[93] Tomasi, J.; Mennucci, B.; Cances, E. *J. Mol. Struct - THEOCHEM* **1999**, *464*, 211–226.

[94] Cammi, R.; Mennucci, B.; Tomasi, J. *J. Phys. Chem. A* **2000**, *104*, 5631–5637.

[95] Cossi, M.; Barone, V. *J. Chem. Phys.* **2000**, *112*, 2427–2435.

[96] Cossi, M.; Barone, V. *J. Chem. Phys.* **2001**, *115*, 4708–4717.

[97] Cossi, M.; Rega, N.; Scalmani, G.; Barone, V. *J. Chem. Phys.* **2001**, *114*, 5691–5701.

[98] Cossi, M.; Scalmani, G.; Rega, N.; Barone, V. *J. Chem. Phys.* **2002**, *117*, 43–54.

[99] Cossi, M.; Rega, N.; Scalmani, G.; Barone, V. *J. Comp. Chem.* **2003**, *24*, 669–681.

[100] Tomasi, J.; Mennucci, B.; Cammi, R. *Chem. Rev.* **2005**, *105*, 2999–3094.

[101] Cramer, C. J.; Truhlar, D. G. *Continuum Solvation Models*; Springer, 2002.

[102] Cramer, C. J. *Essentials of Computational Chemistry: Theories and Models*; John Wiley & Sons, 2013.

[103] Hartwig, J. F. *Nature* **2008**, *455*, 314–322.

[104] Bergman, R. G. *Nature* **2007**, *446*, 391–393.

[105] Godula, K.; Sames, D. *Science* **2006**, *312*, 67–72.

[106] Chen, M. S.; White, M. C. *Science* **2007**, *318*, 783–787.

[107] Chen, K.; Baran, P. S. *Nature* **2009**, *459*, 824–828.

[108] Daugulis, O.; Do, H.-q.; Shabashov, D. *Acc. Chem. Res.* **2009**, *42*, 1074–1086.

[109] Tsang, W. C. P.; Zheng, N.; Buchwald, S. L. *J. Am. Chem. Soc.* **2005**, *127*, 14560–14561.

[110] Yu, J.-Q.; Giri, R.; Chen, X. *Org. Biomol. Chem.* **2006**, *4*, 4041, and references cited therein.

[111] There have been recent reports on the activation of *meta*-C–H activation by TM. See (a) Tang, Ri. -Y.; Li, G.; Yu, J. -Q. *Nature*. **2014**, *507*, 215-220. (b) Leow, D.; Li, G.; Mei, T. -S.; Yu, J. -Q. *Nature* **2012**, *486*, 518–522. (c) Wang, X. -C.; Gong, W.; Fang, L. -Z.; Zhu, R. Y.; Li, S.; Engle, K. M.; Yu, J. -Q. *Nature* **2015**, *519*, 334-338.

[112] Wang, G.-W.; Yuan, T.-T. *J. Org. Chem.* **2010**, *75*, 476–479.

[113] Chen, Q.; Ilies, L.; Nakamura, E. *J. Am. Chem. Soc.* **2011**, *133*, 428–429.

[114] Chen, X.; Goodhue, C. E.; Yu, J.-Q. *J. Am. Chem. Soc.* **2006**, *128*, 12634–12635.

[115] Feng, C.-G.; Ye, M.; Xiao, K.-J.; Li, S.; Yu, J.-Q. *J. Am. Chem. Soc.* **2013**, *135*, 9322–9325.

[116] Ceccarelli, S.; Piarulli, U.; Gennari, C. *J. Org. Chem.* **2000**, *65*, 6254–6256.

[117] Zaitsev, V. G.; Shabashov, D.; Daugulis, O. *J. Am. Chem. Soc.* **2005**, *127*, 13154–13155.

[118] Weibel, J.-M.; Blanc, A.; Pale, P. *Chem. Rev.* **2008**, *108*, 3149–3173.

[119] Wasa, M.; Yu, J.-q. *J. Am. Chem. Soc.* **2008**, *130*, 14058–14059.

[120] Hull, K. L.; Sanford, M. S. *J. Am. Chem. Soc.* **2007**, *129*, 11904–11905.

[121] Dick, A. R.; Sanford, M. S. *Tetrahedron* **2006**, *62*, 2439–2463.

[122] Shilov, A. E.; Shul'pin, G. B. *Chem. Rev.* **1997**, *97*, 2879–2932, and references cited therein.

[123] Muehlhofer, M.; Strassner, T.; Herrmann, W. A. *Angew. Chem. Int. Ed.* **2002**, *41*, 1745–1747.

[124] Stahl, S. S.; Labinger, J. a.; Bercaw, J. E. *Angew. Chem. Int. Ed.* **1998**, *37*, 2180–2192.

[125] Beccalli, E. M.; Broggini, G.; Martinelli, M.; Sottocornola, S. *Chem. Rev.* **2007**, *107*, 5318–5365.

[126] McGlacken, G. P.; Fairlamb, I. J. S. *Eur. J. Org. Chem.* **2009**, *2009*, 4011–4029.

[127] Ackermann, L. *Chem. Rev.* **2011**, *111*, 1315–1345.

[128] Sun, H.-Y.; Gorelsky, S. I.; Stuart, D. R.; Campeau, L.-C.; Fagnou, K. *J. Org. Chem.* **2010**, *75*, 8180–8189.

[129] Suzuki, A. *Chem. Comm.* **2005**, 4759–4763.

[130] Mei, T.-S.; Kou, L.; Ma, S.; Engle, K.; Yu, J.-Q. *Synthesis* **2012**, *44*, 1778–1791.

[131] Louillat, M.-L.; Patureau, F. W. *Chem. Soc. Rev.* **2014**, *43*, 901–910.

[132] Chenna, B. C.; Shinkre, B. A.; King, J. R.; Lucius, A. L.; Narayana, S. V.; Velu, S. E. *Bioorg. Med. Chem. Lett.* **2008**, *18*, 380–385.

[133] Perdew, J. P.; Chevary, J.; Vosko, S.; Jackson, K. A.; Pederson, M. R.; Singh, D.; Fiolhais, C. *Phys. Rev. B* **1992**, *46*, 6671.

[134] Perdew, J. P.; Chevary, J.; Vosko, S.; Jackson, K. A.; Pederson, M. R.; Singh, D.; Fiolhais, C. *Phys. Rev. B* **1993**, *48*, 4978.

[135] Perdew, J. P.; Burke, K.; Wang, Y. *Phys. Rev. B* **1998**, *57*, 14999.

[136] Adamo, C.; Barone, V. *J. Chem. Phys.* **1998**, *108*, 664–675.

[137] Lee, C.; Yang, W.; Parr, R. G. *Phys. Rev., B* **1988**, *37*, 785–789.

[138] Frisch, M. J.; Trucks, G. W.; Schlegel, H. B.; Scuseria, G. E.; Robb, M. A.; Cheeseman, J. R.; Scalmani, G.; Barone, V.; Mennucci, B.; Petersson, G. A.; Nakatsuji, H.; Caricato, M.; Li, X.; Hratchian, H. P.; Izmaylov, A. F.; Bloino, J.; Zheng, G.; Sonnenberg, J. L.; Hada, M.; Ehara, M.; Toyota, K.; Fukuda, R.; Hasegawa, J.; Ishida, M.; Nakajima, T.; Honda, Y.; Kitao, O.; Nakai, H.; Vreven, T.; Montgomery, J. A., Jr.; Peralta, J. E.; Ogliaro, F.; Bearpark, M.; Heyd, J. J.; Brothers, E.; Kudin, K. N.; Staroverov, V. N.; Kobayashi, R.; Normand, J.; Raghavachari, K.; Rendell, A.; Burant, J. C.; Iyengar, S. S.; Tomasi, J.; Cossi, M.; Rega, N.; Millam, J. M.; Klene, M.; Knox, J. E.; Cross, J. B.; Bakken, V.; Adamo, C.; Jaramillo, J.; Gomperts, R.; Stratmann, R. E.; Yazyev, O.; Austin, A. J.; Cammi, R.; Pomelli, C.; Ochterski, J. W.; Martin, R. L.; Morokuma, K.; Zakrzewski, V. G.; Voth, G. A.; Salvador, P.; Dannenberg, J. J.; Dapprich, S.; Daniels, A. D.; Farkas, .; Foresman, J. B.; Ortiz, J. V.; Cioslowski, J.; Fox, D. J. Gaussian09 Revision E.01. Gaussian Inc. Wallingford CT 2009.

[139] Zhao, Y.; Truhlar, D. G. *J. Phys. Chem. A* **2006**, *110*, 13126–13130.

[140] Zhao, Y.; Truhlar, D. G. *J. Chem. Phys.* **2006**, *125*, 194101–194118.

[141] Liu, P.; Xu, X.; Dong, X.; Keitz, B. K.; Herbert, M. B.; Grubbs, R. H.; Houk, K. *J. Am. Chem. Soc.* **2012**, *134*, 1464–1467.

[142] Komagawa, S.; Wang, C.; Morokuma, K.; Saito, S.; Uchiyama, M. *J. Am. Chem. Soc.* **2013**, *135*, 14508–14511.

[143] Wang, Z. J.; Benitez, D.; Tkatchouk, E.; Goddard III, W. A.; Toste, F. D. *J. Am. Chem. Soc.* **2010**, *132*, 13064–13071.

[144] Biswas, S.; Huang, Z.; Choliy, Y.; Wang, D. Y.; Brookhart, M.; Krogh-Jespersen, K.; Goldman, A. S. *J. Am. Chem. Soc.* **2012**, *134*, 13276–13295.

[145] Gonzalez, C.; Schlegel, H. B. *J. Chem. Phys.* **1989**, *90*, 2154–2161.

[146] Gonzalez, C.; Schlegel, H. B. *J. Phys. Chem.* **1990**, *94*, 5523–5527.

[147] Nosova, V. M.; Ustynyuk, Y. A.; Bruk, L. G.; Temkin, O. N.; Kisin, A. V.; Storozhenko, P. A. *Inorg. Chem.* **2011**, *50*, 9300–9310.

[148] Patrick, Y.; Henry, M. *Can. J. Chem.* **1974**, *52*, 1241–1247.

[149] Akhmadullina, N. S.; Cherkashina, N. V.; Kozitsyna, N. Y.; Stolarov, I. P.; Perova, E. V.; Gekhman, A. E.; Nefedov, S. E.; Vargaftik, M. N.; Moiseev, I. I. *Inorg. Chim. Acta* **2009**, *362*, 1943–1951.

[150] Yatsimirsky, A.; Ryabov, A.; Zagorodnikov, V.; Sakodinskaya, I.; Kavetskaya, O.; Berezin, I. *Inorg. Chim. Acta* **1981**, *48*, 163–171.

[151] Skapski, A. C.; Smart, M. L. *Chem. Comm.* **1970**, 658–659.

[152] Bakhmutov, V. I.; Berry, J. F.; Cotton, F. A.; Murillo, C. A.; Box, P. O.; Station, C. *Dalton Trans.* **2005**, 1989–1992.

[153] Newbound, T. D.; Colsman, M. R.; Miller, M.; Wulfsberg, G. P.; Anderson, O. P.; Strauss, S. H. *J. Am. Chem. Soc.* **1989**, *111*, 3762–3764.

[154] Colsman, M. R.; Newbound, T. D.; Marshall, L. J.; Noirot, M. D.; Miller, M.; Wulfsberg, G. P.; Frye, J. S.; Anderson, O. P.; Strauss, S. H. *J. Am. Chem. Soc.* **1990**, *112*, 2349–2362.

[155] Hurlburt, P. K.; Anderson, O. P.; Strauss, S. H. *Can. J. Chem.* **1992**, *70*, 726–731.

[156] Seggen, D. M. V.; Hurlburt, P. K.; Noirot, M. D.; Anderson, Oren, P.; Strauss, S. H. *Inorg. Chem.* **1992**, *31*, 1423–1430.

[157] Seggen, D. M. V.; Hurlburt, P. K.; Anderson, O. P.; Strauss, S. H. *Inorg. Chem.* **1995**, *34*, 3453–3464.

[158] Díaz-Torres, R.; Alvarez, S. *Dalton Trans.* **2011**, *40*, 10742–10750.

[159] Strauss, S. H. *Chem. Rev.* **1993**, *93*, 927–942.

[160] Bihlmeier, A.; Gonsior, M.; Raabe, I.; Trapp, N.; Krossing, I. *Chem. Eur. J.* **2004**, *10*, 5041–5051.

[161] Chipperfield, J. R. *Non-Aqueous Solvents*; Oxford University Press: New York, United States.

[162] To reach the optimum number of DCE molecules, we have considered separated solvated ions with varying number of solvent molecules as well. We optimized complexes $[Cs(DCE)_n]^+$ and $[F(DCE)_n]^-$ for n = 1–4 in the dielectric continuum of DCE. Free energies of these structures were computed with respect to free ion (Cs^+ or F^-) and $(DCE)_n$ cluster. Based on the computed Gibbs free energies, three DCE molecules are found to be the most suitable configuration for both the cation (Cs^+) and the anion (F^-). Hence, we believe that $[CsF(DCE)_6]$ will be a logically correct representation of cesium fluoride in DCE. In other words, a contact ion pair in a moderately polar solvent such as DCE is highly likely.

[163] The coordination through the carbonyl oxygen resulted in higher energy transition states (Figure 2.2).

[164] The energy of the TS without the deprotonation of –NHAr is found to be 13.1 kcal/mol higher than that of **TS1**. See Figure A.1 in the Appendix A for more details. The amidic

N–H activation prior to the C–H activation was earlier noted in other reactions as well (see ref. 54 and 55).

[165] Such transition states involving acetate-assisted C–H activation have been proposed in the cases of different substrates. See references 217 and 220.

[166] Several mechanistic problems in transition metal catalysis have employed infinitely separated reactants as the common reference point. See references 201,208–211.

[167] Zhang, X.-G.; Dai, H.-X.; Wasa, M.; Yu, J.-Q. *J. Am. Chem. Soc.* **2012**, *134*, 11948–11951, Bases (like CsF) are known to deprotonate substrates in BHA reactions. See : Schlummer, B.; Scholz, U. *Adv. Synth. Catal.* **2004**, *346*, 1599–1626.

[168] There are some qualitative proposals wherein homo-bimetallic palladium dimers are suggested to be the active catalyst rather than their monomeric analogue. However, no transition states or details of the potential energy surfaces were reported. (a) Paton, R. S.; Brown, J. M. *Angew. Chem., Int. Ed.* **2012**, *51*, 10448. (b) Powers, D. C.; Ritter, T. *Nature* **2009**, *1*, 302. (c) Christmann, U.; Pantazis, D. A.; Benet- Buchholz, J.; McGrady, J. E.; Maseras, F.; Vilar, R. *J. Am. Chem. Soc.* **2006**, *128*, 6376. (d) Cotton, F. A.; Gu, J.; Murillo, C. A.; Timmons, D. J. *J. Am. Chem. Soc.* **1998**, *120*, 13280.

[169] See Figure A.2 in the Appendix A for other possible higher energy C–H activation transition states. We were also able to locate a few low energy energy C–H activation transition states having trimetallic (Pd–Pd–Ag) interaction as the active catalyst (Figure A.4).

[170] Additional possibilities with one and two molecules of solvent DCE bound to the cesium ion are computed to be of higher energy. See Figure A.3 in the Appendix A.

[171] The Pd–Ag bond distance of 2.9 Å is comparable to earlier experimental reports on palladium–silver bond lengths as reported in reference 224 and 225.

[172] Canty, A. J.; van Koten, G. *Acc. Chem. Res.* **1995**, *28*, 406–413.

[173] Kozitsyna, N. Y.; Nefedov, S. E.; Klyagina, A. P.; Markov, A. A.; Dobrokhotova, Z. V.; Velikodny, Y. A.; Kochubey, D. I.; Zyubina, T. S.; Gekhman, A. E.; Vargaftik, M. N.; Moiseev, I. I. *Inorg. Chim. Acta* **2011**, *370*, 382–387.

[174] Chaudret, B.; Delavaux, B.; Poilblanc, R. *Coord. Chem. Rev.* **1988**, *86*, 191–243.

[175] Richardson, D. E.; Taube, H. *Coord. Chem. Rev.* **1984**, *60*, 107–129.

[176] Adams, R. D.; Captain, B.; Zhu, L. *J. Am. Chem. Soc.* **2006**, *128*, 13672–13673.

[177] Álvarez, R.; de Lera, A. R.; Aurrecoechea, J. M.; Durana, A. *Organometallics* **2007**, *26*, 2799–2802.

[178] Giri, R.; Liang, J.; Lei, J.-G.; Li, J.-J.; Wang, D.-H.; Chen, X.; Naggar, I. C.; Guo, C.; Foxman, B. M.; Yu, J.-Q. *Angew. Chem. Int. Ed.* **2005**, *44*, 7420–7424.

[179] Giri, R.; Chen, X.; Yu, J.-Q. *Angew. Chem. Int. Ed.* **2005**, *44*, 2112–2115.

[180] Giri, R.; Lan, Y.; Liu, P.; Houk, K. N.; Yu, J.-Q. *J. Am. Chem. Soc.* **2012**, *134*, 14118–14126.

[181] Murahashi, T.; Kurosawa, H. *Coord. Chem. Rev.* **2002**, *231*, 207–228.

[182] Petretto, G. L.; Rourke, J. P.; Maidich, L.; Stoccoro, S.; Cinellu, M. A.; Minghetti, G.; Clarkson, G. J.; Zucca, A. *Organometallics* **2012**, *31*, 2971–2977.

[183] Tang, R.-Y.; Li, G.; Yu, J.-Q. *Nature* **2014**, *507*, 215–220.

[184] Hyster, T. K.; Knorr, L.; Ward, T. R.; Rovis, T. *Science* **2012**, *338*, 500–503.

[185] Jazzar, R.; Hitce, J.; Renaudat, A.; Sofack-Kreutzer, J.; Baudoin, O. *Chem. Eur. J.* **2010**, *16*, 2654–2672.

[186] Davies, H. M. L.; Du Bois, J.; Yu, J.-Q. *Chem. Soc. Rev.* **2011**, *40*, 1855–1856.

[187] Crabtree, R. H. *J. Chem. Soc., Dalton Trans.* **2001**, 2437–2450.

[188] Labinger, J. A.; Bercaw, J. E. *Nature* **2002**, *417*, 507–514.

[189] McNally, A.; Haffemayer, B.; Collins, B. S. L.; Gaunt, M. J. *Nature* **2014**, *510*, 129–133.

[190] Dupont, J.; Consorti, C. S.; Spencer, J. *Chem. Rev.* **2005**, *105*, 2527–2571.

[191] Stürmer, R. *Angew. Chem. Int. Ed.* **1999**, *38*, 3307–3308.

[192] Tobisu, M.; Ano, Y.; Chatani, N. *Org. Lett.* **2009**, *11*, 3250–3252.

[193] Achonduh, G. T.; Hadei, N.; Valente, C.; Avola, S.; O'Brien, C. J.; Organ, M. G. *Chem. Commun.* **2010**, *46*, 4109–4111.

[194] Stuart, D. R.; Fagnou, K. *Science* **2007**, *316*, 1172–1175.

[195] Phipps, R. J.; Gaunt, M. J. *Science* **2009**, *323*, 1593–1597.

[196] Nishikata, T.; Abela, A. R.; Huang, S.; Lipshutz, B. H. *J. Am. Chem. Soc.* **2010**, *132*, 4978–4979.

[197] Meng, X.; Kim, S. *Org. Lett.* **2013**, *15*, 1910–1913.

[198] Board, J.; Cosman, J. L.; Rantanen, T.; Singh, S. P.; Snieckus, V. *Platinum Met. Rev.* **2013**, *57*, 234–258.

[199] Some of the computational studies on C–N bond forming reactions are the following: (a) Kretschmer, R.; Schlangen, M.; Schwarz, H. *Angew. Chem. Int. Ed.* **2012**, *5*, 3483–3488. (b) Guimond, N.; Gorelsky, S. I.; Fagnou, K. *J. Am. Chem. Soc.* **2011**, *133*, 6449–6457. (c) Ke, Z.; Cundari, T. R. *Organometallics* **2010**, *29*, 821–834. (d) Senn, H. M.; Blöchl, P. E.; Togni, A. *J. Am. Chem. Soc.* **2000**, *122*, 4098–4107.

[200] Figg, T. M.; Wasa, M.; Yu, J.-Q.; Musaev, D. G. *J. Am. Chem. Soc.* **2013**, *135*, 14206–14214.

[201] Yang, Y.-F.; Cheng, G.-J.; Liu, P.; Leow, D.; Sun, T.-Y.; Chen, P.; Zhang, X.; Yu, J.-Q.; Wu, Y.-D.; Houk, K. *J. Am. Chem. Soc.* **2014**, *136*, 344–355.

[202] Anand, M.; Sunoj, R. B.; Schaefer III, H. F. *J. Am. Chem. Soc.* **2014**, *136*, 5535–5538.

[203] There are several examples of complexes with Pd–Ag bond with one or more bridging ligands in literature, which alludes to such a possibility. See : (a) Kozitsyna, N. Y.; Nefedov, S. E.; Klyagina, A. P.; Markov, A. A.; Dobrokhotova, Z. V.; Velikodny, Y. A.; Kochubey, D. I.; Zyubina, T. S.; Gekhman, A. E.; Vargaftik, M. N.; Moi- seev, I. I. *J. Org. Chem.* **2013**, *362*, 13754–13755. (b) Alonso, E.; Fornie, J.; Fortun, C.; Orpen, A. G. *Organometallics* **2003**, *22*, 5011–5019. (c) Lande, S. V.; Sharma, N.; Kumar, A.; Jasra, R. V. *Int. J. Spectro.* **2014**, *2014*, 1–6. (d) Neo, Y. C.; Vittal, J. J.; Andy Hor, T. S. *J. Chem. Soc., Dalton Trans.* **2002**, *2*, 337–342. (e) Langrick, C. R.; Shaw, B. L.; Pringle, P. G.; Shaw, B. L. *Inorg. Chim. Acta* **1983**, *76*, L263 L264.

[204] The solvent used was 1,4-dioxane for the reaction without any additive, toluene when cesium flouride was the exclusive additive, and DCE when both additives (silver acetate and cesium flouride) were employed. The aminating reagent used in the first two cases (no additive and with just cesium flouride) was *O*–benzoyl hydroxylmorpholine, whereas it was *O*–benzoyl hydroxylpiperidine in the presence of both additives,

wherein a maximum (97%) yield was reported. To enable uniform comparison, we have employed *O*–benzoyl hydroxylpiperidine with DCE as the solvent in all the three scenarios. The results should not differ much because of the chemical similarity between the aminating reagents as well as the dielectric of these three solvents.

[205] Stephens, P. J.; Devlin, F. J.; Chabalowski, C. F. *J. Phys. Chem.* **1994**, *98*, 11623–11627.

[206] Godbout, N.; Salahub, D. R.; Andzelm, J.; Wimmer, E. *Can. J. Chem.* **1992**, *70*, 560–571.

[207] Weigend, F.; Ahlrichs, R. *Phys. Chem. Chem. Phys.* **2005**, *7*, 3297–3305.

[208] Cheng, G.-J.; Yang, Y.-F.; Liu, P.; Chen, P.; Sun, T.-Y.; Li, G.; Zhang, X.; Houk, K. N.; Yu, J.-Q.; Wu, Y.-D. *J. Am. Chem. Soc.* **2014**, *136*, 894–897.

[209] Zhang, S.; Shi, L.; Ding, Y. *J. Am. Chem. Soc.* **2011**, *133*, 20218–20229.

[210] Balcells, D.; Nova, A.; Clot, E.; Gnanamgari, D.; Crabtree, R. H.; Eisenstein, O. *Organometallics* **2008**, *27*, 2529–2535.

[211] Nova, A.; Balcells, D.; Schley, N. D.; Dobereiner, G. E.; Crabtree, R. H.; Eisenstein, O. *Organometallics* **2010**, *29*, 6548–6558.

[212] Nosova, V. M.; Ustynyuk, Y. A.; Bruk, L. G.; Temkin, O. N.; Kisin, A. V.; Storozhenko, P. A. *Inorg. Chem.* **2011**, *50*, 9300–9310.

[213] Coordination via the amidic nitrogen of the directing group (–CONHR, where R = alkyl or aryl group) is preferred over the carbonyl oxygen. Similar features have been noticed in other palladium-catalyzed reactions as well. See refs 54, 55 and 200. After O–Cs bond formation in **A**, only the nitrogen coordination site is available for binding to

[Pd(μ−OAc)$_3$Ag] (Scheme 3). If there were no cesium fluoride in the reaction mixture, then the acetate of palladium acetate or silver acetate would have deprotonated –CONHAr.

[214] These possibilities also include trimetallic arrangements consisting of Pd–Pd–Ag arrangments.

[215] Powers, D. C.; Benitez, D.; Tkatchouk, E.; Goddard, W. A.; Ritter, T. *J. Am. Chem. Soc.* **2010**, *132*, 14092–14103.

[216] Powers, D. C.; Ritter, T. *Acc. Chem. Res.* **2012**, *45*, 840–850.

[217] Davies, D. L.; Donald, S. M. A.; Macgregor, S. A. *J. Am. Chem. Soc.* **2005**, *127*, 13754–13755.

[218] Lapointe, D.; Fagnou, K. *Chem. Lett.* **2010**, *39*, 1118–1126.

[219] Boutadla, Y.; Davies, D. L.; Macgregor, S. A.; Poblador-Bahamonde, A. I. *Dalton Trans.* **2009**, 5887–5893.

[220] Ess, D. H.; Bischof, S. M.; Oxgaard, J.; Periana, R. A.; Goddard, W. A. *Organometallics* **2008**, *27*, 6440–6445.

[221] Omae, I. *J. Organomet. Chem.* **2007**, *692*, 2608–2632.

[222] Although the molecular origin has not been established, some of the unique features of cesium such as large ionic radius, low charge density, and high polarizability are suggested as beneficial to palladium catalysis. See the following: Khader, K. K. A.; Sajith, A. M.; Padusha, M. S. A.; Nagaswarupa, H. P.; Muralidharan, A. *New J. Chem.* **2014**, *38*, 1294–1305.

[223] Khranenko, S. P.; Baidina, I. A.; Gromilov, S. A.; Belyaev, A. V. *J. Struct. Chem.* **2005**, *46*, 1060–1065.

[224] Braunstein, P.; Frison, C.; Oberbeckmann-Winter, N.; Morise, X.; Messaoudi, A.; Bénard, M.; Rohmer, M.-M.; Welter, R. *Angew. Chem. Int. Ed.* **2004**, *43*, 6120–6125.

[225] Kickham, J. E.; Loeb, S. J. *Organometallics* **1995**, *14*, 3584–3587.

[226] Braunstein, P.; Chetcuti, M. J.; Welter, R. *Chem. Commun.* **2001**, 2508–2509.

[227] Bratko, I.; Gómez, M. *Dalton Trans.* **2013**, *42*, 10664–10681.

[228] Ariafard, A.; Rajabi, N. A.; Jalali Atashgah, M.; Canty, A. J.; Yates, B. F. *ACS Catal.* **2014**, *4*, 860–869.

[229] Mata, J. A.; Hahn, F. E.; Peris, E. *Chem. Sci.* **2014**, *5*, 1723–1732.

[230] Jimeno, C.; Christmann, U.; Escudero-Adán, E. C.; Vilar, R.; Pericàs, M. A. *Chem. Eur. J.* **2012**, *18*, 16510–16516.

[231] Park, J.; Hong, S. *Chem. Soc. Rev.* **2012**, *41*, 6931–6943.

[232] Powers, D. C.; Ritter, T. *Nat. Chem.* **2009**, *1*, 302–309.

[233] Gray, T. G.; Veige, A. S.; Nocera, D. G. *J. Am. Chem. Soc.* **2004**, *126*, 9760–9768.

[234] Zhang, L.; Fang, D.-C. *J. Org. Chem.* **2013**, *78*, 2405–2412.

[235] Crespo, O.; Laguna, A.; Fernández, E. J.; López-de Luzuriaga, J. M.; Jones, P. G.; Teichert, M.; Monge, M.; Pyykkö, P.; Runeberg, N.; Schütz, M.; Werner, H. J. *Inorg. Chem.* **2000**, *39*, 4786–4792.

[236] Yamaguchi, T.; Yamazaki, F.; Ito, T. *J. Chem. Soc., Dalton Trans.* **1999**, 273–274.

[237] Balch, A. L.; Catalano, V. J.; Olmstead, M. M. *Inorg. Chem.* **1990**, *29*, 585–586.

[238] Xia, B.-H.; Zhang, H.-X.; Che, C.-M.; Leung, K.-H.; Phillips, D. L.; Zhu, N.; Zhou, Z.-Y. *J. Am. Chem. Soc.* **2003**, *125*, 10362–10374.

[239] Ebihara, M.; Tsuchiya, M.; Yamada, M.; Tokoro, K.; Kawamura, T. *Inorg. Chim. Acta* **1995**, *231*, 35–43.

[240] Crespo, O.; Gimeno, M. C.; Laguna, A.; Lehtonen, O.; Ospino, I.; Pyykkö, P.; Villacampa, M. D. *Chem. Eur. J.* **2014**, *20*, 3120–3127.

[241] Tanaka, S.-i.; Hoh, H.; Akahane, Y.; Tsutsuminai, S.; Komine, N.; Hirano, M.; Komiya, S. *J. Organomet. Chem.* **2007**, *692*, 26–35.

[242] The natural charge on palladium decreases from 0.504 in $\mathbf{TS(2–3)_a}$ to 0.488 in $\mathbf{TS(2–3)_c}$, indicating a relatively better Pd to Ag charge transfer in $\mathbf{TS(2–3)_c}$ and hence cooperativity between the two metals. Additional orbital interaction analysis revealed overlap between the Pd and Ag orbitals (see Figure B.5 in the appendix A) that offers improved clarity on the intermetallic interaction. Topological analysis of the electron density using the Atoms-in-Molecules (AIM) exhibited bond paths between Pd and Ag as well as a bond critical point. For a representative system, see Figure B.4 in the appendix A.

[243] Koszinowski, K.; Schröder, D.; Schwarz, H. *J. Am. Chem. Soc.* **2003**, *125*, 3676–3677.

[244] Musaev, D. G.; Liebeskind, L. S. *Organometallics* **2009**, *28*, 4639–4642.

[245] Ritleng, V.; Chetcuti, M. J. *Chem. Rev.* **2007**, *107*, 797–858.

[246] Ceccon, A.; Santi, S.; Orian, L.; Bisello, A. *Coord. Chem. Rev.* **2004**, *248*, 683–724.

[247] Wheatley, N.; Kalck, P. *Chem. Rev.* **1999**, *99*, 3379–3420.

[248] Attempts to locate N–O activation transition states by positioning cesium at other places in the complex failed, suggesting **TS(5–6)$_b$** to be the most likely transition state when cesium flouride is the only additive.

[249] The natural charge on palladium in **TS(5–6)$_a$** is 0.648 while that on **TS(5–6)$_c$** is 0.418. Pd(II) donates more electron density to Ag(III) in **TS(5–6)$_c$**.

[250] **TS(5–6)$_d$** and **TS(5–6)** are the lowest-energy TSs of all other N–O activation TSs with the same stoichiometry.

[251] Sundermann, A.; Uzan, O.; Martin, J. M. *Chem. Eur. J.* **2001**, *7*, 1703–1711.

[252] Furuya, T.; Benitez, D.; Tkatchouk, E.; Strom, A. E.; Tang, P.; Goddard III, W. A.; Ritter, T. *J. Am. Chem. Soc.* **2010**, *132*, 3793–3807.

[253] Transition-state geometries with a trans disposition of the Pd– Ag bond and Pd–NR_2 bonds could not be located.

[254] Simmons, E. M.; Hartwig, J. F. *Nature* **2012**, *483*, 70–73.

[255] Yang, L.; Huang, H. *Chem. Rev.* **2015**, *115*, 3468–3517.

[256] Wencel-Delord, J.; Dröge, T.; Liu, F.; Glorius, F. *Chem. Soc. Rev.* **2011**, *40*, 4740–4761.

[257] Hickman, A. J.; Sanford, M. S. *Nature* **2012**, *484*, 177–185.

[258] Magano, J.; Dunetz, J. R. *Chem. Rev.* **2011**, *111*, 2177–2250.

[259] Johansson Seechurn, C. C.; Kitching, M. O.; Colacot, T. J.; Snieckus, V. *Angew. Chem. Int. Ed.* **2012**, *51*, 5062–5085.

[260] García-Melchor, M.; Braga, A. A.; Lledós, A.; Ujaque, G.; Maseras, F. *Acc. Chem. Res.* **2013**, *46*, 2626–2634.

[261] Gorelsky, S. I.; Lapointe, D.; Fagnou, K. *J. Am. Chem. Soc.* **2008**, *130*, 10848–10849.

[262] Decharin, N.; Stahl, S. S. *J. Am. Chem. Soc.* **2011**, *133*, 5732–5735.

[263] Wickens, Z. K.; Guzmán, P. E.; Grubbs, R. H. *Angew. Chem. Int. Ed.* **2015**, *54*, 236–240.

[264] Gary, J. B.; Cook, A. K.; Sanford, M. S. *ACS Catal.* **2013**, *3*, 700–703.

[265] Chan, K. S.; Wasa, M.; Chu, L.; Laforteza, B. N.; Miura, M.; Yu, J.-Q. *Nature Chem.* **2014**, *6*, 146–150.

[266] Deng, Y.; Yu, J.-Q. *Angew. Chem. Int. Ed.* **2015**, *54*, 888–891.

[267] Hay, P. J.; Wadt, W. R. *J. Chem. Phys.* **1985**, *82*, 270283.

[268] Hay, P. J.; Wadt, W. R. *J. Chem. Phys.* **1985**, *82*, 284298.

[269] Hay, P. J.; Wadt, W. R. *J. Chem. Phys.* **1985**, *82*, 299310.

[270] Wurz, G.; Hofer, O.; Greger, H. *Nat. Prod. Lett.* **1993**, *3*, 177–182.

[271] Hassan, J.; Sevignon, M.; Gozzi, C.; Schulz, E.; Lemaire, M. *Chem. Rev.* **2002**, *102*, 1359–1470.

[272] Smalley, A. P.; Gaunt, M. J. *J. Am. Chem. Soc.* **2015**, *137*, 10632–10641.

[273] Dang, Y.; Qu, S.; Nelson, J. W.; Pham, H. D.; Wang, Z.-X.; Wang, X. *J. Am. Chem. Soc.* **2015**, *137*, 2006–2014.

[274] Gillie, A.; Stille, J. *J. Am. Chem. Soc.* **1980**, *102*, 4933–4941.

[275] Anand, M.; Sunoj, R. B.; Schaefer III, H. F. *ACS Catal.* **2015**, *6*, 696–708.

[276] Petretto, G. L.; Rourke, J. P.; Maidich, L.; Stoccoro, S.; Cinellu, M. A.; Minghetti, G.; Clarkson, G. J.; Zucca, A. *Organometallics* **2012**, *31*, 2971–2977.

[277] Wang, G.-W.; Yuan, T.-T.; Li, D.-D. *Angew. Chem. Int. Ed.* **2011**, *50*, 1380–1383.

[278] Gibbs, G.; Downs, R.; Prewitt, C.; Rosso, K. M.; Ross, N.; Cox, D. F. *J. Phys. Chem. B* **2005**, *109*, 21788–21795.

[279] Shaik, S.; Danovich, D.; Wu, W.; Hiberty, P. C. *Nat. Chem.* **2009**, *1*, 443–449.

[280] Ponec, R.; Yuzhakov, G.; Sundberg, M. R. *J. Comp. Chem.* **2005**, *26*, 447–454.

[281] Wu, L.-C.; Hsu, C.-W.; Chuang, Y.-C.; Lee, G.-H.; Tsai, Y.-C.; Wang, Y. *J. Phys. Chem. A* **2011**, *115*, 12602–12615.

[282] (a) Bader, R. F. W. *Atoms in Molecules: A Quantum Theory*, Oxford University Press, New York, 1990. (b) Bader, R. F. W. A quantum theory of molecular structure and its applications. *Chem. Rev.* **1991**, *91*, 893.

[283] Grabowski, S. J. *Chem. Rev.* **2011**, *111*, 2597–2625.